(2)

NAVAL POSTGRADUATE SCHOOL

Monterey, California

THESIS

STRUCTURAL DESIGN, ANALYSIS,
AND MODAL TESTING OF THE
PETITE AMATEUR NAVY SATELLITE
(PANSAT)

by

Daniel J. Sakoda

September 1992

Thesis Advisor: Prof. Ramesh Kolar

REPORT DOCUMENTATION PAGE

Form Approved OMB No. 0704-0188

1a. REPORT SECURITY CLASSIFICATION: UNCLASSIFIED	1b. RESTRICTIVE MARKINGS
2a. SECURITY CLASSIFICATION AUTHORITY	3. DISTRIBUTION/AVAILABILITY OF REPORT: Approved for public release; distribution is unlimited.
2b. DECLASSIFICATION/DOWNGRADING SCHEDULE	
4 PERFORMING ORGANIZATION REPORT NUMBER(S)	5. MONITORING ORGANIZATION REPORT NUMBER(S)
6a. NAME OF PERFORMING ORGANIZATION: Naval Postgraduate School; 6b. OFFICE SYMBOL (If applicable)	7a. NAME OF MONITORING ORGANIZATION: Naval Postgraduate School
6c. ADDRESS (City, State, and ZIP Code): Monterey, CA 93943-5000	7b. ADDRESS (City, State, and ZIP Code): Monterey, CA 93943-5000
8a. NAME OF FUNDING/SPONSORING ORGANIZATION; 8b. OFFICE SYMBOL (If applicable)	9 PROCUREMENT INSTRUMENT IDENTIFICATION NUMBER
8c. ADDRESS (City, State, and ZIP Code)	10 SOURCE OF FUNDING NUMBERS: PROGRAM ELEMENT NO. / PROJECT NO. / TASK NO / WORK UNIT ACCESSION NO

11. TITLE (Include Security Classification)
STRUCTURAL DESIGN, ANALYSIS, AND MODAL TESTING OF THE PETITE AMATEUR NAVY SATELLITE (PANSAT)

12. PERSONAL AUTHOR(S)
Sakoda, Daniel June

13a. TYPE OF REPORT	13b. TIME COVERED	14. DATE OF REPORT (Year, Month, Day)	15. PAGE COUNT
Master's Thesis	FROM _____ TO _____	1992 September	89

16. SUPPLEMENTARY NOTATION The views expressed in this thesis are those of the author and do not reflect the official policy or position of the Department of Defense or the U.S. Government.

17. COSATI CODES		
FIELD	GROUP	SUB-GROUP

18. SUBJECT TERMS (Continue on reverse if necessary and identify by block number)
PANSAT Satellite, Small Self-Contained Payload (SSCP), Get away Special (GAS), Complex Autonomous Payload (CAP), Finite Element Analysis (FEA), Modal Analysis

19. ABSTRACT (Continue on reverse if necessary and identify by block number)

The Naval Postgraduate School's (NPS) Space Systems Academic Group is developing the Petite Amateur Navy Satellite (PANSAT), a small satellite for digital store-and-forward communication in the amateur frequency band. PANSAT is intended to be a payload of opportunity amendable to a number of launch vehicles. The Shuttle Small Self-Contained Payload (SSCP) program was chosen as a design baseline because of its high margins of safety as a manned system. The PANSAT structure design is presented for the launch requirements of a Shuttle SSCP. A finite element model was developed and studied for the design loads of a SSCP. The results showed the structure to be very robust and likely to accommodate the requirements of other launch vehicles. The finite element analysis was verified by model testing, correlating the fundamental mode of the finite element model with that of an engineering test structure.

20. DISTRIBUTION/AVAILABILITY OF ABSTRACT	21. ABSTRACT SECURITY CLASSIFICATION	
☒ UNCLASSIFIED/UNLIMITED ☐ SAME AS RPT ☐ DTIC USERS	UNCLASSIFIED	
22a NAME OF RESPONSIBLE INDIVIDUAL: KOLAR, Ramesh	22b. TELEPHONE (Include Area Code): (408) 646-2936	22c. OFFICE SYMBOL: AA/Kj

Approved for public release; distribution is unlimited.

Structural Design, Analysis, and Modal Testing
of the Petite Amateur Navy Satellite (PANSAT)

by

Daniel J. Sakoda
B.S., University of Illinois, 1986

Submitted in partial fulfillment of the
requirements for the degree of

MASTER OF SCIENCE IN ASTRONAUTICAL ENGINEERING

from the

NAVAL POSTGRADUATE SCHOOL

September 1992

Author: 
Daniel J. Sakoda

Approved by: 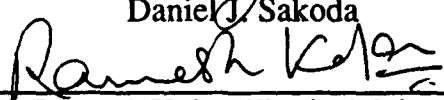
Ramesh Kolar, Thesis Advisor


Brij N. Agrawal, Second Reader

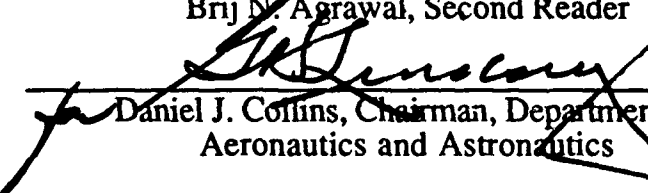
Daniel J. Collins, Chairman, Department of
Aeronautics and Astronautics

ABSTRACT

The Naval Postgraduate School's (NPS) Space Systems Academic Group is developing the Petite Amateur Navy Satellite (PANSAT), a small satellite for digital store-and-forward communication in the amateur frequency band. PANSAT is intended to be a payload of opportunity amenable to a number of launch vehicles. The Shuttle Small Self-Contained Payload (SSCP) program was chosen as a design baseline because of its high margins of safety as a manned system. The PANSAT structure design is presented for the launch requirements of a Shuttle SSCP. A finite element model was developed and studied for the design loads of a SSCP. The results showed the structure to be very robust and likely to accommodate the requirements of other launch vehicles. The finite element analysis was verified by modal testing, correlating the fundamental mode of the finite element model with that of an engineering test structure.

TABLE OF CONTENTS

LIST OF TABLES

LIST OF FIGURES

ACKNOWLEDGMENTS

Many thanks are due for this endeavor. I would like to express my sincere appreciation to Rudy Panholzer, my supervisor, for his encouragement and support; Ramesh Kolar for his patience and advice as my thesis advisor; and the great folks in the Space Systems Academic Group with whom I have had the privilege of working: David, Ron, Jim, Gian, Glenn, Sue. David P. and James. Additionally, I would like to express my gratitude to Prof. Young Shin for his time and vote of confidence. I would also like to thank my parents for their love and support; and my brother, Robin, for introducing me to Monterey and the Naval Postgraduate School.

I. PANSAT MISSION OVERVIEW

The Naval Postgraduate School's (NPS) Space Systems Academic Group is developing the Petite Amateur Navy Satellite (PANSAT), a small satellite for digital communication in the amateur frequency band centered at 437.25 MHz (960 kHz bandwidth). Direct sequence spread spectrum will be used to provide store-and-forward packet radio communication. The PANSAT project has three objectives: (1) to provide an educational tool for the officer students at NPS, (2) to perform and evaluate digital communications using spread spectrum in the amateur radio band from a small satellite, and (3) to provide a low-cost, space-based platform for small experiments.

The spacecraft will require no attitude control and encompasses only the structure, electric power, computer, and communication subsystems. The lack of attitude control reduces performance, but with a considerable reduction in response time, reliability concerns, and safety issues. Telemetry, tracking, and control (TT&C) functions will be distributed among the communication and computer subsystems. PANSAT can be launched from the Shuttle or an expendable launch vehicle. A typical Shuttle orbit of 480 km altitude and 28.5° inclination will provide sufficient coverage for up to ten minutes of communication between the spacecraft and NPS. The Shuttle launch was chosen as a conservative design constraint since it is a manned system. PANSAT would fly as a Small Self-Contained Payload (SSCP). SSCPs utilize the Get Away Special (GAS) and the Complex Autonomous Payload (CAP) programs. The launch sequence as a SSCP CAP is shown in Fig. 1. A pictorial representation of the mission overview is shown in Fig. 2.

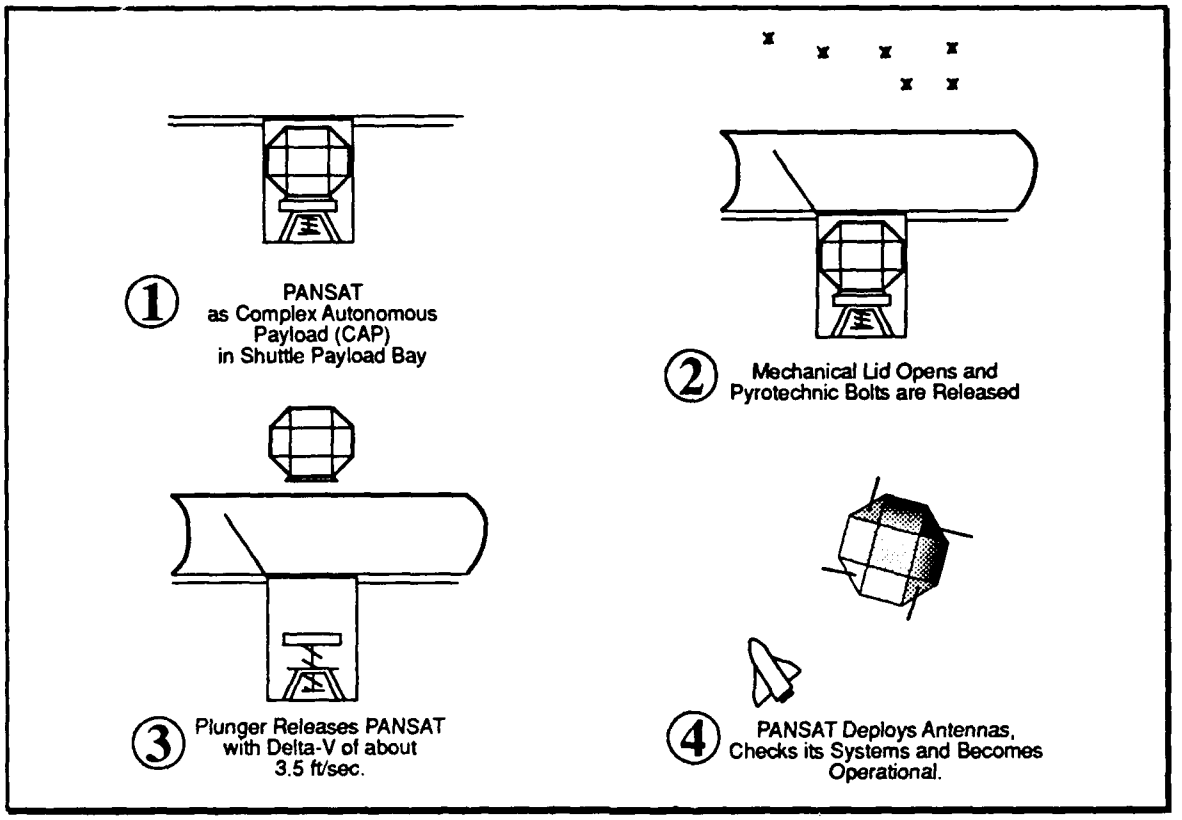

Figure 1. PANSAT Launch Sequence as a CAP Payload

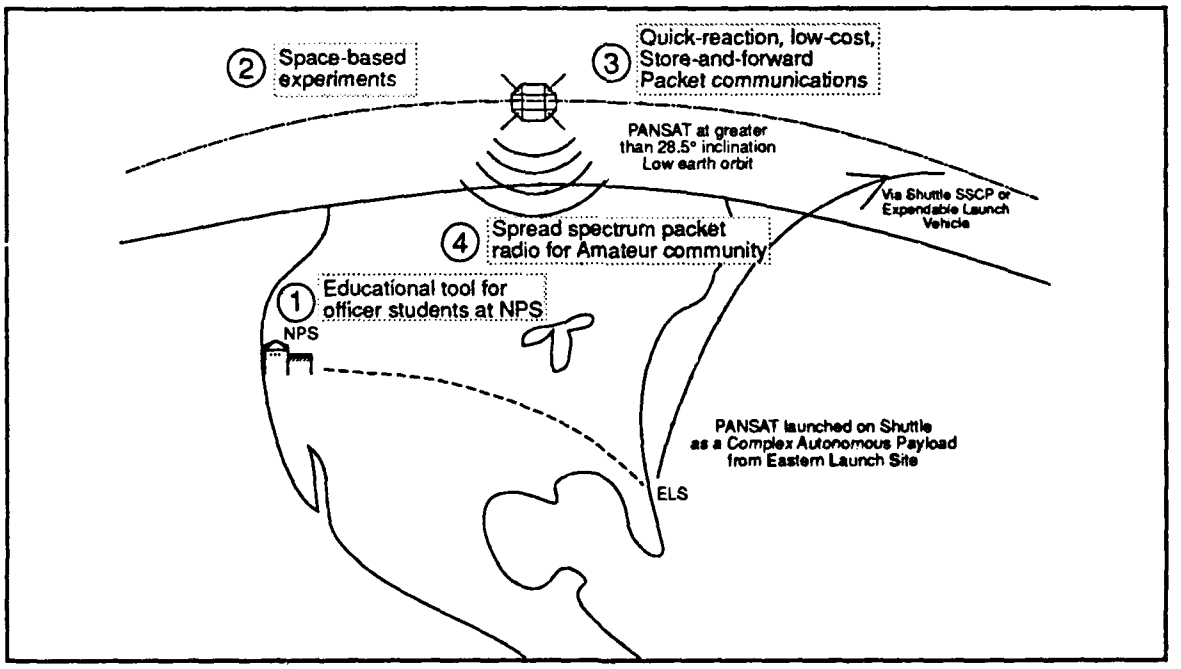

Figure 2. PANSAT Mission Overview

II. SHUTTLE SMALL SELF-CONTAINED PAYLOADS

A Shuttle Small Self-Contained Payload (SSCP) launch was chosen as a conservative design constraint. SSCPs utilize the Get Away Special (GAS) and Complex Autonomous Payload (CAP) programs. Both GAS payloads and CAPs utilize Get Away Special canisters which fly in the Shuttle payload bay. The main difference between CAPs and GAS payloads is that the CAP is more complex and may require additional services not provided by a standard GAS canister. Additionally, CAPs are queued differently than GAS payloads for a launch. The terms 'GAS' and 'CAP' are used interchangeably in this report.

A number of restrictions for safety concerns as well as compatibility as a secondary payload arise from a manned Shuttle launch. SSCP experiments are flown on a space/weight available basis [Ref. 1, p. 50]. Canisters are typically mounted in the Shuttle payload bay along the longerons. Figure 3 shows a canister mounted just below the Shuttle Remote Manipulator System (RMS) arm. PANSAT will require a modified GAS canister as a free-flier experiment. This includes a motorized door assembly, and a launch mechanism. These requirements distinguish PANSAT as a CAP rather than a GAS payload. The conservative SSCP design constraints allow PANSAT ease in qualification for other launch vehicles, such as a Scout or Pegasus flight, as a secondary payload.

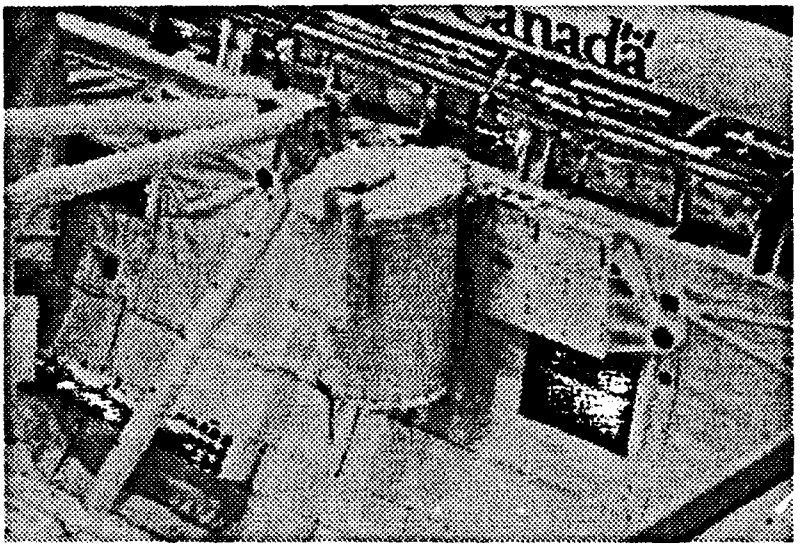

Figure 3. CAP Canister Mounted in Shuttle Payload Bay

Actual space flight assignment for PANSAT is the task of the Department of Defense (DoD) Space Test Program (STP). STP is responsible for the acquisition of space flight opportunities and payload integration. DoD experiments are assigned a priority based on rankings from the tri-service meeting where sponsoring agencies brief their experiment [Ref. 1, p. 16]. PANSAT is reviewed annually through the Navy Call for Experiments followed by the tri-service meeting. The initial step in the process is the filing of DD Form 1721, the STP request for space flight. [Ref. 1, pp. 25-29]

The information in DD Form 1721 determines the launch vehicle by experiment requirements. These include orbit parameters, sortie (retrieved) or free-flier (not retrieved) mode, power requirements, experiment orientation, and other user requirements. DD Form 1721 also outlines the objectives of the experiment, especially as to their military relevance. Correspondence with the STP office continues after receiving a launch opportunity for scheduling and

coordinating payload integration. This is because a number of DoD experiments may fly on a single launch opportunity as a suite.

The experimenter will also correspond directly with the NASA GAS program office if the flight is in a GAS canister. The GAS program office, located at the Goddard Space Flight Center (GSFC), is responsible for ensuring the requirements imposed by NHB 1700.7B, *Safety Policy and Requirements for Payloads Using the Space Transportation System (STS),* are fulfilled. The first document required is the Payload Accommodation Requirements (PAR). This document outlines the experiment's requirements of the GAS canister and any astronaut interfaces. The NASA GAS Safety Office requires a detailed analysis of the experiment in the form of a Safety Data Package (SDP). These documents are updated and approved in a three-phase process until launch.

A. PAYLOAD ENVELOPE

The payload envelope for a CAP equipped with the NASA standard ejection mechanism is 150 lbs weight, and 19.0 in. diameter by 18.5 in. height. The launch mechanism, as shown in Fig. 4, consists of a pedestal with a spring-loaded plunger. The spring is attached to the spacecraft by means of a Marman Clamp retention system. Two pyrotechnic bolts release the spring and thrust the spacecraft out of the shuttle at approximately 3.5 fps [Ref. 1, p. 52]. The motorized door assembly is shown in Fig. 5.

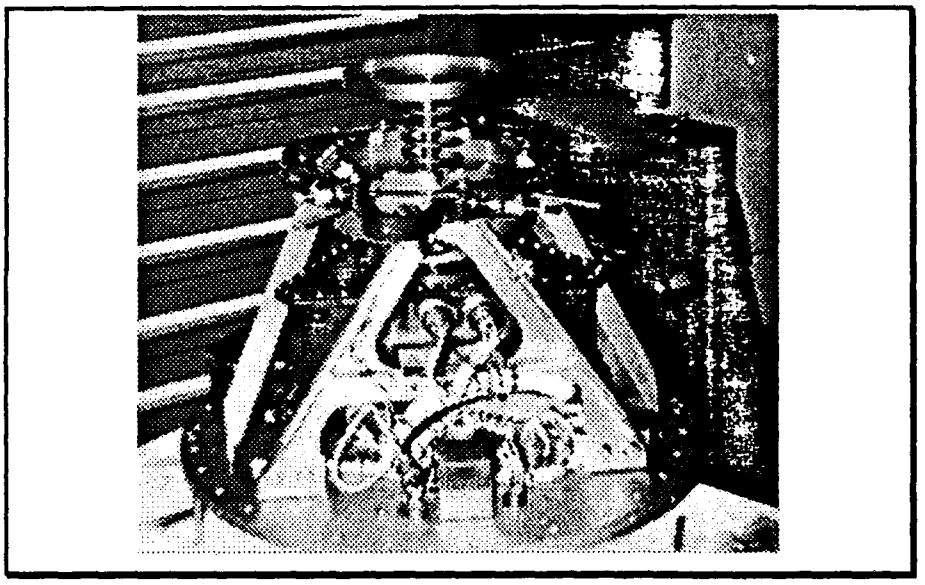

Figure 4. CAP Launch Mechanism

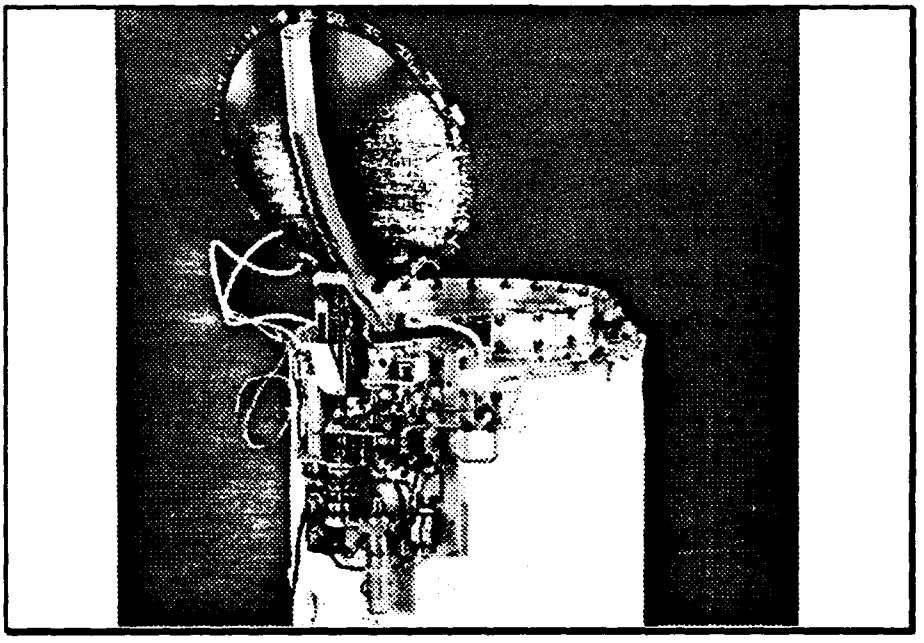

Figure 5. CAP Motorized Door Assembly

B. LAUNCH ENVIRONMENT

Launch loads for the Shuttle are due to the acoustic environment of the payload bay and thrust forces. A Shuttle SSCP must be able to withstand the load vectors given in Table 1 for analysis verified by test. [Ref. 2, p. A5]

TABLE 1. LOAD VECTORS FOR ANALYSIS VERIFIED BY TEST

Direction	Limit Load (g's)	Yield Load (g's)	Ultimate Load (g's)
± X	6.0	7.5	9.0
± Y	6.0	7.5	9.0
± Z	10.0	12.5	15.0

The yield factor of safety is 1.25 and the Ultimate factor of safety is 1.5. The direction referred corresponds to the Shuttle orbiter coordinate system shown in Fig. 6. Analysis not verified by test requires a yield factor of safety of 1.5 and ultimate factor of safety of 2.0. PANSAT will undergo verification of static loads by applying a low-frequency sine burst. The sine burst is 14.5 g's in each axis, not to exceed 20 Hz. The test is 5 cycles at 100 percent of the test loads. [Ref. 2, p. A-7]

Random vibration is not a requirement for GAS payloads. A random vibration test is planned for PANSAT, however, to ensure the structural integrity of the integrated spacecraft. The random vibration level for payloads inside a GAS canister is shown in Fig. 7.

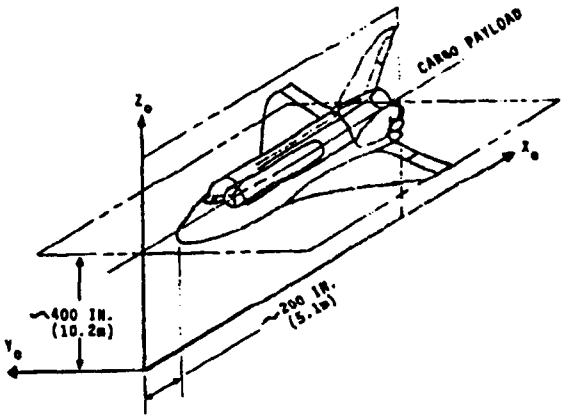

TYPE: ROTATING, ORBITER REFERENCED

ORIGIN: APPROXIMATELY 200 (9.1m) INCHES AHEAD OF THE NOSE AND APPROXIMATELY 400 INCHES (10.2m) BELOW THE CENTERLINE OF THE CARGO BAY

ORIENTATION AND LABELING:

THE X AXIS IS PARALLEL TO THE CENTERLINE OF THE CARGO BAY, NEGATIVE IN THE DIRECTION OF LAUNCH

THE Z AXIS IS POSITIVE UPWARD IN LANDING ATTITUDE

THE Y AXIS COMPLETES THE RIGHT-HANDED SYSTEM

THE STANDARD SUBSCRIPT IS 0

Figure 6. Orbiter Coordinate System [Ref. 2, p. A-7]

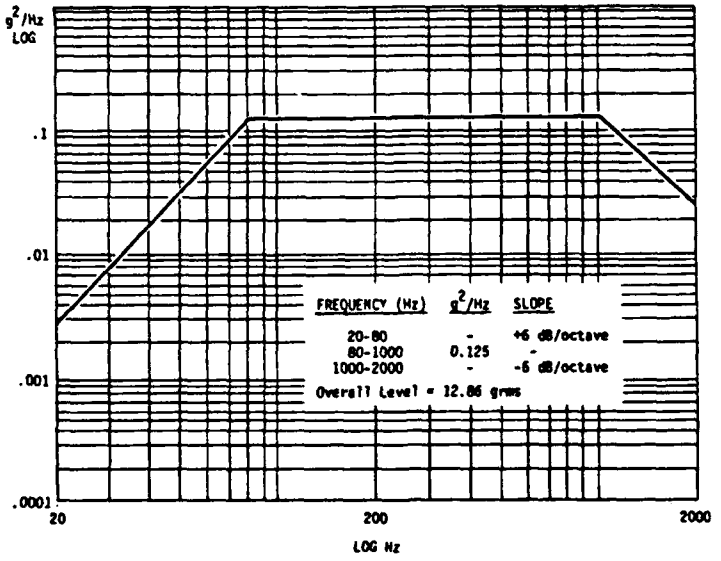

Figure 7. Random Vibration Level for Payloads Inside GAS Canisters (40 sec/mission/axis) [Ref. 2, p. A-15]

III. STRUCTURAL DESIGN

The PANSAT structure is designed to support 17 solar arrays about the spacecraft, a base-plate to interface with the launch vehicle (via a Marman clamp retention system), antenna mounting surfaces, space-viewing surfaces for experiments, and sufficient space within for mounting electronic components of the communication, computer, and electric power subsystems. Design considerations include simplicity and low-cost in fabrication and materials while minimizing weight. The spacecraft configuration is a twenty-six sided polyhedron with edges of length 7 1/8 in. (18.10 cm), similar to a sphere of radius 9.3 in. (23.6 cm). The configuration provides the most uniform distribution of solar energy on the solar arrays for the tumbling spacecraft. Figure 8 shows the PANSAT configuration.

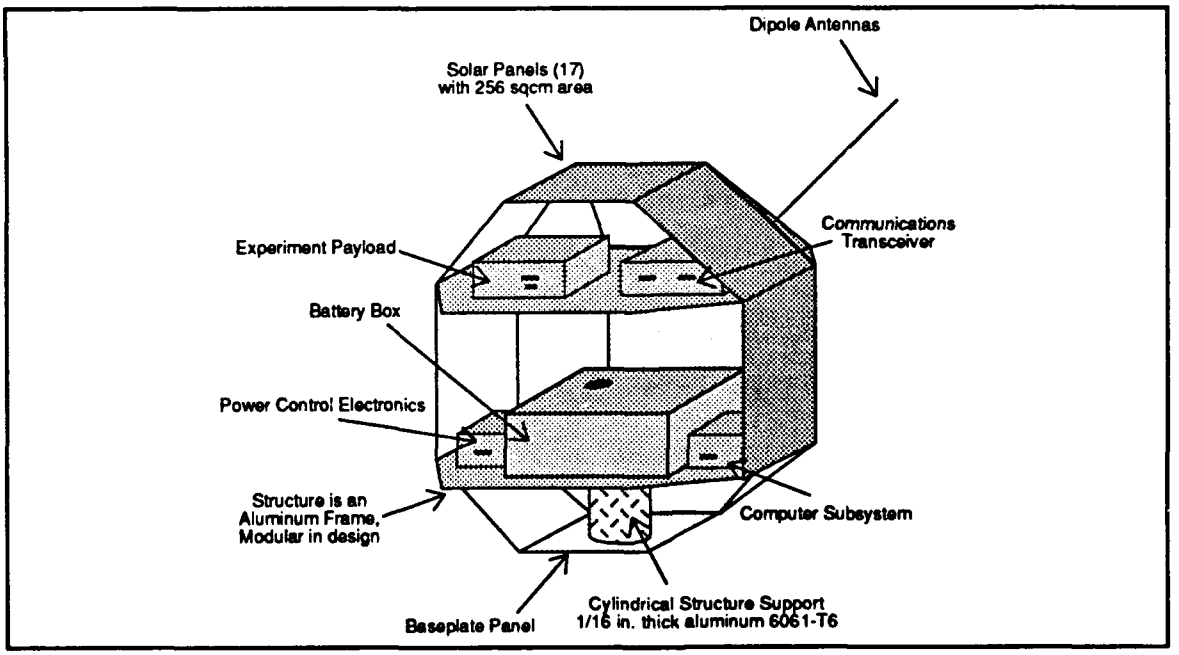

Figure 8. PANSAT Configuration

The design employs aluminum 6061-T6 throughout, which has a high strength-to-weight ratio and good machining properties. The structure incorporates modularity with frame-type elements providing both stiffeners and a shearing-plate in a single uniform component. The frame panels provide stiffness for the structure as well as a surface (7 1/8 in. x 7 1/8 in. x 1/16 in. thick) for mounting the solar array. The stiffeners also provide a surface for mounting solar panels not acting as structural members.

Loads are transferred from the spacecraft to the launch vehicle interface by means of a cylindrical shell. A 1/16 in. (0.159 cm) thick cylinder is sufficient to provide a margin of safety of 263% (see Appendix A), for a combined load of 150 lbf x 20 g's compression and 150 lbf x 12 in. x 12 g's moment.

Subsystem components are mounted to the structure by means of two equipment plates. The lower equipment plate is mounted directly to the support cylinder and carries most of the component mass. It is designed to carry 85 lbs of equipment (57% of spacecraft mass). The lower equipment plate requires only 1/8 in. thickness because of the added stiffness from the support cylinder; whereas the upper equipment plate is 1/4 in. thick. The upper equipment plate is capable of carrying 37.5 lbs of equipment (25% of spacecraft mass).

The structure elements are fastened together with screws. 10-24 screws are used where higher stresses are expected, and 4-40 screws are used elsewhere. Series 300, 404, 430, or 444 stainless steel are satisfactory for a GAS payload [Ref. 3]. Coil-threaded inserts are used for mating the fasteners with the parent material. This is done for increased strength and for reducing wear on the parent material.

Appendix B shows the drawings used to fabricate the modal test structure. This structure will be used for future flight qualification testing and for mock-up purposes. The actual flight unit will be built with materials having full documentation and traceability.

IV. FINITE ELEMENT ANALYSIS

A finite element analysis (FEA) was performed using the GIFTS software package by CASA/GIFTS® [Ref. 4] on a MicroVAX cluster (2000 series) in the Department of Aeronautics and Astronautics CAD/CAE Laboratory. Both static and dynamic analyses were performed for the structure. Static analysis was done for the loads prescribed in Table 1 with estimates of component masses. Dynamic analysis was performed to identify the fundamental vibration frequencies and mode shapes.

A. MODELING THE DESIGN

GIFTS provides an interactive environment for building the computer model. The software is composed of processor modules which the user accesses to input element structural parameters, create the structure's geometry, apply loads and boundary conditions, or perform the iterative routines for finding deflections, stresses, vibration frequencies, and mode shapes. Figure 9 shows the analysis process for PANSAT.

Two beam cross-sections were created for the structure. The first cross-section was used for the webbing on the panel faces, (0.44 in. x 0.063 in.). The addition of webbing is a design modification to provide support while milling aluminum sections. The second beam cross-section (0.44 in. x 0.125 in.) was used to model the boundary of the panel members.

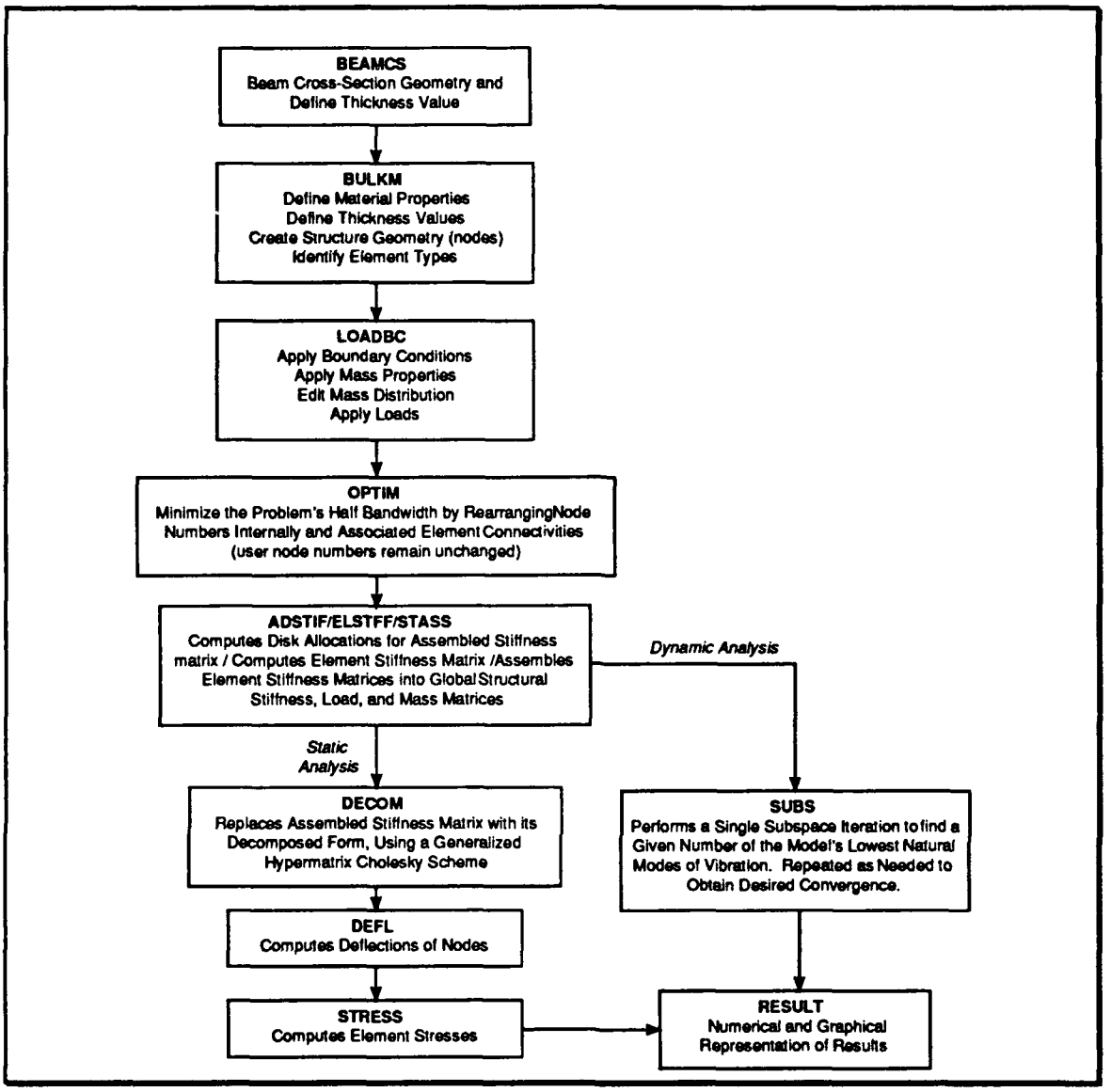

Figure 9. Processor Flow Diagram for PANSAT Analysis [Ref. 2, Sec. 4]

The origin of the model was located at the center of the base plate which lies in the 'xy' plane. This allows ease in generating the key nodes because of the spacecraft configuration's symmetry. Lines were then generated by connecting key nodes. Lines can be generated as beam elements or non-structural (geometric) lines. The user specifies the number of nodes to be distributed on a line. GIFTS will distribute the nodes evenly between the key nodes unless a

biasing factor is used. The number of nodes specified requires some discrimination by the user. This is because in generating the structural elements, by means of grids, compatibility is required on the grid boundary. The opposing lines on a grid bounded by four lines must have an equal number of nodes. On a grid bounded by three lines, all lines must have the same number of nodes.

The structural properties of the model are attributed to the grids by thickness values and material properties. The thickness values correspond to the thicknesses of the equipment plates, panels, and beam cross-sections. The material properties of aluminum were used throughout the model. Aluminum 6061-T6 is defined as an isotropic material with yield stress of 36 ksi, Young's modulus of 9.9×10^6 psi, Poisson ratio of 0.33, and density of 0.098 lb/in^3 (2.54×10^{-4} $slugs/in^3$). English units were used mainly because of their use in the aerospace industry and from vendor information on aluminum. Figure 10 shows the finite element model of the spacecraft structure.

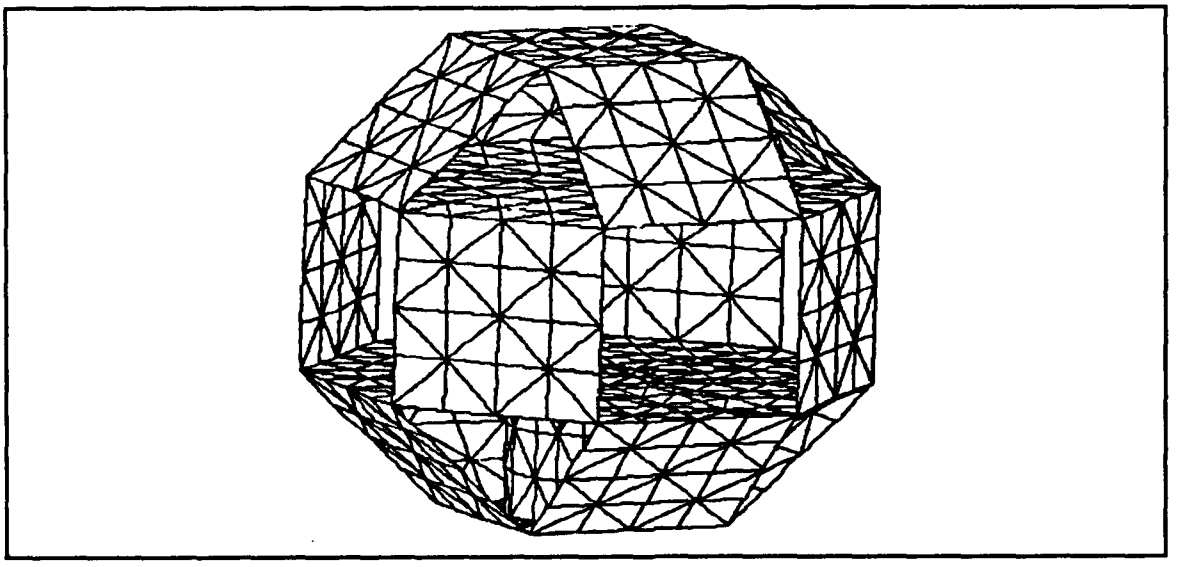

Figure 10. Finite Element Model of Structure

The model used for dynamic analysis is identical except that component masses are not added. Modal testing of the structure without component mass was used for verification of the finite element model.

B. FINITE ELEMENT ANALYSIS RESULTS

1. Static Loading

Finite element analysis results show that the structure is capable of withstanding the loads of a Shuttle GAS launch. Von Mises, or maximum octahedral shear stress, failure criterion was used to determine the margins of safety for all structural elements. Analysis for individual load cases were performed for the X, Y, and Z directions (as shown in Fig. 6). The load cases were combined and the failure criterion calculated to yield margins of safety under worst-possible-case loads. Table 2 shows the margins of safety for the various structural elements.

TABLE 2. MARGINS OF SAFETY OF STRUCTURE MEMBERS

Member	X			Y			Z			Combined		
	Ele. No.	Type	M.S.	Ele. No.	Type	M.S.	Ele. No.	Type	M.S.	Ele. No.	Type	M.S.
Top Plate	190	TB3	216	184	TB3	216	192	TB3	51.9	186	TB3	47.1
Upper-Deck, +x	69	Beam	89.9	69	Beam	61.5	1077	Beam	1.49	1073	Beam	1.48
Upper-Deck, -y	77	Beam	61.5	77	Beam	89.9	1026	Beam	1.49	1025	Beam	1.46
Upper-Deck, -x	85	Beam	89.9	85	Beam	61.5	1061	Beam	1.49	1041	Beam	1.49
Upper-Deck, +y	93	Beam	61.5	93	Beam	89.9	1045	Beam	1.49	1041	Beam	1.49
Mid-Deck, +x+y	37	Beam	26.0	33	Beam	25.3	1096	Beam	1.40	1096	Beam	1.48
Mid-Deck,+x,-y	41	Beam	26.0	45	Beam	25.3	1108	Beam	1.40	1108	Beam	1.36
Mid-Deck, -x,-y	53	Beam	26.0	49	Beam	25.3	1128	Beam	1.40	1128	Beam	1.33
Mid-Deck, -x,+y	57	Beam	26.0	61	Beam	25.3	1140	Beam	1.40	1144	Beam	1.42
Lower-Deck, +x	1157	Beam	8.43	1157	Beam	7.06	1160	Beam	2.58	1156	Beam	2.39
Lower-Deck, -y	1173	Beam	7.13	1173	Beam	8.26	1173	Beam	3.61	1173	Beam	1.23
Lower-Deck, -x	1189	Beam	8.43	1189	Beam	7.06	1188	Beam	2.58	1185	Beam	1.70
Lower-Deck, +y	1205	Beam	7.13	1205	Beam	8.26	1205	Beam	3.61	1205	Beam	3.29
Upper Eqp. Plate	615	TB3	110	609	TB3	111	640	TB3	4.30	576	TB3	4.25
Lower Eqp. Plate	416	TB3	26.4	382	TB3	25.4	448	TB3	2.40	448	TB3	2.27
Bottom Plate	160	TB3	4.98	159	TB3	4.90	160	TB3	6.75	159	TB3	1.49
Cylinder	271	TB3	1.86	247	TB3	1.86	247	TB3	6.57	241	TB3	0.59

2. Dynamic Modeling

Dynamic analysis through FEA was done considering the two cases of the structure alone and with component mass added (as described earlier). Free boundary conditions were used to yield the vibration modes allowing the highest number of degrees of freedom. The study shows that the dynamic characteristics of the upper equipment plate predominates. Ten modes were taken including the rigid body modes (first 6). The seventh mode is the fundamental vibration mode. Table 3 gives the frequencies for the first three modes of the structure alone and with component masses added.

TABLE 3. FEA DYNAMIC ANALYSIS RESULTS

Mode	Structure only (Hz)	Structure with masses (Hz)
1	2.3109E+02	5.0646E+01
2	4.6214E+02	7.0929E+01
3	4.6216E+02	7.8491E+01

The dynamic analysis of the structure without component masses is of particular importance in verifying the FEA model. Modal testing of the engineering qualification model is used for finite element model verification. Figures 11 through 13 show the computed mode shapes for the first three modes. The figure on the left shows all the elements shrunk 10% with the dashed lines representing the undeformed shape.

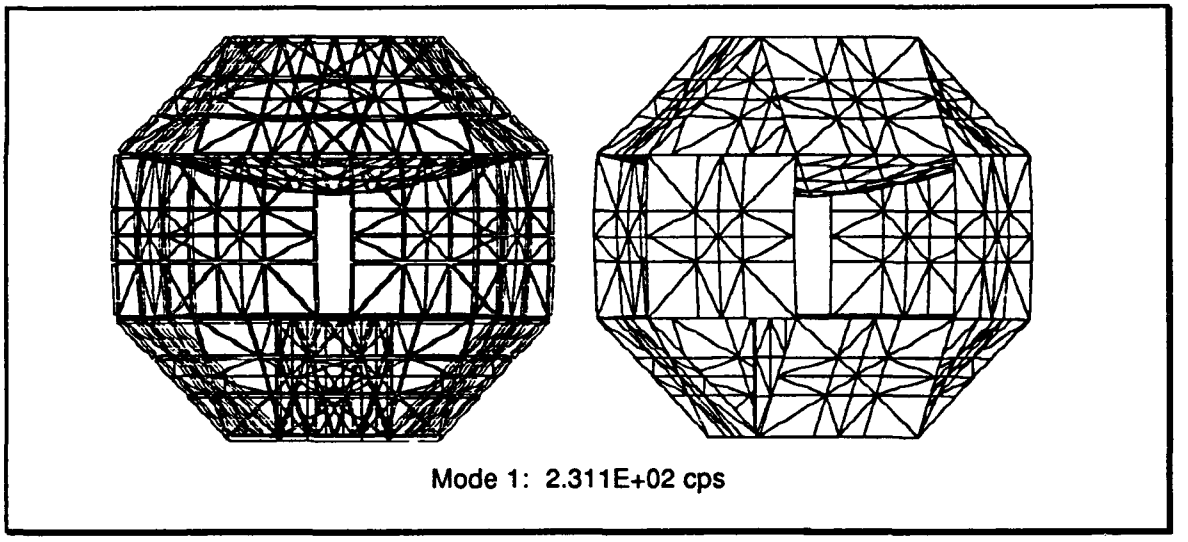

Figure 11. First Mode Shape (FEA)

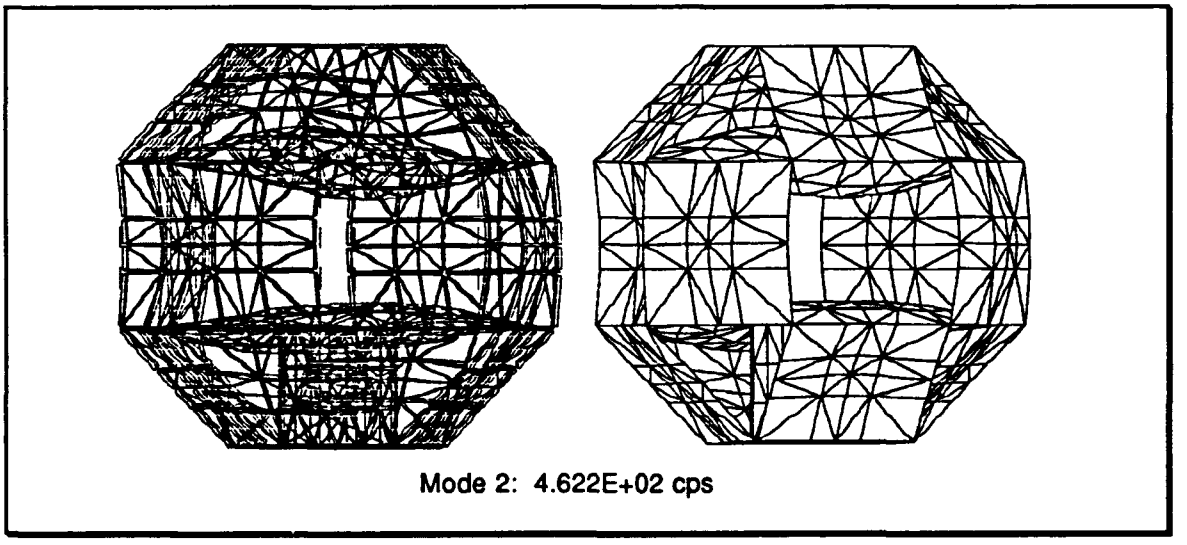

Figure 12. Second Mode Shape (FEA)

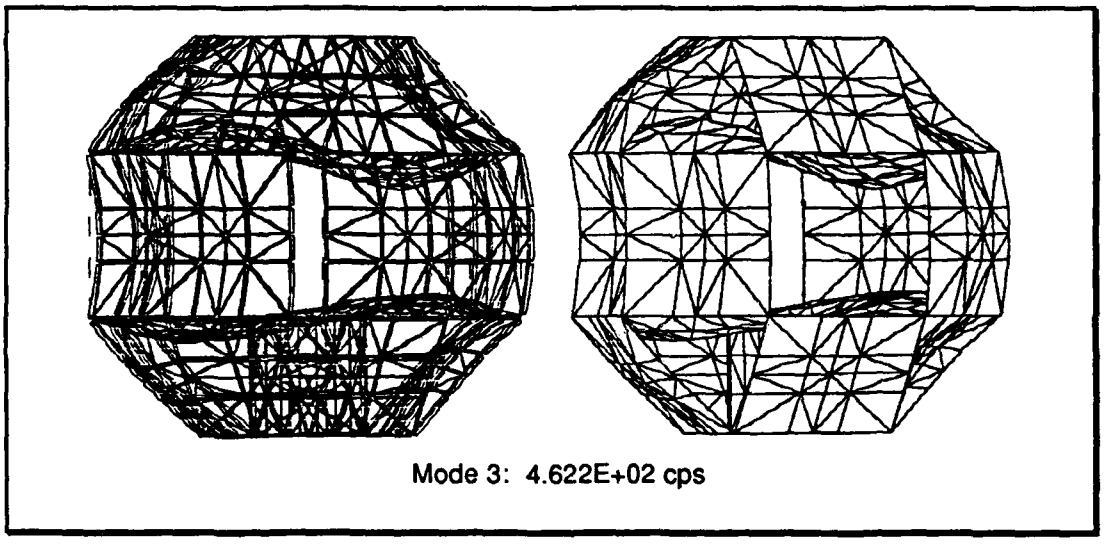

Figure 13. Third Mode Shape (FEA)

V. MODAL TESTING OF STRUCTURE

A test structure was built from fabrication drawings (Appendix B) at NPS for verification of the finite element model. Verification was done by means of modal testing. The structure was excited by a dynamic shaker and measurements about the structure were taken with accelerometers. The test data was then analyzed to identify the modal or resonant frequencies and mode shapes of the structure. Although only a few transducers are required to identify the modal frequencies, a number of measurement points (degrees of freedom) are needed to derive the mode shapes associated with the frequencies.

A. TEST APPARATUS

The apparatus used for modal testing of the PANSAT structure included a Hewlett-Packard (HP) 3565S data acquisition system, a MB Dynamics PM500A dynamic shaker, an aluminum support structure used for suspending the device under test, a Hewlett-Packard 9000 model 360CH Unix workstation providing software control, and piezoelectric accelerometers. Figure 14 shows the experimental setup.

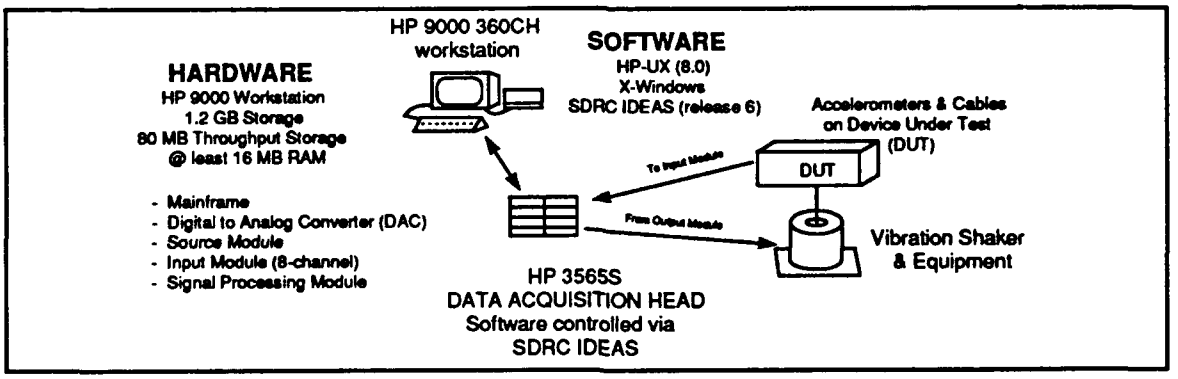

Figure 14. Vibration Test Setup

The HP 3565S data acquisition system as configured allows simultaneous sampling of 8 input channels. The sample rate is automatically set by specifying the resolution and measurement bandwidth. The hardware also provides a source module to output a signal for excitation and a signal processing module for data processing while acquisition is taking place. The HP 3565S transfers data directly to the computer workstation via a Hewlett-Packard Interface Bus (HPIB). The workstation also communicates with the data acquisition system via the HPIB interface. All data acquisition parameters are controlled by software via the Structural Dynamics Research Corp. (SDRC) IDEAS software application [Ref. 5]. Figure 15 shows the process undertaken for modal testing.

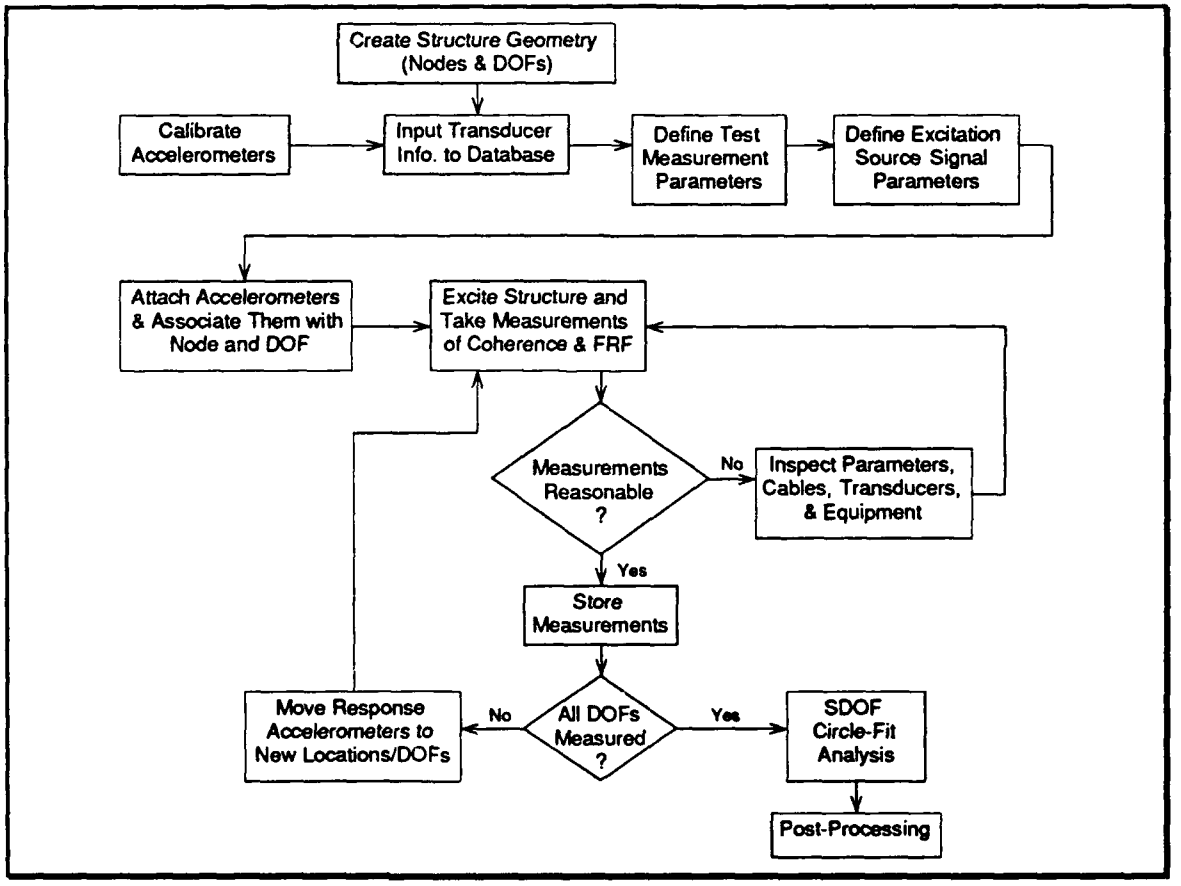

Figure 15. Process Flow for Modal Testing

1. Test Preparation

A computer-generated test model was constructed prior to any test runs. This model constructs the degrees of freedom similar to the finite element model. Each node of a test model generally signifies at least 1 of 6 degrees of freedom (3 in translation and 3 in rotation). For the PANSAT structure, each node denotes 1 translational degree of freedom; and is associated with the actual geometry of the structure. This was done in the SDRC IDEAS Model Preparation task. The model geometry and degrees of freedom are shown in Fig. 16.

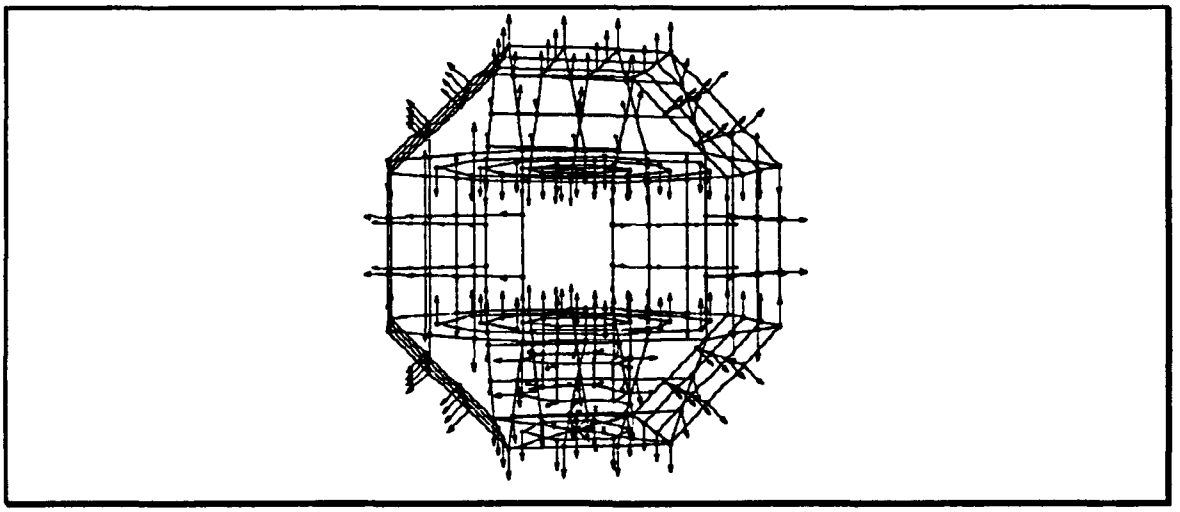

Figure 16. Test Model Geometry

The next step prior to test data acquisition is the calibration of the transducers. The transducers used were model numbers 309A, 303A12, and 303A03 manufactured by PCB Piezotronics, Inc. These accelerometers are integrated circuit piezoelectric (ICP) or voltage mode type accelerometers with linear response between 5 and 10,000 Hz and low mass. A power supply is required for operation, preferably a constant-current power supply. The transducers were calibrated using a Brüel & Kjær (B&K) type 4294 calibration exciter and a Hewlett-Packard 3561A dynamic signal analyzer. The B&K 4294

calibration exciter provides sinusoidal excitation at 159.2 Hz and 10 m/sec^2. The sensitivity of an accelerometer can be found by attaching it to the calibration exciter and deriving the ratio of its output in millivolts to the acceleration in g's of the excitation (mV/g). These values are input into the SDRC IDEAS database along with the model type and serial number. The transducer can then be identified with the geometry node and degree of freedom where the measurement is taken.

2. Boundary Conditions

The PANSAT structure was suspended from an aluminum support structure via shock cords. Suspension provides a simulation of a free-free boundary condition. Four shock cords were used to suspend the structure over the dynamic shaker where a stainless steel rod was attached between the shaker and the base plate of the device under test. The stainless steel rod provides force input to the test structure at a single point along a single axis. Figure 17 shows the test configuration.

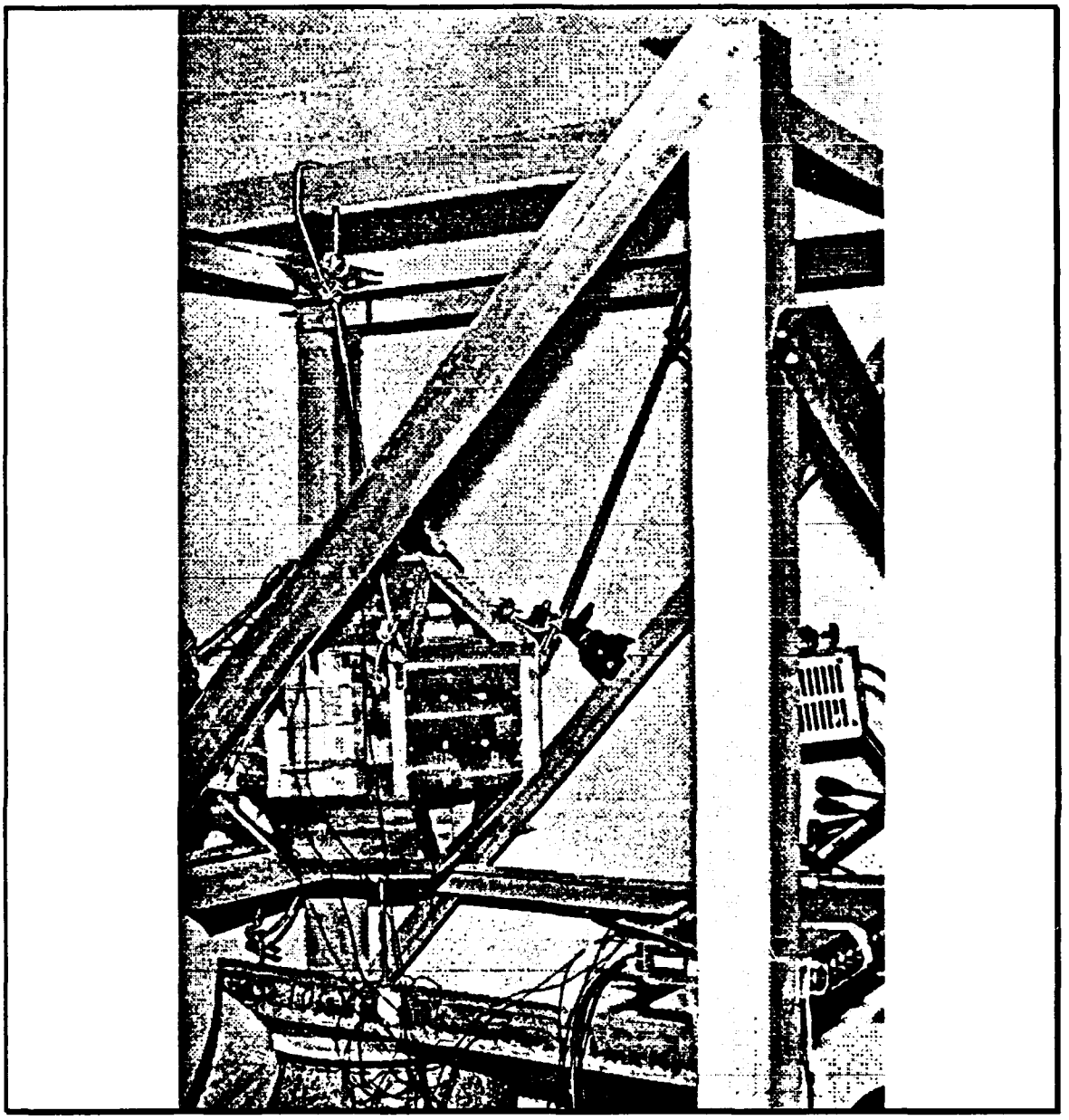

Figure 17. PANSAT Test Configuration

3. Measurement Parameters

Excitation of the structure was done using burst random noise. The frequency range was set from 0 Hz to 800 Hz with 400 spectral lines of resolution. This resulted in a sampling frequency of 2048.0 Hz and a frame length of 0.5 sec. A Hanning Broadband window was applied on the data; and

averaging was used with 10 averages for each measurement. The frequency response function (FRF) and ordinary coherence were stored for each response node on the structure referenced to an accelerometer attached to the shaker head.

The data acquisition system is capable of simultaneously sampling 8 input channels at one time. The computer generated test model, having 236 nodes plus the reference point at the shaker head, required a number of measurement runs to obtain FRFs at all the degrees of freedom on the model. This was done by measuring and recording the data at 7 nodes and then moving the accelerometers to new locations. This was possible because frequency response and ordinary coherence functions are frequency dependent and not time dependent. A typical FRF measurement is shown in Fig. 18.

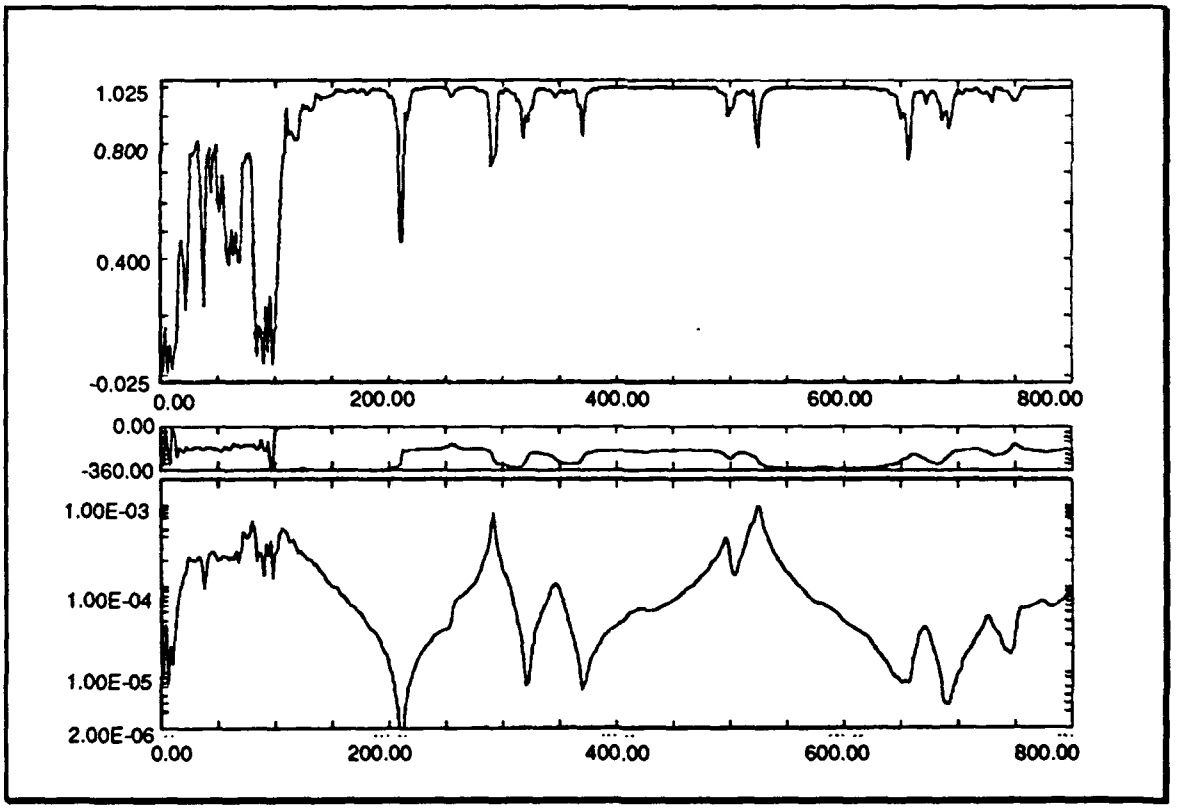

Figure 18. FRF and Coherence Measurement

C. EXPERIMENTAL MODAL ANALYSIS

A number of methods are available for modal analysis on a frequency response function (FRF). The methods can generally be separated into two categories: single degree of freedom (SDOF) analysis and multiple degrees of freedom (MDOF) analysis. This study considers the SDOF analysis case where it is assumed that the contribution of the response near a resonance is predominantly that of the closest mode.

1. SDOF Analysis Background

The simplest SDOF analysis is to search for the peaks of a FRF to identify the resonances of a structure. The peak is assumed to be at the natural frequency and the damping can be found using the half-power method. The modal properties are then derived from the amplitude, natural frequency, and damping resulting in an analytical representation of the mode. This type of analysis, however, does not work well for cases where modes are close to each other, or when the structure is not proportionally damped. Additionally, the natural frequency is wholly dependent on the single point of the peak amplitude in question.

A second approach, more detailed type of SDOF analysis, is the circle-fit method. The circle-fit method is derived from the fact that for a SDOF system a Nyquist plot of a FRF will result in a circle in the Argand plane. The following summarizes the circle-fit analysis method [Ref. 6, pp. 158-165]. The SDOF assumption is applied to a more general FRF for a small frequency range about a natural frequency of mode r. The main assumption is that the dominant term of the FRF series expansion is the one associated with mode r.

That is, for receptance $\alpha_{jk}(\omega)$ (displacement as the response parameter),

$$\alpha_{jk}(\omega) = \frac{x}{f} = \sum_{s=1}^{N} \frac{{}_sA_{jk}}{\omega_s^2 - \omega^2 + i\eta_s\omega_s^2}, \tag{5.1}$$

where ${}_sA_{jk}$ is the modal constant, a complex coefficient for mode s linking coordinates j and k;

ω_s is the natural frequency of mode s; and

η_s is the damping loss factor for mode s.

Equation 5.1 can be rewritten as the following, by isolating mode r.

$$\alpha_{jk}(\omega) = \frac{{}_rA_{jk}}{\omega_r^2 - \omega^2 + i\eta_r\omega_r^2} + \sum_{\substack{s=1 \\ \neq r}}^{N} \frac{{}_sA_{jk}}{\omega_s^2 - \omega^2 + i\eta_s\omega_s^2} \tag{5.2}$$

The SDOF assumption for the mode r will make the second term approximately independent of frequency ω. The expression can then be written as,

$$\alpha_{jk}(\omega)_{\omega=\omega_r} \approx \frac{{}_rA_{jk}}{\omega_r^2 - \omega^2 + i\eta_r\omega_r^2} + {}_rB_{jk} \tag{5.3}$$

noting that the plot of both terms yields a circle in the Argand plane. Note that for this r^{th} mode, the origin is offset by an amount determined by the contribution of all other modes. The contribution of the second term in Eq. 5.3 is nearly constant for the frequency range of interest. It is apparent that the modal constant acts to size the circle by its magnitude and to rotate the circle by an angle $\angle {}_rA_{jk}$. The equation of interest for receptance then becomes

$$\alpha_{jk}(\omega) = \frac{1}{\omega_r^2\left[1 - (\omega/\omega_r)^2 + i\eta_r\right]} \tag{5.4}$$

which after multiplying the numerator and denominator by the complex conjugate $[1-(\omega/\omega_r)^2 - i\eta_r]$, yields a formula for a circle,

$$\alpha_{jk}(\omega) = \frac{1-\left(\omega/\omega_r\right)^2 - i\eta_r}{\omega_r^2\left[\left\{1-\left(\omega/\omega_r\right)^2\right\}^2 + \eta_r^2\right]}$$

2. Properties of a Modal Circle

The properties of a modal circle can be exemplified through Eq. 5.4 and Fig. 19 to obtain modal parameters. The discussion begins with the following relationships. [Ref. 6, pp. 162-164]

$$\tan(\gamma) = \frac{\eta_r}{1-(\omega/\omega_r)^2}$$

$$\tan(90°-\gamma) = \tan(\theta/2) = \frac{1-(\omega/\omega_r)^2}{\eta_r} \qquad (5.6)$$

Rearranging Eq. 5.6 yields,

$$\omega^2 = \omega_r^2(1-\eta_r \tan(\theta/2)) \qquad (5.7)$$

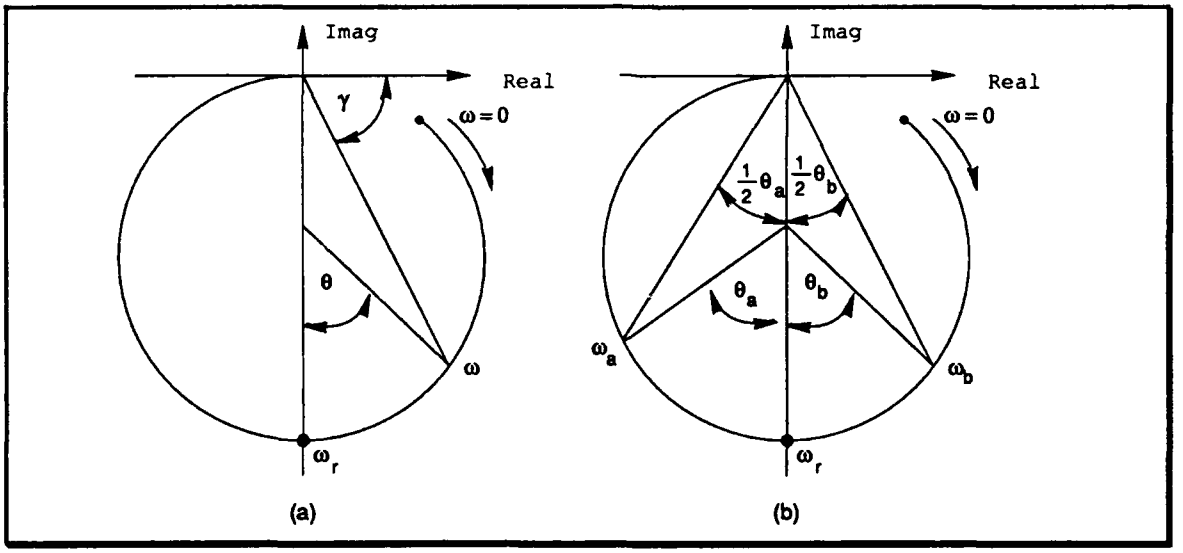

Figure 19. Modal Circle Properties

Differentiating Eq. 5.7 with respect to θ yields the following.

$$\frac{d\omega^2}{d\theta} = \frac{-\omega_r^2\eta_r}{2}\left[1+\frac{\left\{1-(\omega/\omega_r)^2\right\}^2}{\eta_r^2}\right] \qquad (5.8)$$

The reciprocal of Eq. 5.8 displays the sweep rate of the points which make up the circle. This sweep rate is shown to reach a maximum value when $\omega = \omega_r$. That is, the derivative of Eq. 5.8, when taken with respect to frequency $(d/d\omega)$, equals 0 when $(\omega_r^2 - \omega^2) = 0$. It is also important to note that the reciprocal of Eq. 5.8 when $\omega = \omega_r$ provides an estimate for damping.

$$\left.\frac{d\theta}{d\omega^2}\right|_{\omega=\omega_r} = -2/(\omega_r^2\eta_r)$$

Damping can also be derived from two specific points on the circle, a point above and a point below the natural frequency. Referring again to Fig. 18(b) and Eq. 5.6, the damping of the mode can be found by the expression,

$$\eta_r = \frac{\omega_a^2 - \omega_b^2}{\omega_r^2[\tan(\theta_a/2) + \tan(\theta_b/2)]} \qquad (5.9)$$

which is an exact expression that applies to all levels of damping.

The diameter of the circle is the final property of the modal circle which is indicated by the term $1/\omega_r^2\eta_r$. The actual diameter of the modal circle is found by combining the $1/\omega_r^2\eta_r$ term with the magnitude of the modal constant.

$${}_rD_{jk} = \frac{|{}_rA_{jk}|}{\omega_r^2\eta_r} \qquad (5.10)$$

The value of $\angle {}_rA_{jk}$ denotes the angle of rotation of the principal diameter, which passes through the natural frequency point (ω_r), from the negative imaginary axis.

3. Experiment Results

The large number of measurements at the various degrees of freedom provides a choice of FRFs from which to derive modal parameters. There is no guarantee that a single measurement will provide a good representation of all the modes of a test structure. This may be because the measurement was taken at or

near a nodal point of resonance (not to be confused with a finite element node or test model degree of freedom node).

The procedure for analyzing modal test data using the SDOF circle-fit method is summarized as follows: [Ref. 6, p.165]

- Select a frequency range (the points to construct the circle)
- Construct a circle and calculate the quality of fit
- Locate the natural frequency and obtain a damping estimate
- Determine the modal constant

The modal parameters obtained from the circle-fit analysis can then be used to construct an analytical SDOF FRF. The analytical FRF can be displayed on top of the original test data. The mode shape of the structure is then derived utilizing all the FRFs of the test data at the natural frequency of the mode. Figures 20, 21, and 22 show the modal circle constructed for the first mode, the analytical FRF generated, and the mode shape of the test model, respectively.

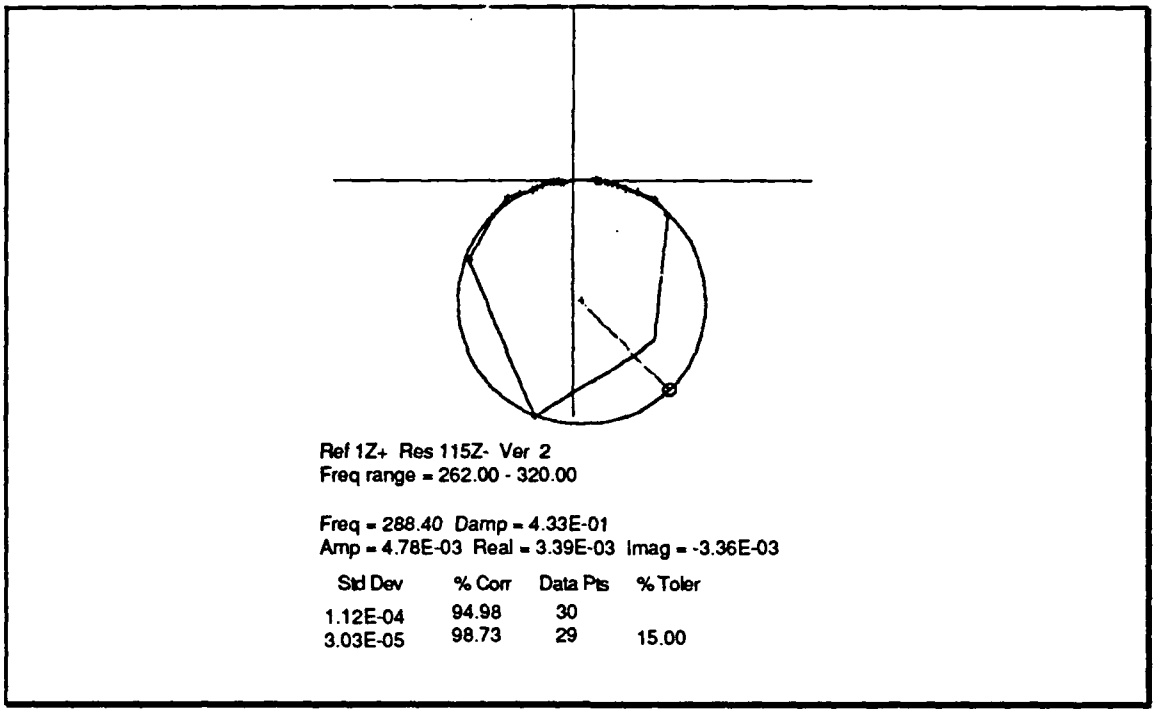

Figure 20. Circle Fit of Test Data for First Mode

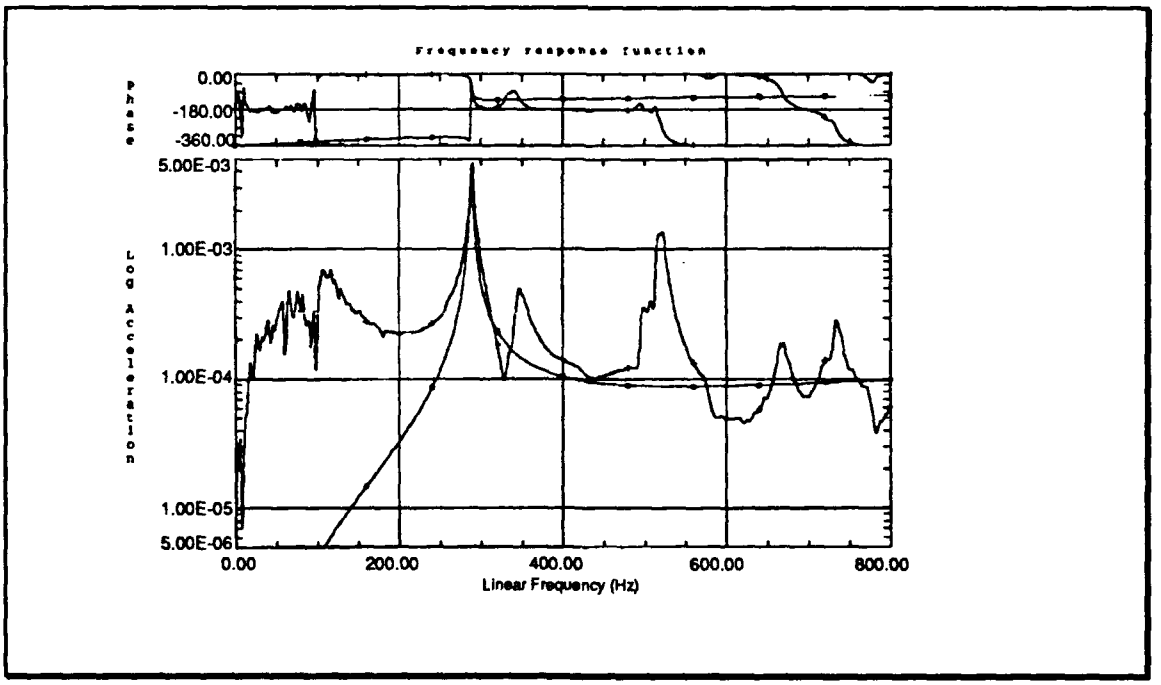

Figure 21. Analytical FRF of First Mode Superimposed on Test Data

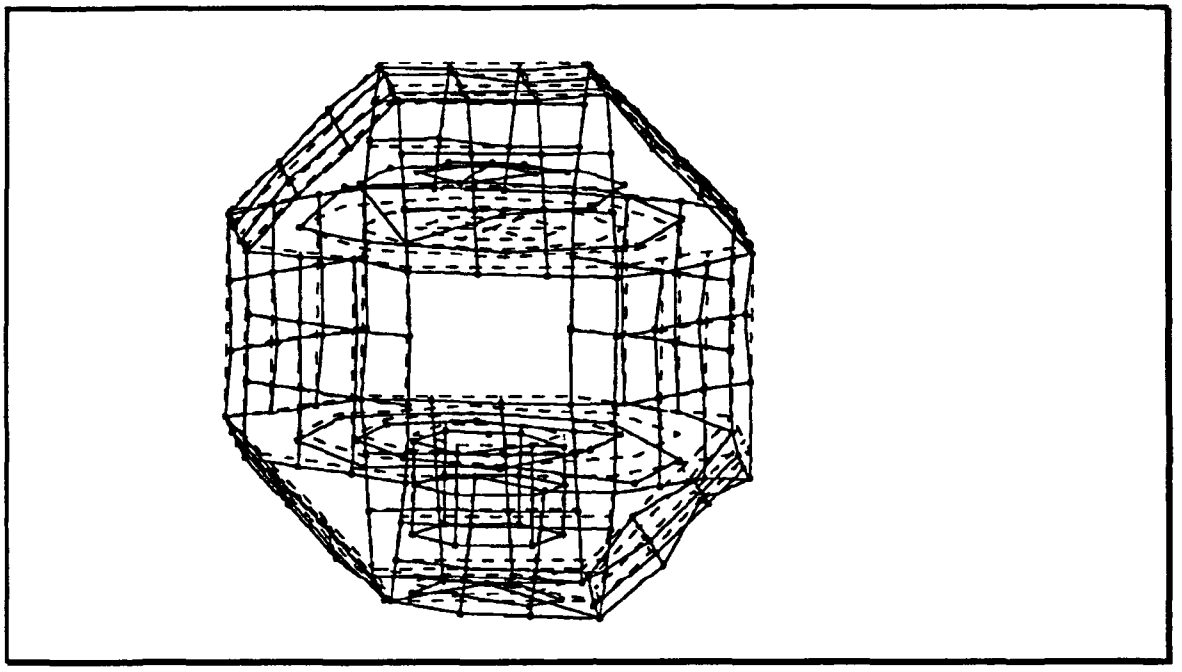

Figure 22. Mode Shape from Test Data of First Mode

The mode shape depicted by this first mode shows a local mode of the structure which is the fundamental bending mode of a plate. Agreement should be expected between the fundamental mode of the test analysis and the fundamental mode of the finite element analysis. The degree of correlation between test and FEA generally decreases with the higher modes. The fundamental mode shape agrees with that of the finite element model. However, the frequency of the fundamental mode of the test model varies with the finite element model by approximately 25%. This indicates a problem with either the accuracy of the finite element model or the quality of the test data taken. Inspection of FRFs taken at other points on the structure dispute the latter possibility. Another possibility for poor correlation may lie in the fabrication of the test structure. This is discussed later. A second iteration in finite element modeling was performed to study the possibility of the FEA model as the source of error.

The SDOF circle-fit analysis method was again utilized for the next four modes apparent in the FRFs. The plots of the constructed modal circles, generated FRFs, and mode shapes are given in Appendix C. The experimental modal analysis results are summarized in Table 4. The frequency range used in the circle-fit analysis is given along with the natural frequency of the mode and the damping.

Table 4 shows the presence of a mode at 345.4 Hz which was hidden from FEA. The Nyquist plot shows this to be a valid mode although the FRF peak is much lower than those which correlate to modes presented in FEA results. It is difficult to determine exactly why the test results show modes which are hidden from FEA; however, with complex structures it is impossible to precisely model boundary conditions imposed by the joining of actual structural pieces with fasteners and other anomalies resulting from fabrication and integration. The focus here, however, lies mainly on correlation of the fundamental mode derived from test data analysis with that from FEA. Acceptable correlation is required for validation of the FEA model, ensuring the structure can withstand the loads imposed by launch and maintain structural integrity.

TABLE 4. MODAL TEST SUMMARY

Mode	Frequency Range (Hz)	Frequency (Hz)	Damping
1	262.0 - 320.0	288.4	4.33E-01
2	326.0 - 364.0	345.4	1.52E+00
3	470.0 - 496.0	495.8	1.28E+00
4	510.0 - 578.0	522.6	6.83E-01
5	648.0 - 688.0	671.4	8.25E-01

VI. FEA MODELING REVISITED

The PANSAT structure was again modeled for finite element analysis (FEA). The finite element modeling capabilities of the SDRC IDEAS software were invoked for this iteration following the experimental modal analysis which used IDEAS test and measurement tools. Processing speed and accessibility afforded by the computer workstation were other reasons for this selection. Both the GIFTS finite element model and the SDRC IDEAS finite element model used exclusively plate and beam elements; however, more care was taken in defining various beam cross-sections to construct the geometry in the latter. The GIFTS model used only rectangular cross-sections for all beam elements because the initial model was concerned mainly with the structure's ability to withstand acceleration loads. The PANSAT spacecraft structure, however, incorporates a number of irregular geometric shapes. Modeling using *IDEAS* was performed with greater attention to the actual geometry of the fabricated test structure.

The GIFTS model was used to optimize the number of elements for the IDEAS model. The GIFTS model consisted of 1216 nodes, whereas the IDEAS model was reduced to 361. The number of elements on the exterior panel members of the spacecraft was reduced resulting in many fewer nodes. The equipment plates yield the largest deflections, as indicated by the GIFTS model, and therefore, remained well discretized. The SDRC IDEAS model allowed reduced processing time with little loss in fidelity. Figure 23 shows the SDRC IDEAS finite element model. The image on the right shows the model with two panels blanked in order to show the interior and support cylinder.

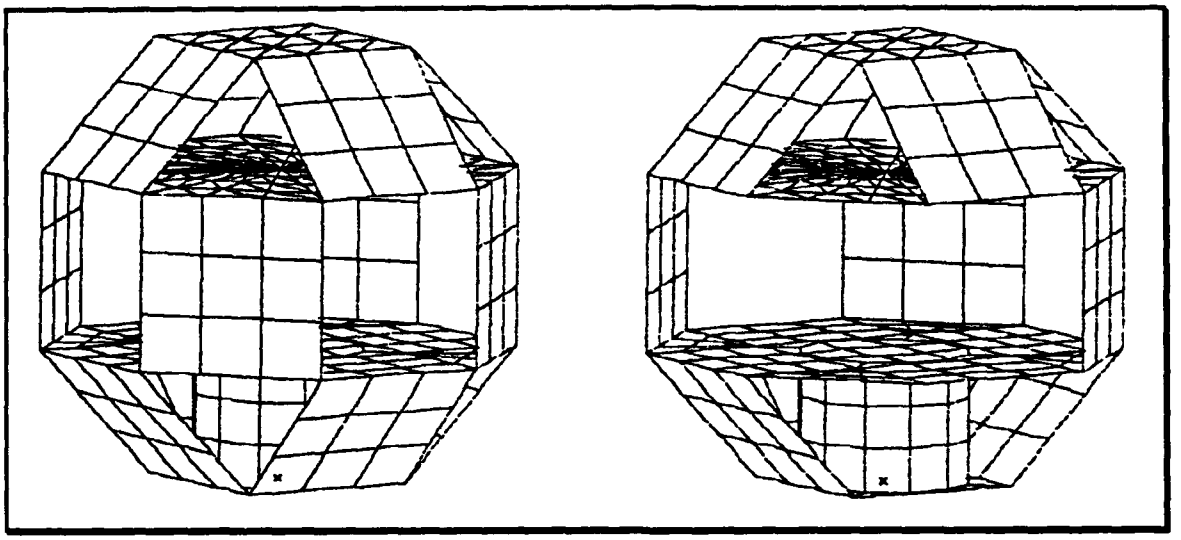

Figure 23. PANSAT Second FEA Model

The IDEAS finite element application is similar to the GIFTS software in that the process involves the utilization of modules to perform certain tasks in the progress of the analysis. Processor modules are defined as 'Tasks' in the IDEAS nomenclature. The process flow for the IDEAS FEA software is shown in Fig. 24. The finite element modeling tools are provided in the following tasks. [Ref. 7]

- **Geometry Modeling**: creates the geometry of the structure (points, lines, surfaces) without any material properties
- **Beam Section Modeling**: creates the cross section of beam elements and derive/modify the properties
- **Mesh Creation**: creates nodes, elements; defines material properties and physical properties; defines and generate element meshes; and performs quality checks for coincident nodes and elements
- **Boundary Conditions**: defines case sets; creates DOF sets, restraint sets, and load sets
- **Model Solution**: defines type of analysis, case sets used, and solution parameters to create data analysis sets
- **Post-Processing**: chooses data analysis sets; displays deformed geometry, stress contours, and animation of mode shapes; manipulates data analysis sets to create combined loads

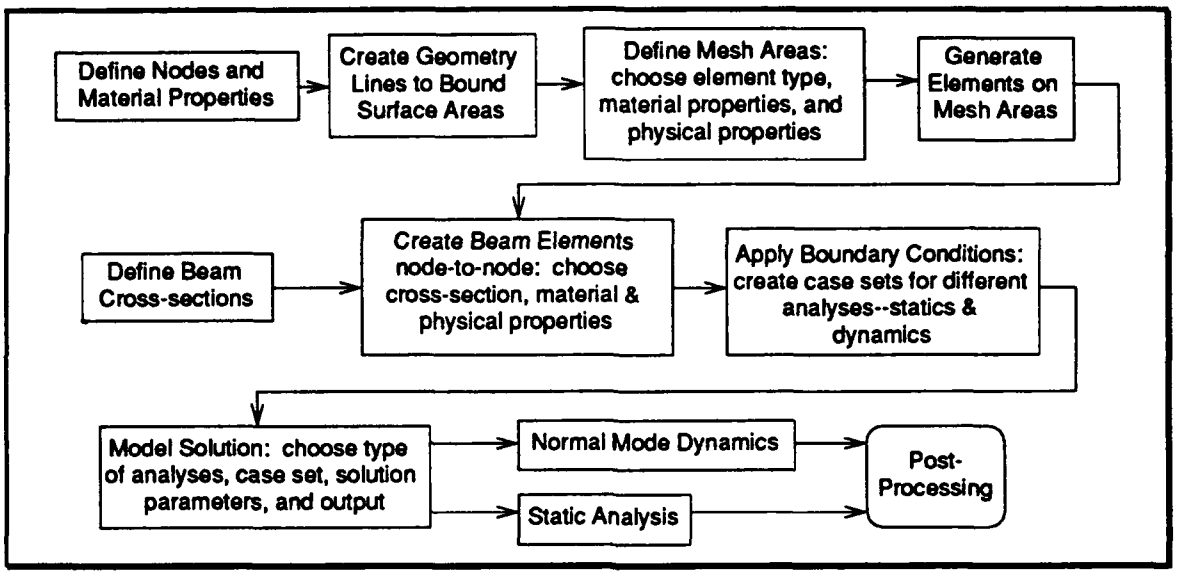

Figure 24. IDEAS FEA Process Flow

A. DYNAMIC ANALYSIS RESULTS

Normal mode dynamic analysis performed on the IDEAS FEA model resulted in much better correlation for the fundamental mode. The structure's FEA fundamental mode was again that of the upper equipment plate bending. The frequency was 270.32 Hz (6.27% variation from the test results). This correlation provides sufficient support for validation of the IDEAS FEA model. The frequencies resulting from this second FEA iteration are given in Table 5; including results when component mass was added. The additional mass was added at nodes as lumped mass elements (evenly distributed on the equipment plates). The upper equipment plate had 37.5 lbs, as before, and the lower equipment plate had 85.5 lbs; less than the GIFTS model because of an increase in the mass of the model itself.

A few of the frequencies shown in Table 5 are very close to each other due to symmetry in the structure. The mode shapes for the IDEAS FEA model are given in Appendix D for the structure alone and with the component mass added. These

mode shapes show general agreement with the results from the previous finite element analysis, but have higher frequencies. The beam cross-sections used in the second model provided additional stiffness to the structure as a whole, thus increasing the modal frequencies. The second mode derived by test data analysis (at 345.4 Hz) once more was not observed in FEA results. Again, this can be attributed to the inability to model exactly the boundary conditions of structural joints and other anomalies due to fabrication and integration.

TABLE 5. SDRC IDEAS FEA MODAL SUMMARY

Mode	Frequency, Hz (structure alone)	Frequency, Hz (mass added)
1	270.32	67.26
2	554.95	144.78
3	555.01	148.68
4	738.20	148.68
5	738.29	163.08
6	818.19	163.09

B. STATIC ANALYSIS

A static analysis was performed for the validated IDEAS FEA model. The same acceleration loads prescribed in Table 1 were applied. Analysis results again show favorable results for loading in all three axes and with combined loads. This would be expected since the higher stiffness implies smaller deflections which relate to lower stresses. A contour plot of the Von Mises stresses of the structure due to the combined load of 15 g's in the Z, 9 g's in the X, and 9 g's in Y is shown in Fig. 23. Again, 2 panels have been blanked to show the interior of the structure.

Table 6 shows the maximum and average values of Von Mises stress for the individual load cases and for the combined load case. The X and Y load cases are

identical because of symmetry, so another load case was studied. The XY load case impo.. .he 9 g's lateral acceleration in the vector direction [X=1, Y=1, Z=0]. Margins of safety (M.S.) are also given. The resulting maximum Von Mises stresses are much lower than the 36 ksi yield stress value for aluminum 6061-T6.

TABLE 6. MAXIMUM VON MISES STRESS VALUES

Load Case	Ele. #	Max. Von Mises Stress (psi)	Average Von Mises Stress (psi)	Smallest M. S.
X (9 g's)	155	2.911×10^3	5.17×10^2	11.37
Y (9 g's)	144	2.911×10^3	5.17×10^2	11.37
XY (9 g's)	145	3.005×10^3	4.99×10^2	10.98
Z (15 g's)	379	4.884×10^3	1.414×10^3	6.37
Combined	379	4.884×10^3	1.777×10^3	6.37

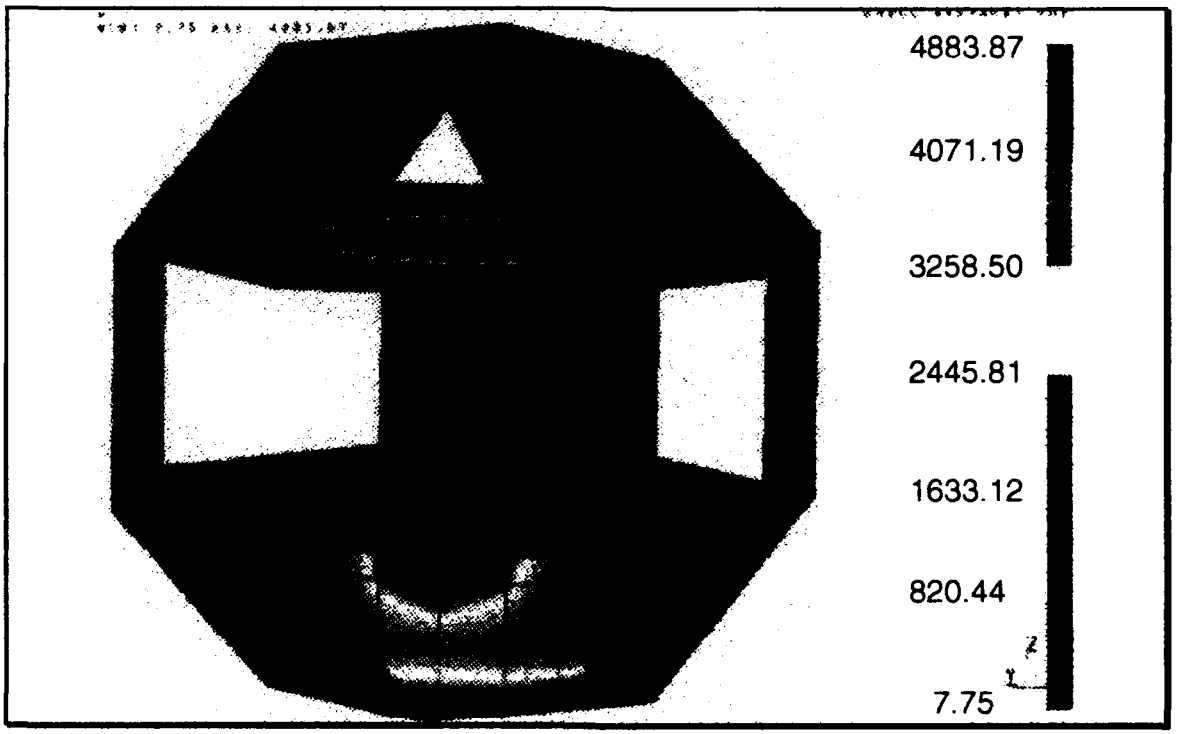

Figure 25. Von Mises Stress Contours for Combined Loads

VII. SOURCES OF ERROR

A number of possibilities exist which may explain the 6% deviation of the fundamental frequency between test data analysis and FEA. Certainly, computer-aided modeling of a real structure can only provide so much fidelity. The other obvious considerations are the experiment setup and the manufacturing of the test structure. The experiment setup includes boundary conditions, type of excitation, sampling parameters, and signal processing. Manufacturing includes adherence to design tolerances.

The free boundary condition was created by the use of shock cords which provide a reasonably good simulation. The structure was, however, attached to a 500 lb_f shaker by a threaded steel rod. This may induce mass loading as well as a loss in the free boundary condition. A plastic rod might be suggested. Different attachment points may also be explored. The random noise excitation may be substituted with sine-sweep excitation utilizing narrow-band windowing. A sine-sweep capability was not available.

Propagated manufacturing errors can result in parts that do not adequately fit, as was the case with the test structure. The 4 panels that support the lower equipment plate were misaligned with the through-holes provided for fasteners by approximately 1/8 in. This resulted in forcing the panels inward (toward the center of the structure) in order to fasten the lower equipment plate to the support panels. Additionally, the support cylinder did not agree with the design drawings by approximately 1/10 in., yielding a gap between the cylinder and the lower equipment plate which it was intended to support. This second discrepancy resulted in the addition of a shim to accommodate the gap.

The fundamental mode shape of the structure is a local bending mode of the upper equipment plate. This might imply that the anomalies introduced due to poor fabrication would not greatly affect the results. However, the structure as a whole becomes more stiff as a result of its pre-stressed state. The lower equipment plate is somewhat analogous to a drumhead which when more tension is applied, the pitch rises, i.e., its natural frequencies rise. How the pre-stressed state of the lower equipment plate affects the fundamental frequency of the structure as a whole is complex and needs careful modeling. Finite element normal mode dynamic analysis does not allow the introduction of forces or loads to the system. The disagreement between the finite element analysis results and the test data analysis results is likely a combined effect of fabrication anomalies, errors introduced by testing, and approximations involved in the finite element analysis methods.

VIII. CONCLUSIONS

This study shows the iterative process involved in engineering design. The structural design of the Petite Amateur Navy Satellite (PANSAT) was presented utilizing the payload requirements typical for a Shuttle Get Away Special (GAS) payload. The Shuttle GAS design requirements were used as a baseline having high margins of safety for a manned launch vehicle. Finite element analysis (FEA) showed the structure was capable of withstanding the launch loads. An engineering prototype was built for modal testing of the designed satellite structure. The test results and the FEA dynamic analysis results differed; the fundamental frequency deviating by as much as 25%. A second iteration in finite element modeling was performed yielding satisfactory results for agreement with the modal testing. Static analysis was then performed on the validated finite element model showing compatibility with the launch requirements of a Shuttle GAS payload. The performance of the structure under the loads prescribed show the structural integrity and its compatibility with other launch vehicles that may have more severe structural requirements.

APPENDIX A

The support cylinder for the structure is analyzed assuming a worst-case compression load of the spacecraft weight at 20 g's (150 lbf x 20 g's); and moment acting at 12 inches from the launch vehicle interface at 12 g's (150 lbf x 12 in. x 12 g's). Torsion is considered negligible. The support cylinder is made of aluminum 6061-T6 with outer diameter of 4.625 in. and 0.0625 in. thickness.

TABLE 7. CYLINDER ANALYSIS PARAMETERS

Young's Modulus, E	Compressive Load	Moment
9.9×10^6 psi	3000 lbf	21,600 in-lb
Thickness, t = 0.0625 in.		Radius, r = 2.312 in.

The analysis for the cylinder for the combined load of axial compression and bending is as follows. [Ref. 8]

The design allowable buckling stress for a circular cylinder under axial load is given by

$$\sigma_{cr} = C_c E \frac{t}{R}$$

where,

C_C = buckling stress coefficient
t = thickness
R = radius.

C_C is given as 0.25 from empirical results for clamped edges in the long-cylinder domain (Z > 80), with

$$Z = \frac{L^2}{R t}\sqrt{1 - \mu^2}$$

where, L is the length, and μ is the Poisson ratio (0.3).

The design allowable buckling stress for a circular cylinder under a bending load is given by

$$\sigma_{cr} = C_b E \frac{t}{R}$$

where, C_b is the buckling-stress coefficient for bending on clamped-edge cylinders with $Z > 80$. C_c is 0.35 for this case.

The stress ratio for axial compression is

$$R_c = \frac{P}{\sigma_{cr}} = 0.045$$

and for bending

$$R_b = \frac{M}{\sigma_{cr}} = 0.231$$

The margin of safety for the combined load is given as $\frac{1}{R_c + R_b} - 1 = 2.63$, or 263% [Ref. 9, p.215].

APPENDIX B

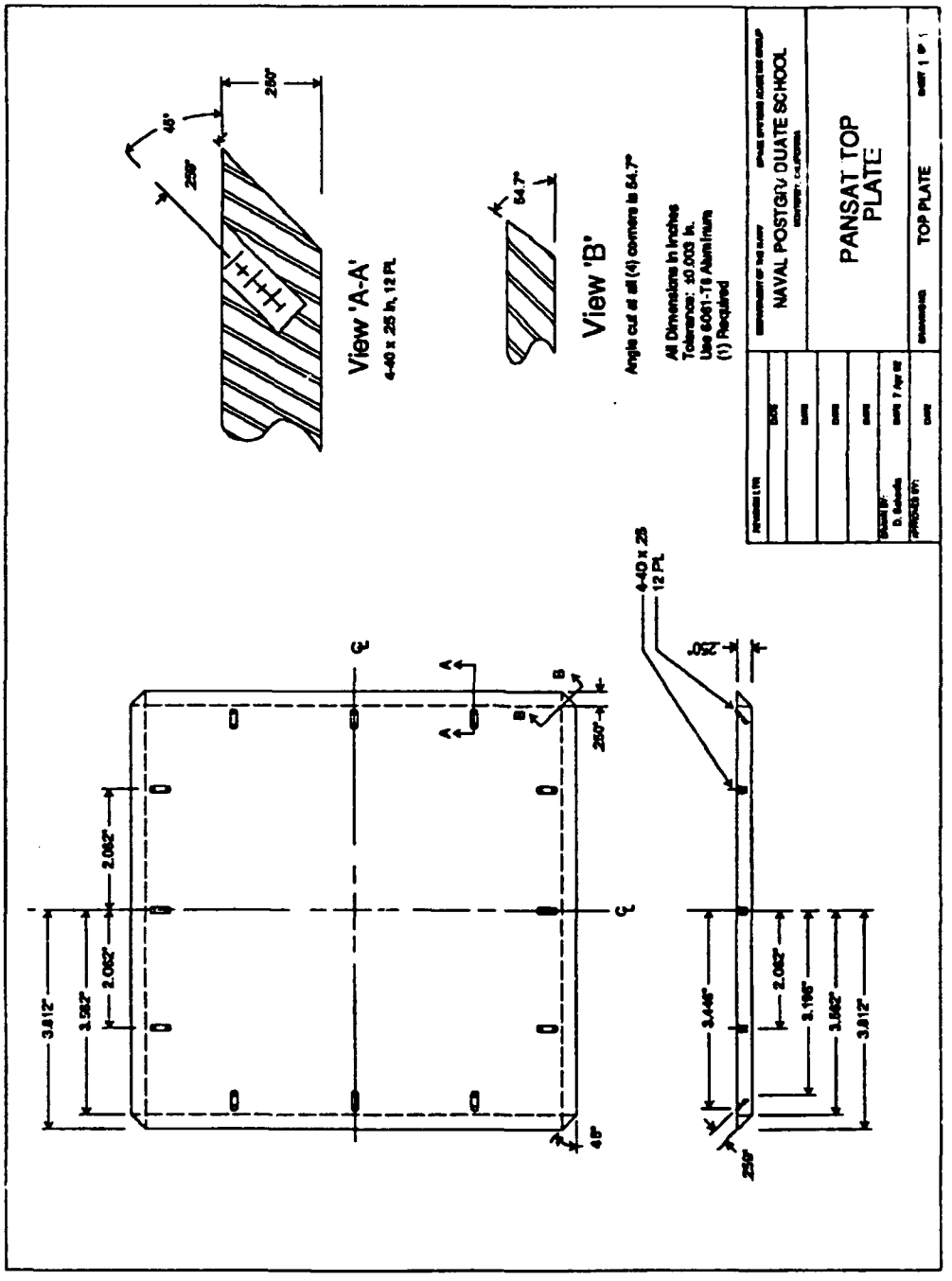

Figure 26. Top Plate

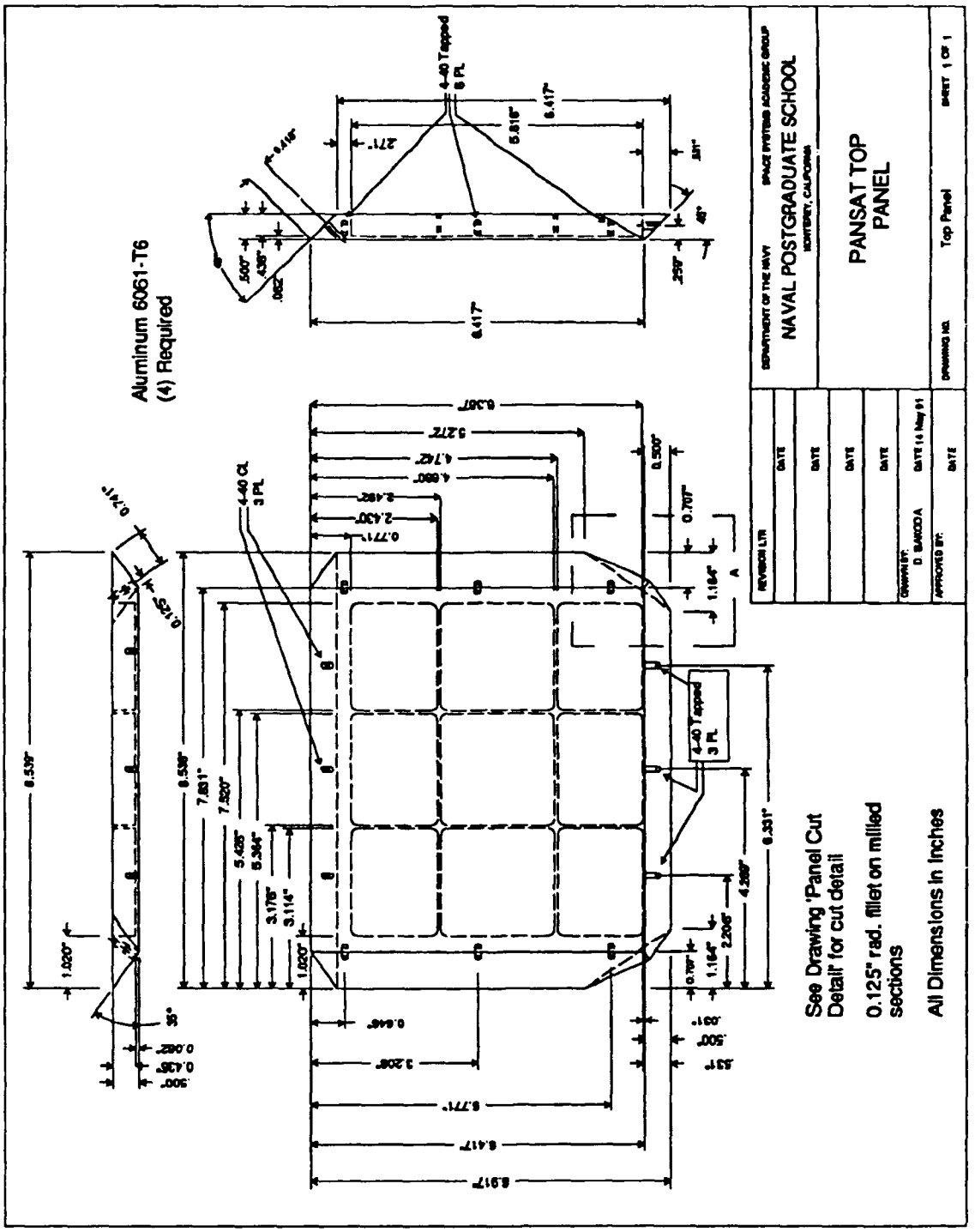

Figure 27. Upper-Deck Support Panel

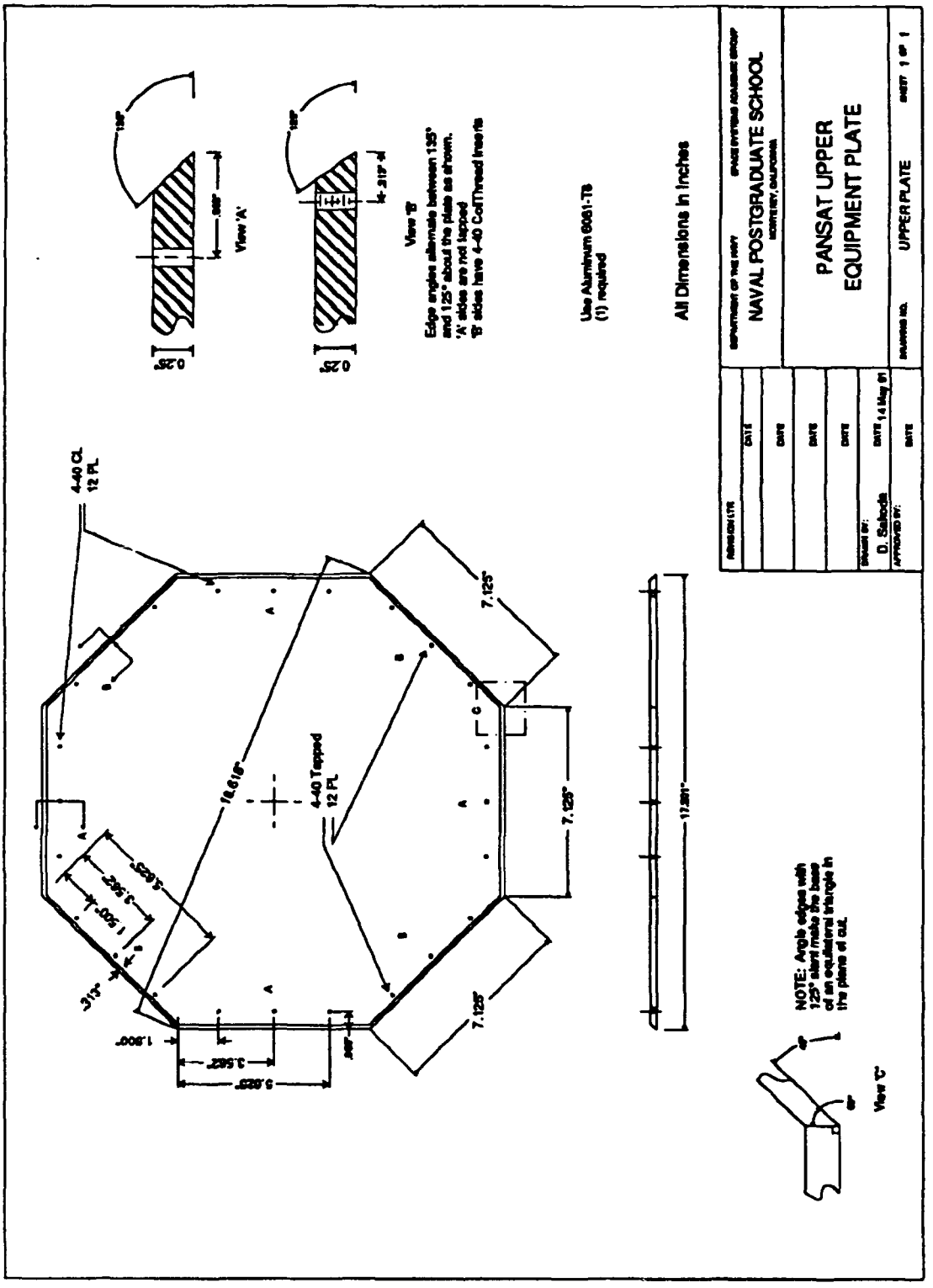

Figure 28. Upper Equipment Plate

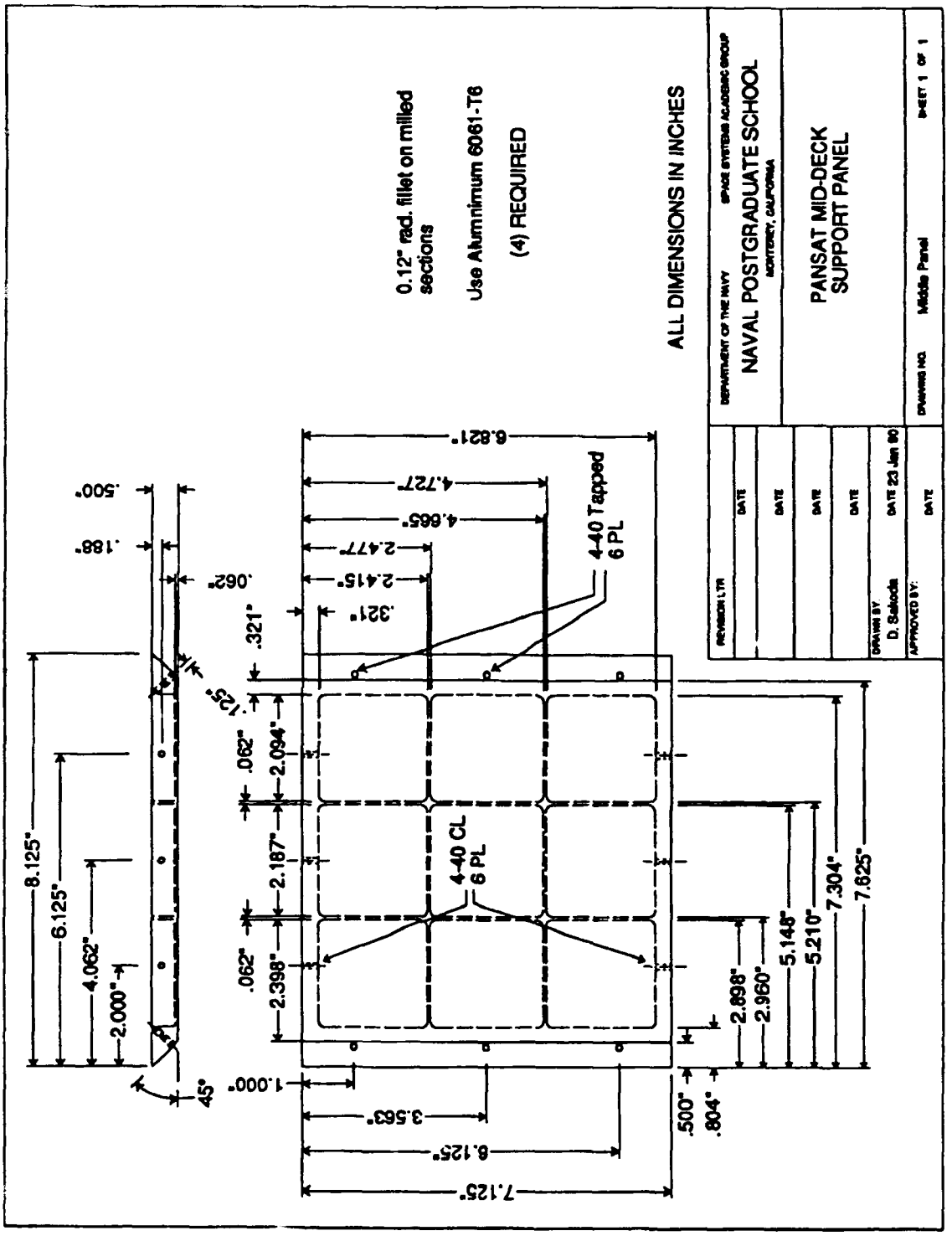

Figure 29. Mid-Deck Support Panel

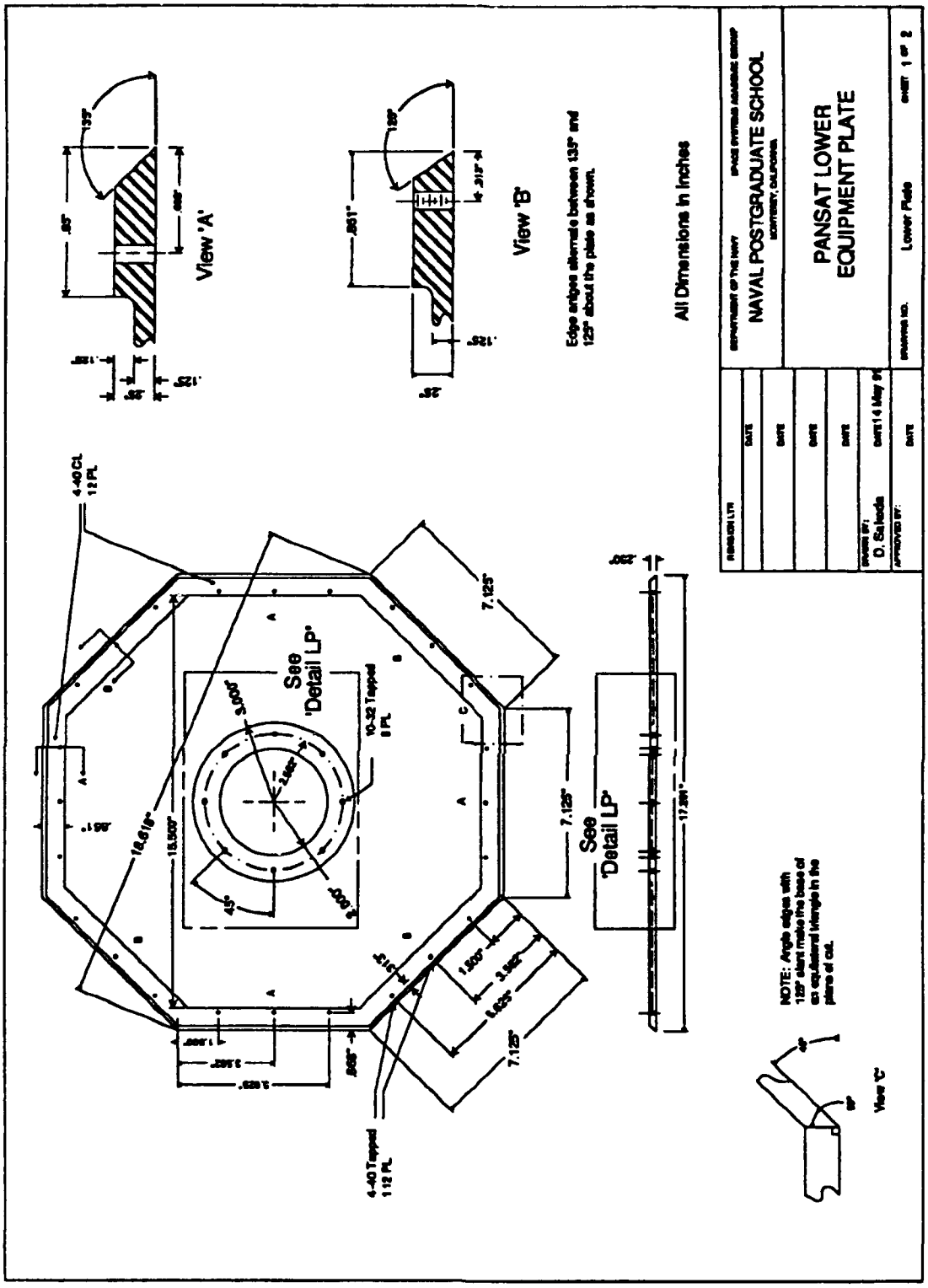

Figure 30. Lower Equipment Plate

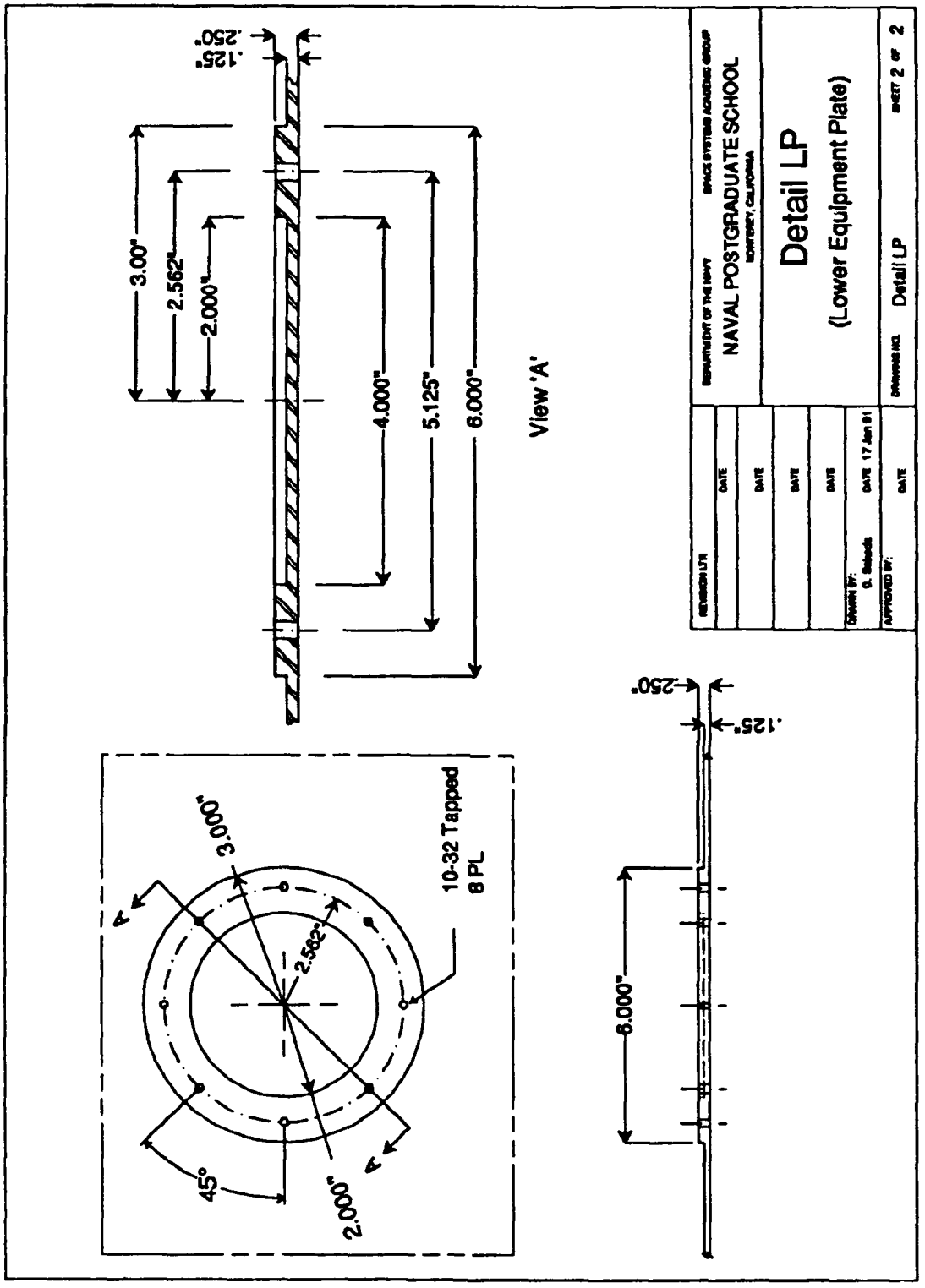

Figure 31. Detail of Upper Equipment Plate

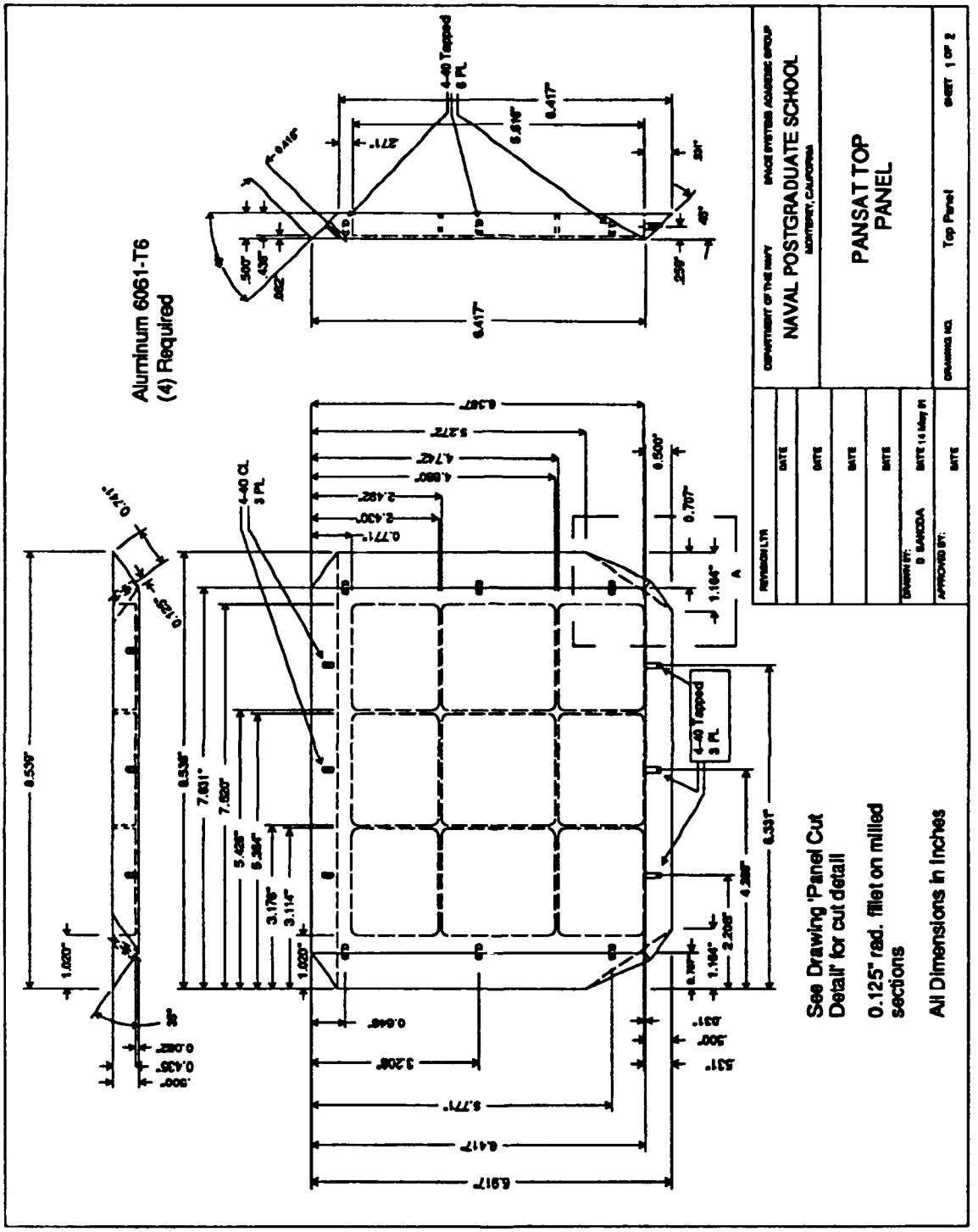

Figure 32. Lower-Deck Panel Support

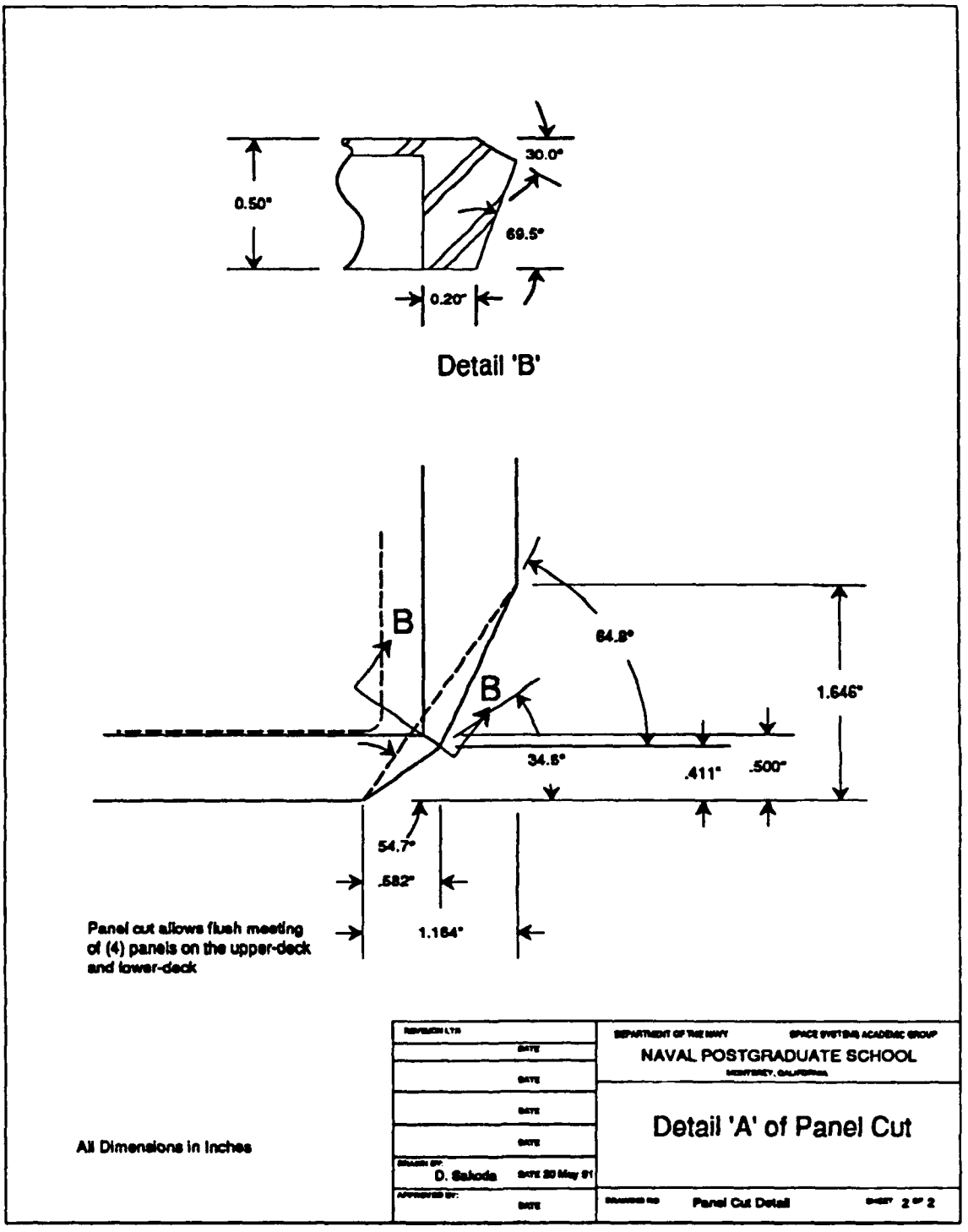

Figure 33. Detail of Upper and Lower Deck Panel Cut

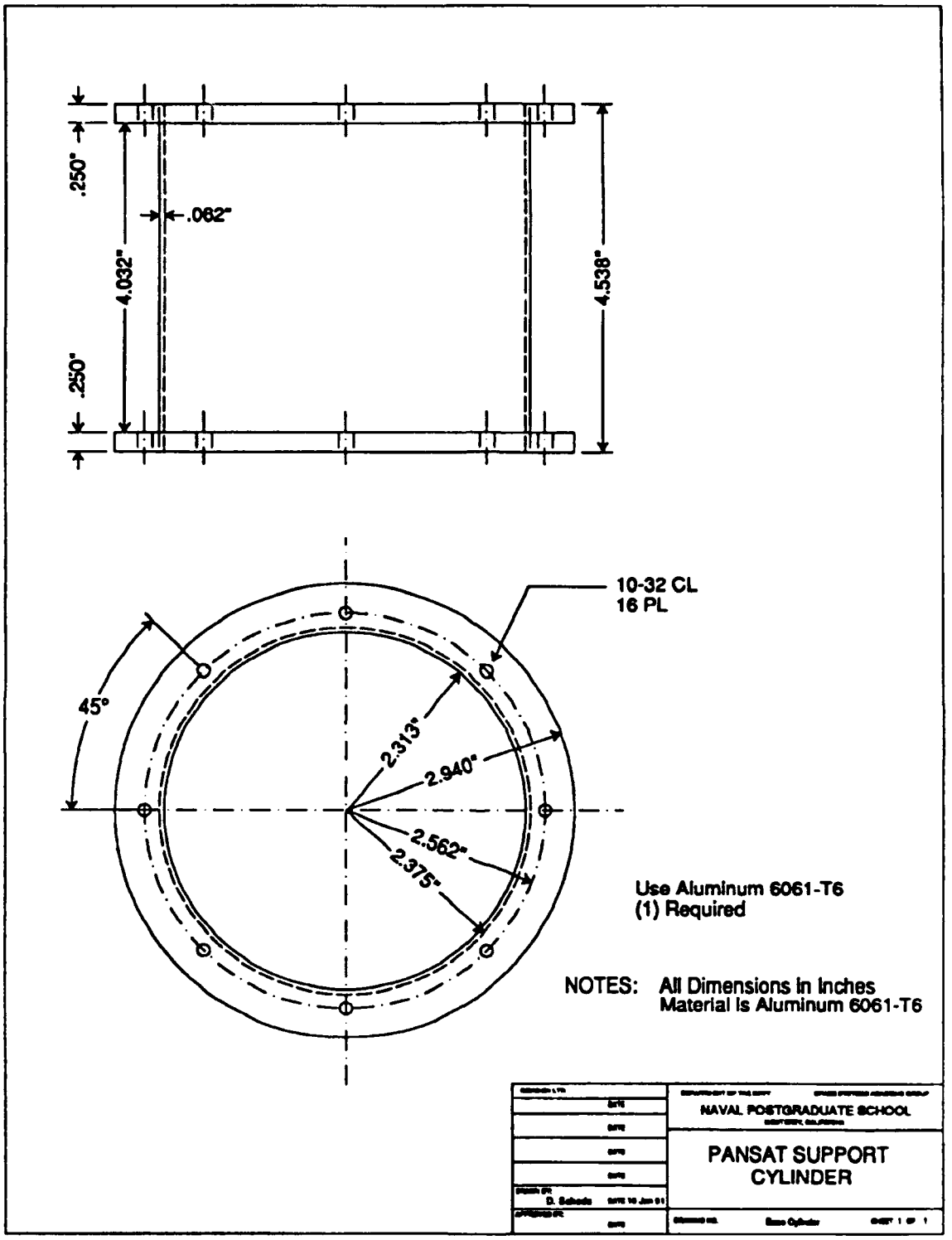

Figure 34. Base Cylindrical Support

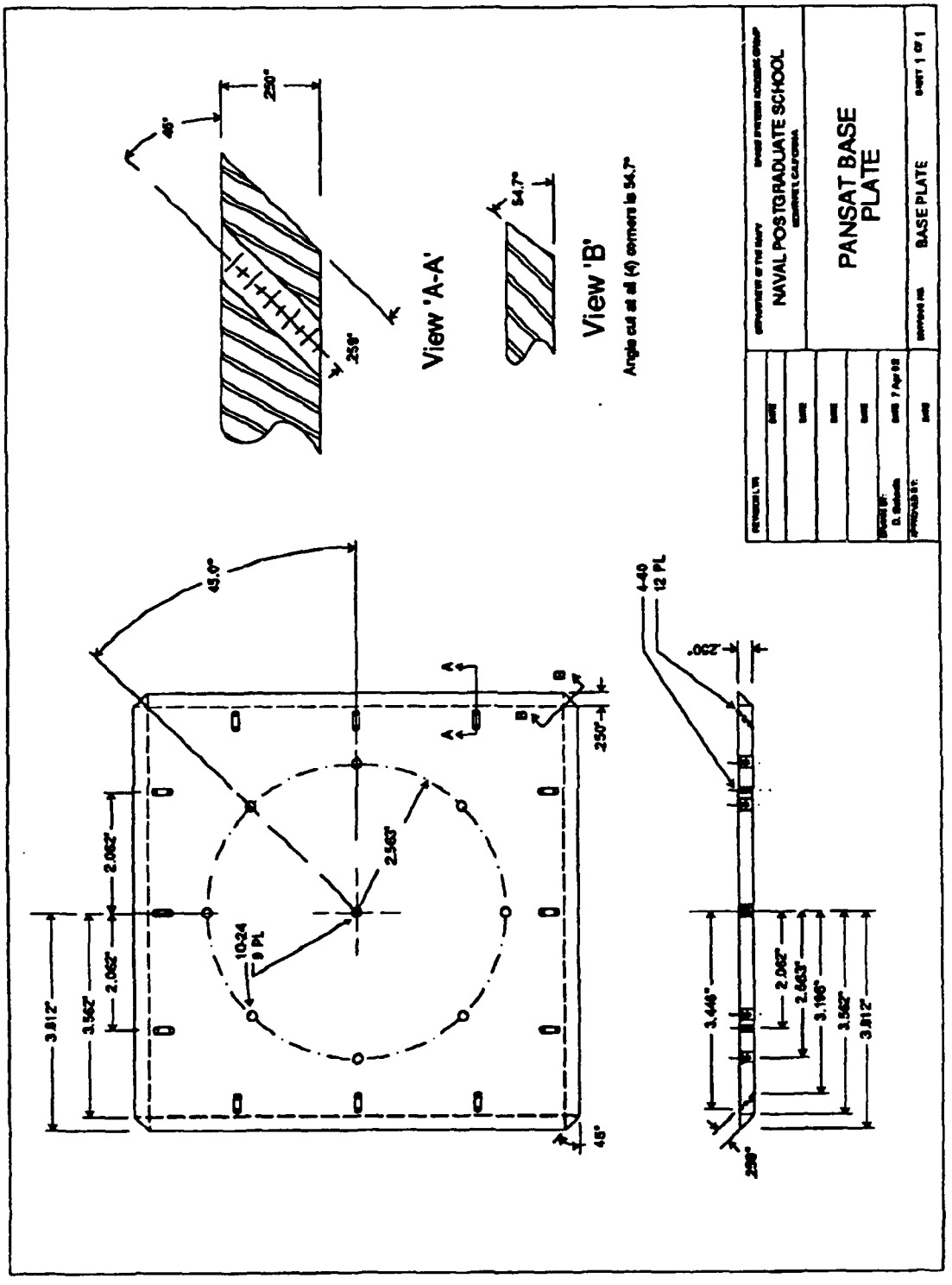

Figure 35. Bottom Plate

APPENDIX C

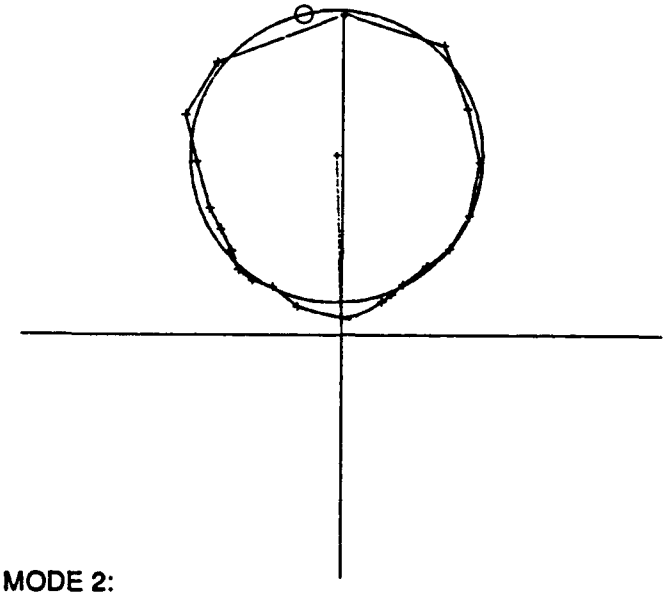

MODE 2:

Ref 1Z+ Res 51Z- Ver 2
Freq range = 326.00 - 364.00

Freq = 345.40 Damp = 1.52E+00
Amp = 1.01E-04 Real = -3.39E-06 Imag = 1.01E-04

Std Dev	% Corr	Data Pts	% Toler
2.00E-06	96.04	20	
2.00E-06	96.04	20	15.00

Figure 36. Mode 2, Test Data Nyquist Plot

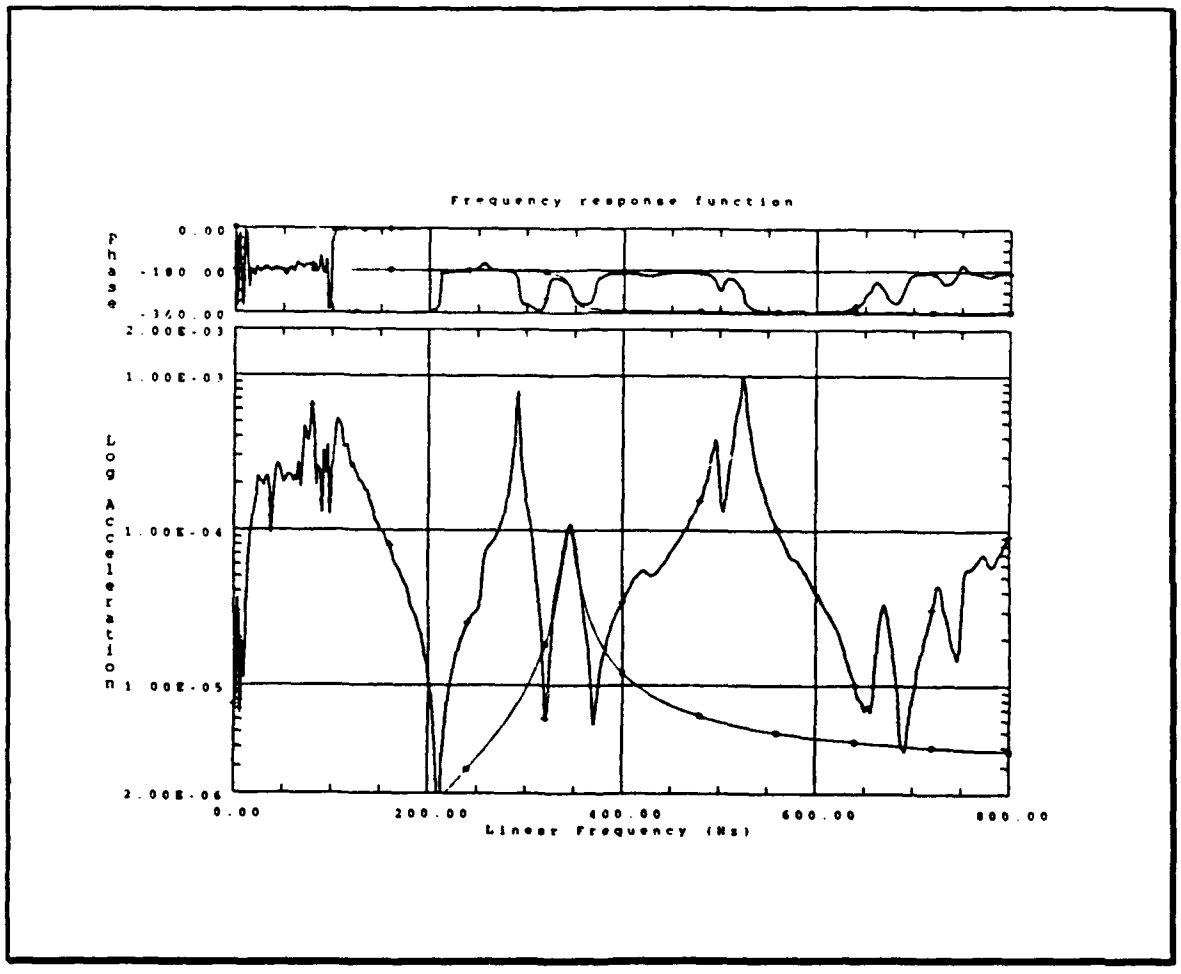

Figure 37. Mode 2, FRF Curve-Fit

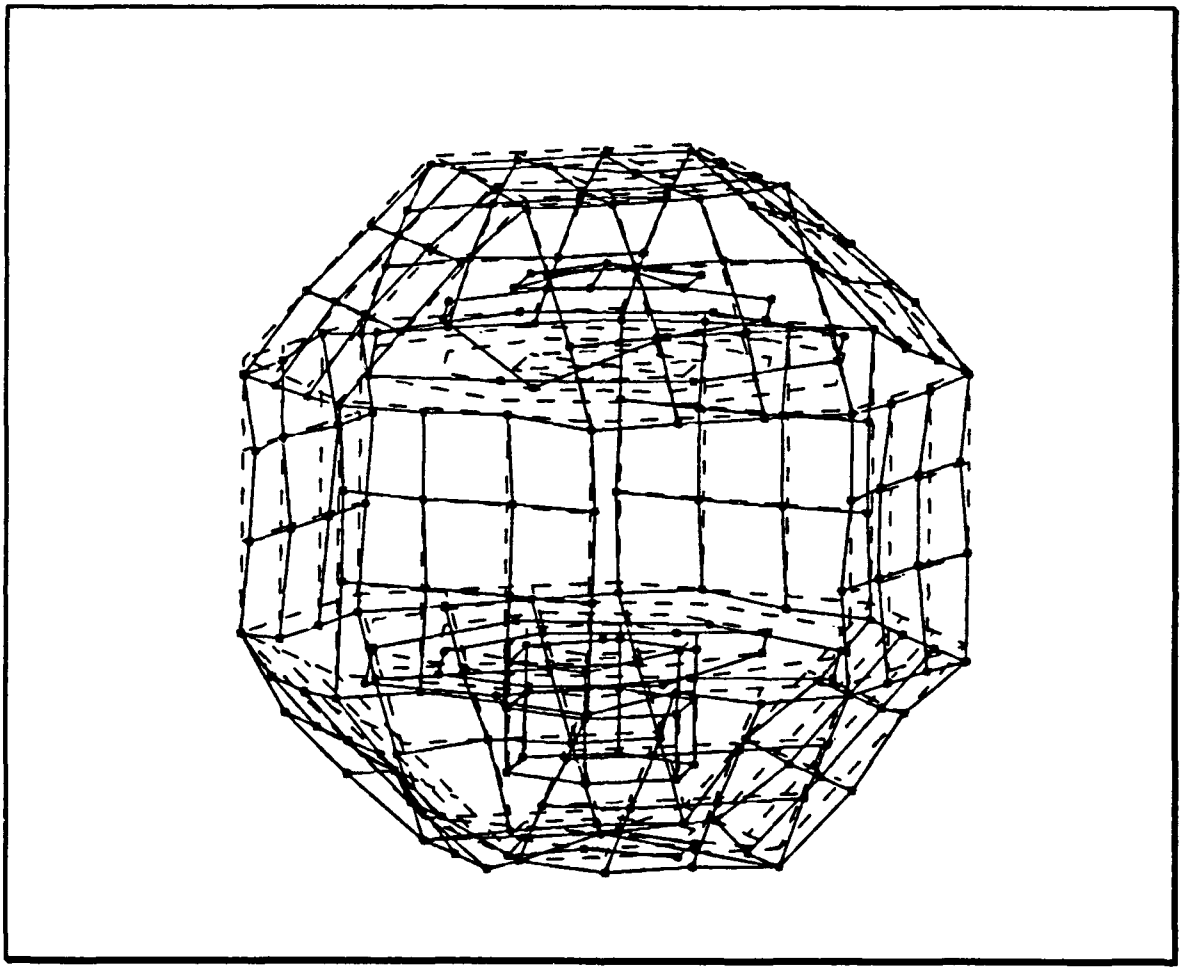

Figure 38. Mode 2, Deformed Geometry

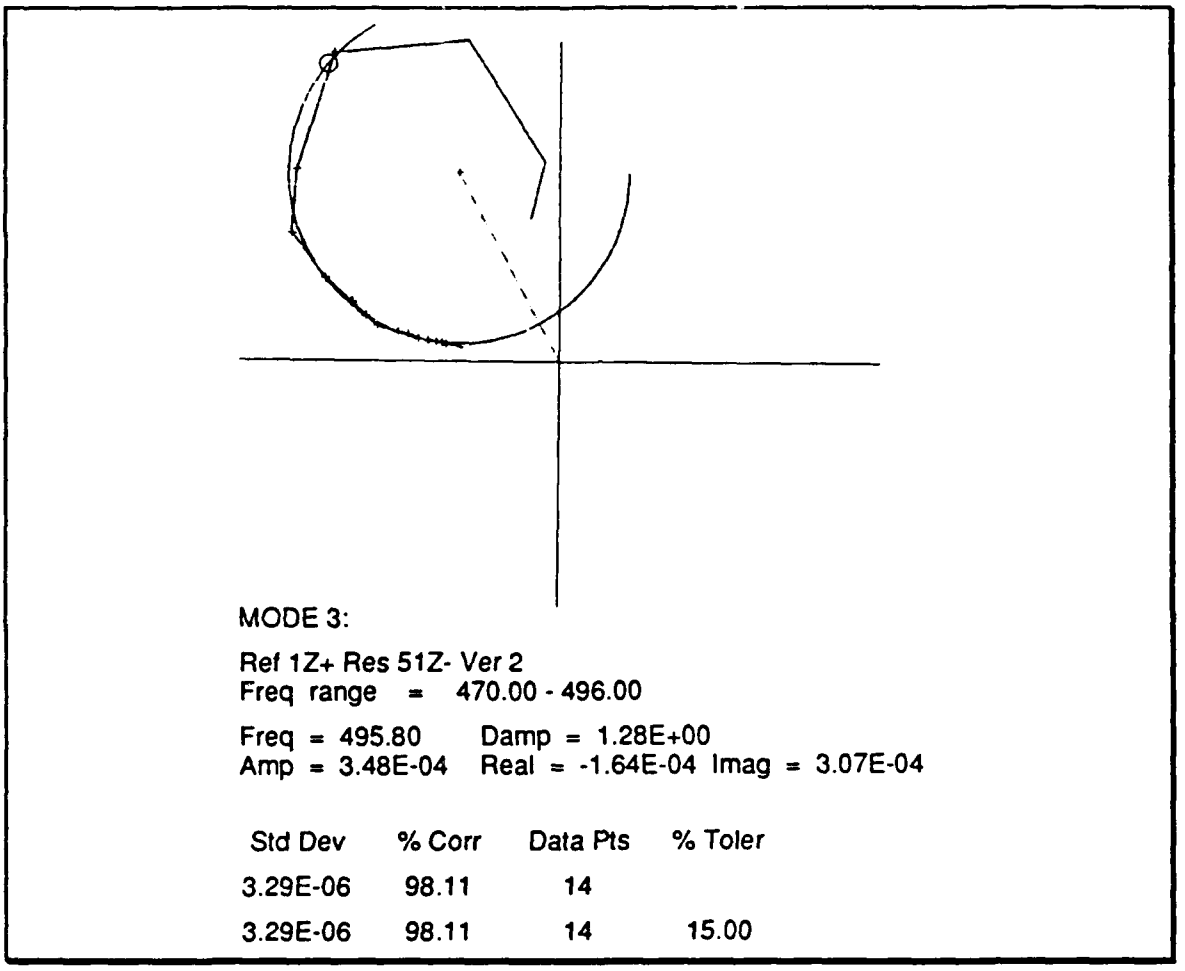

Figure 39. Mode 3, Test Data Nyquist Plot

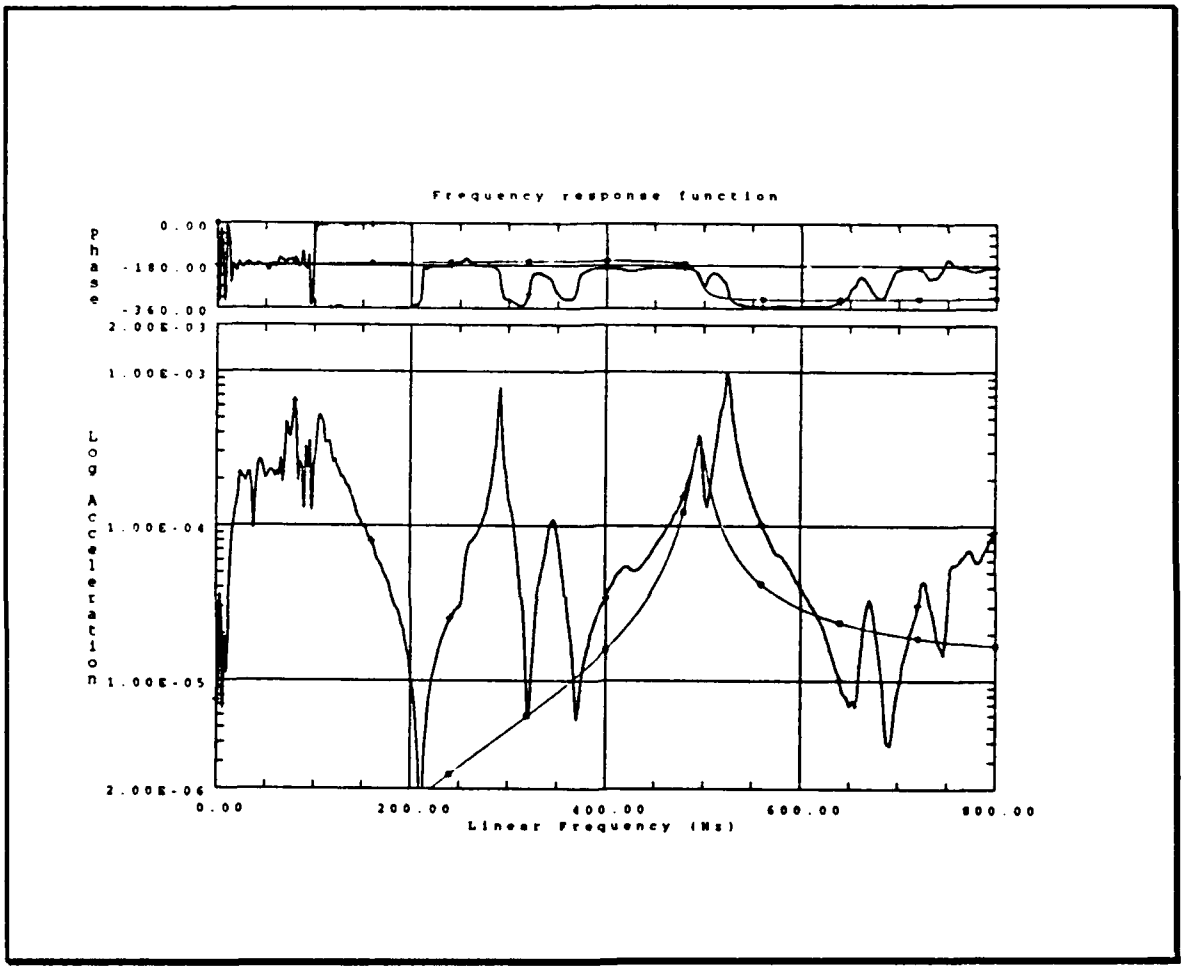

Figure 40. Mode 3, FRF Curve-Fit

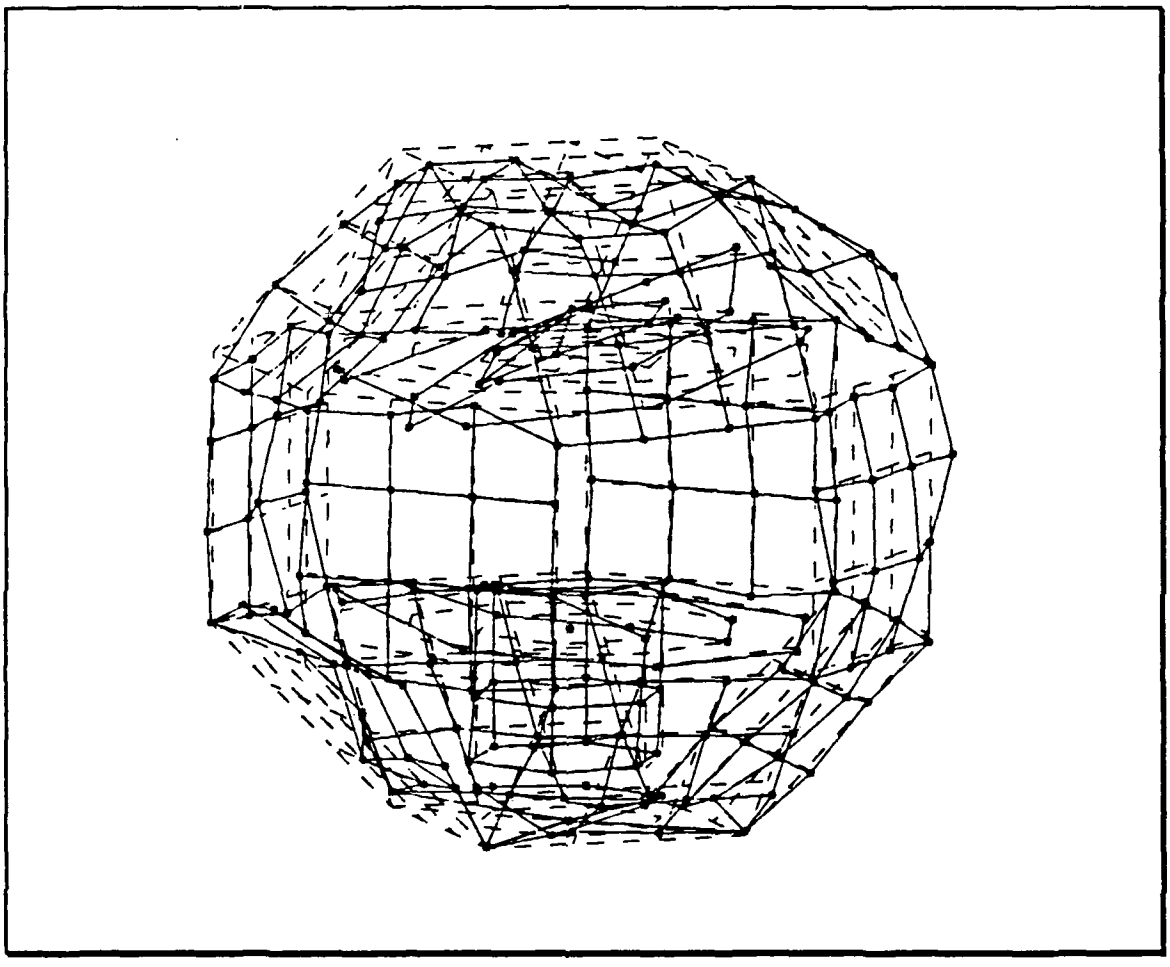

Figure 41. Mode 3, Deformed Geometry

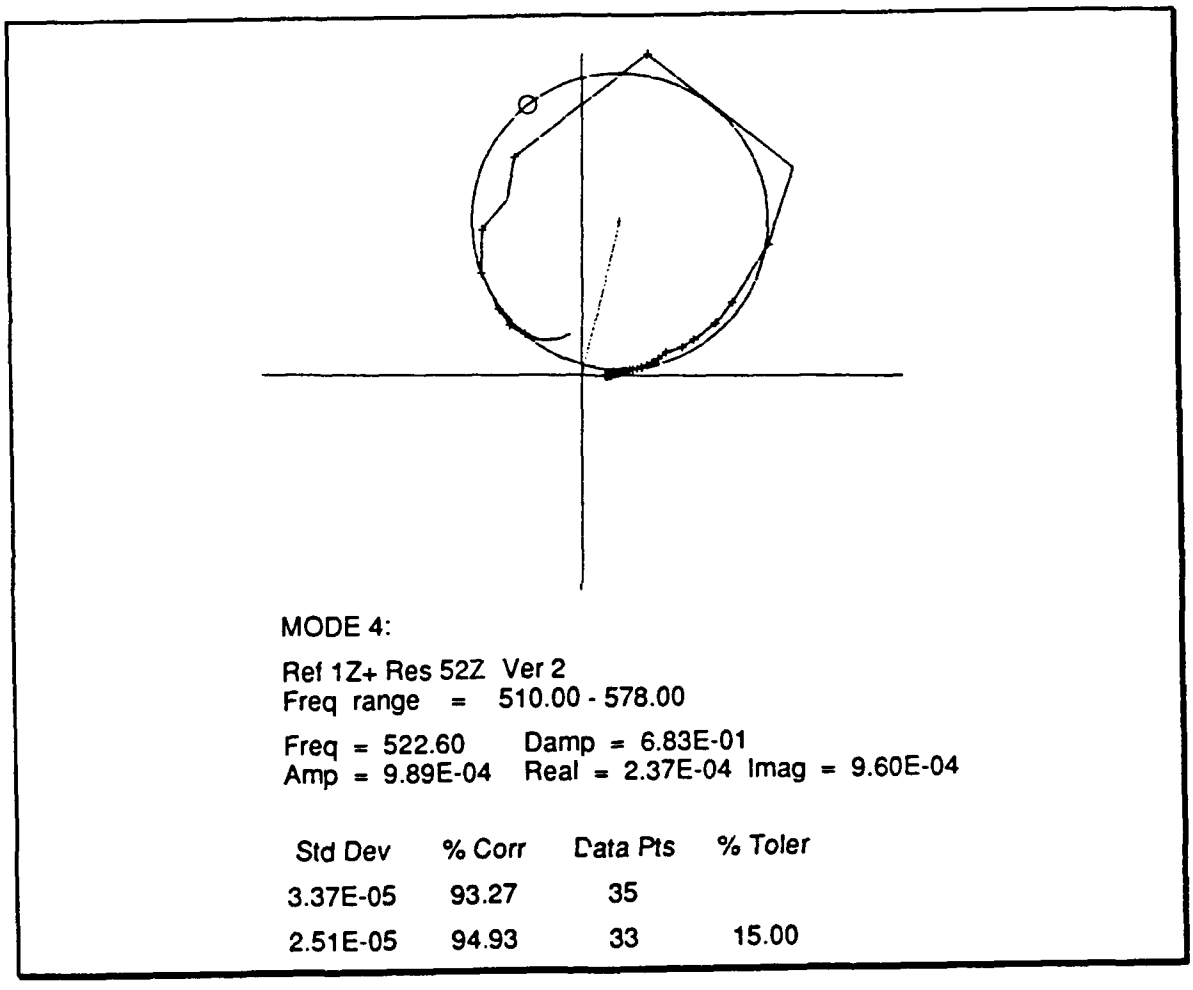

Figure 42. Mode 4, Test Data Nyquist Plot

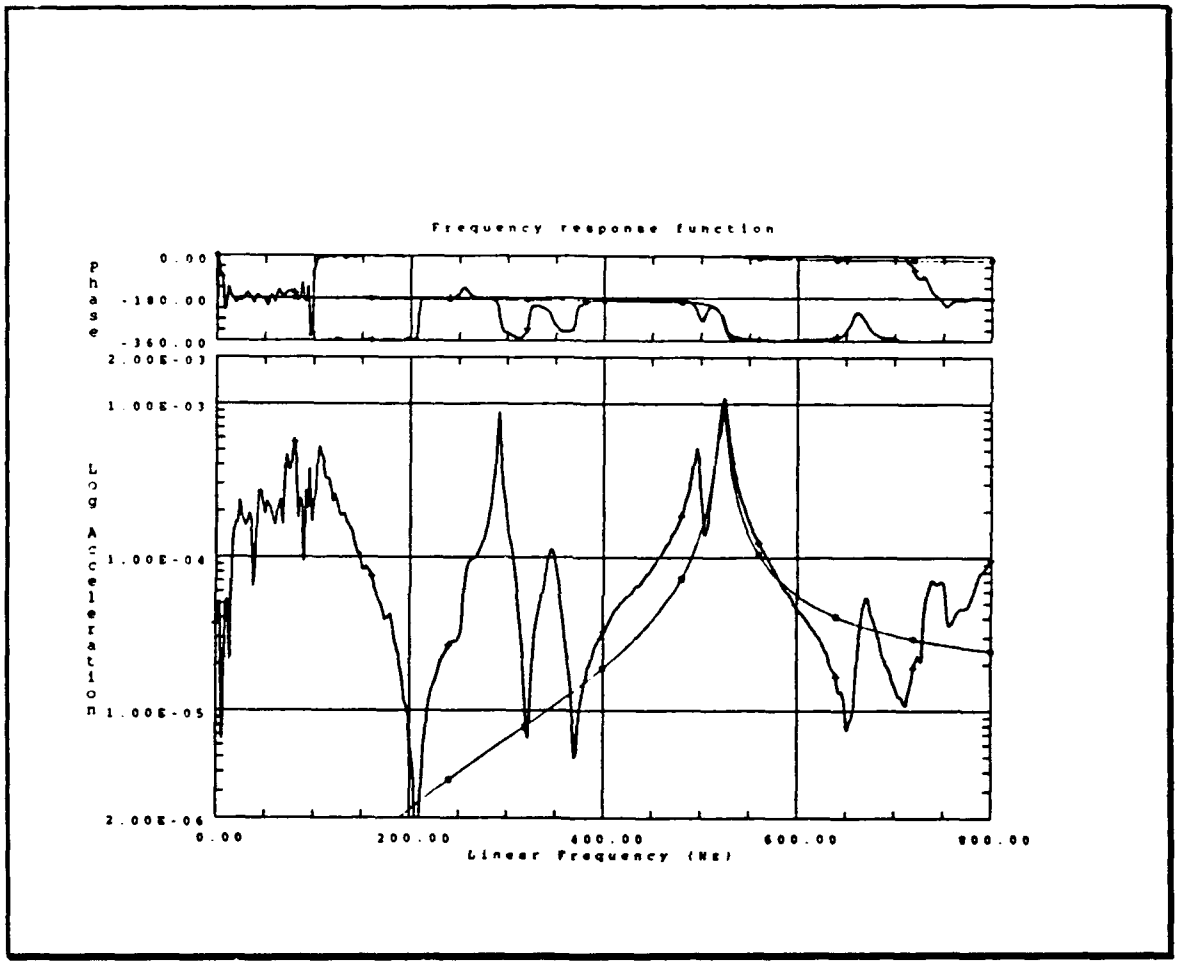

Figure 43. Mode 4, FRF Curve-Fit

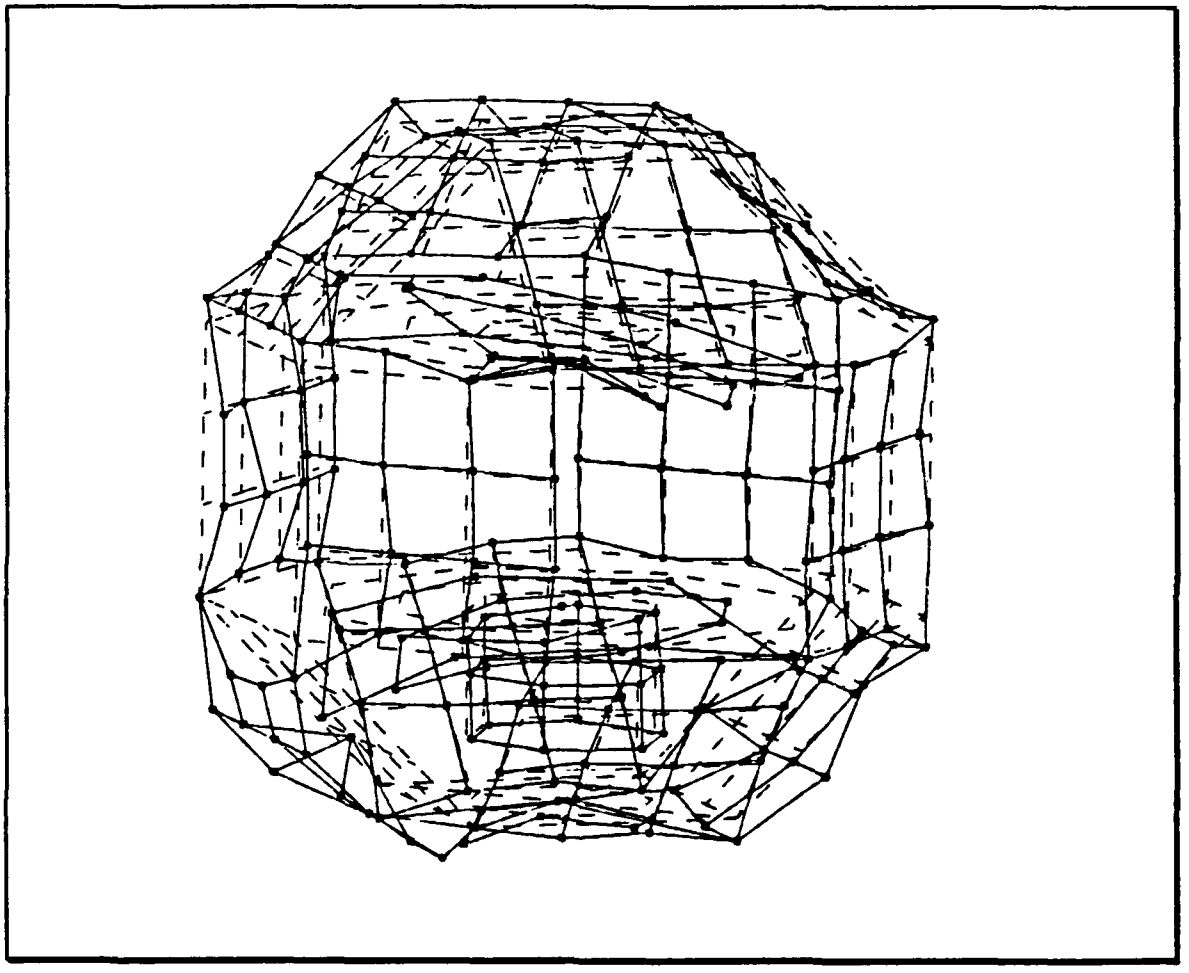

Figure 44. Mode 4, Deformed Geometry

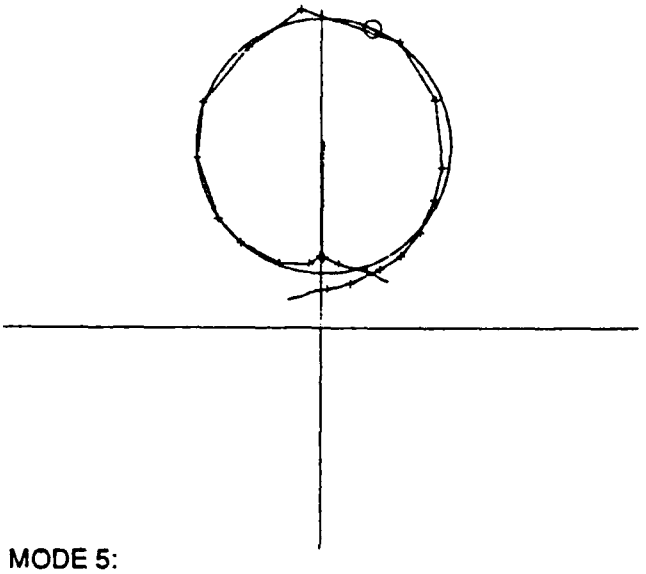

MODE 5:

Ref 1Z+ Res 51Z- Ver 2
Freq range = 648.00 - 688.00

Freq = 671.40 Damp = 8.25E-01
Amp = 2.67E-05 Real = 3.68E-07 Imag = 2.67E-05

Std Dev	% Corr	Data Pts	% Toler
8.84E-07	93.39	21	
8.84E-07	93.39	21	15.00

Figure 45. Mode 5, Test Data Nyquist Plot

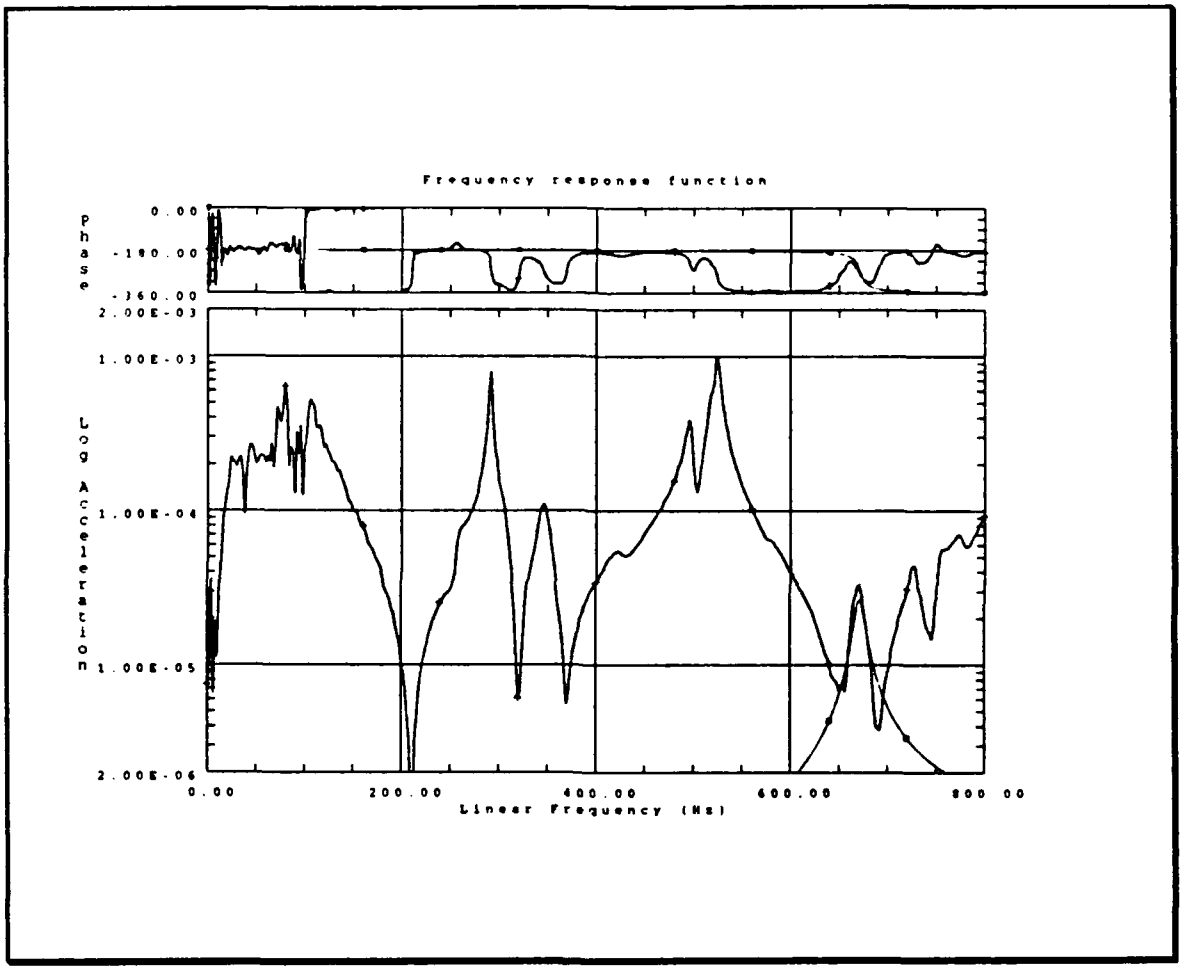

Figure 46. Mode 5, FRF Curve-Fit

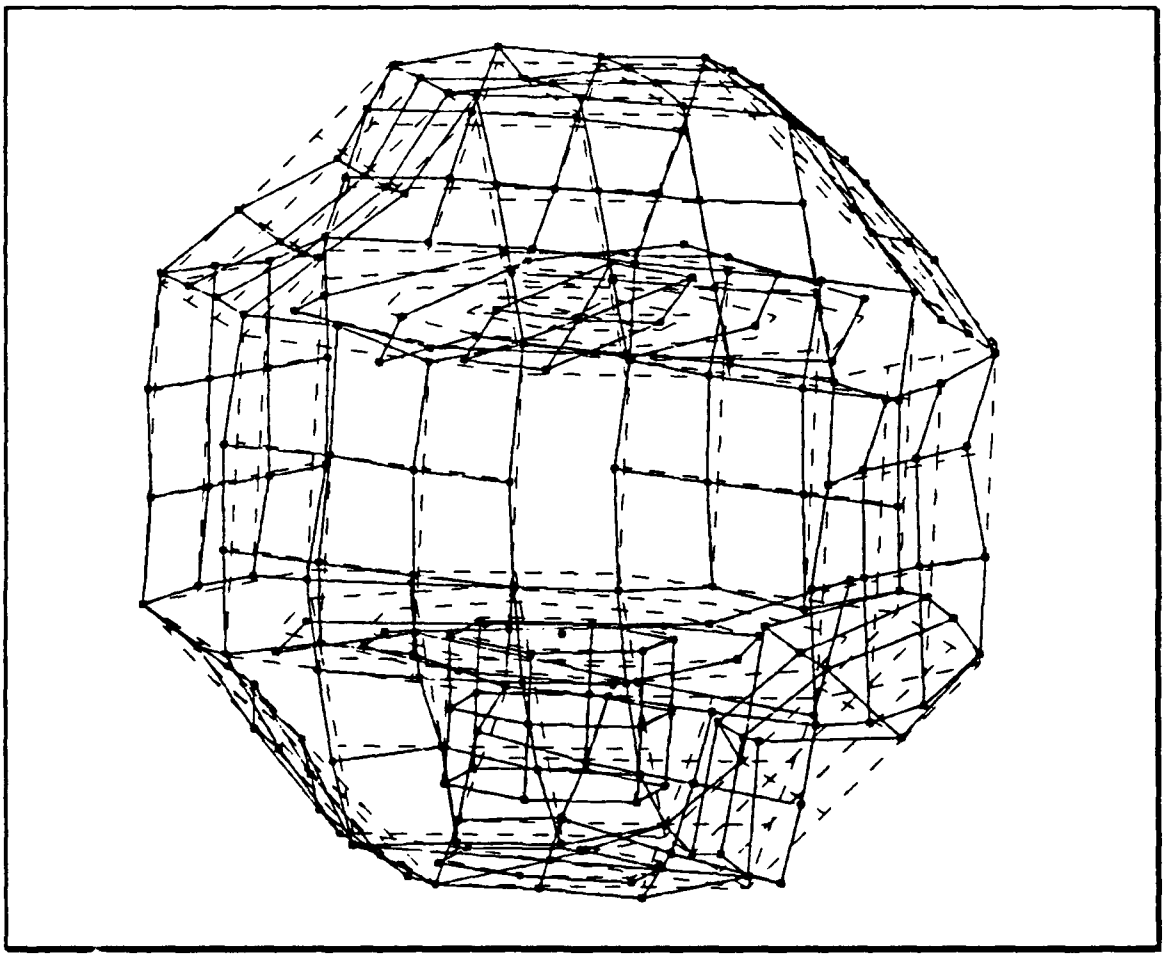

Figure 47. Mode 5, Deformed Geometry

APPENDIX D

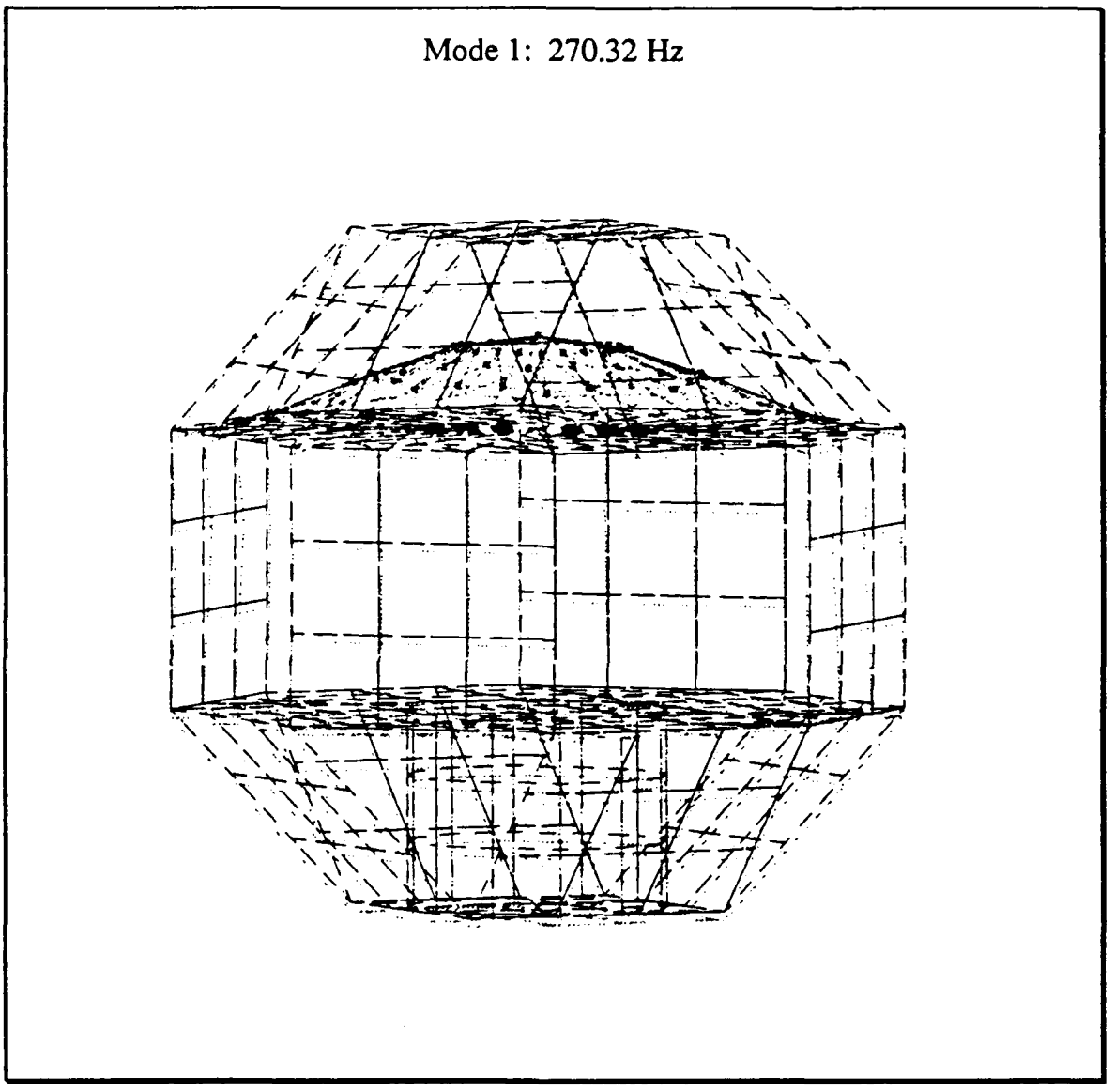

Figure 48. Mode 1, Structure Alone

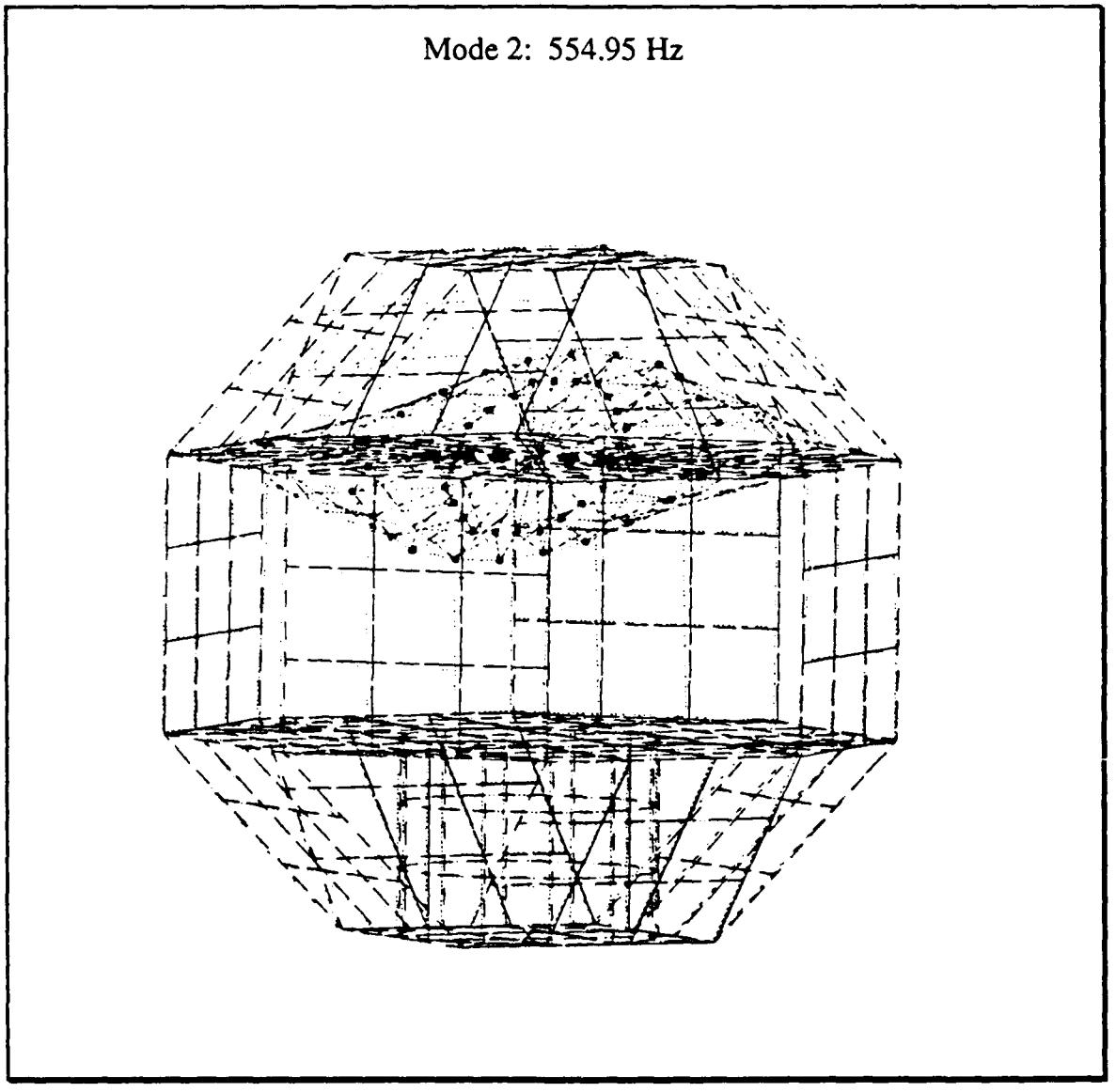

Figure 49. Mode 2, Structure Alone

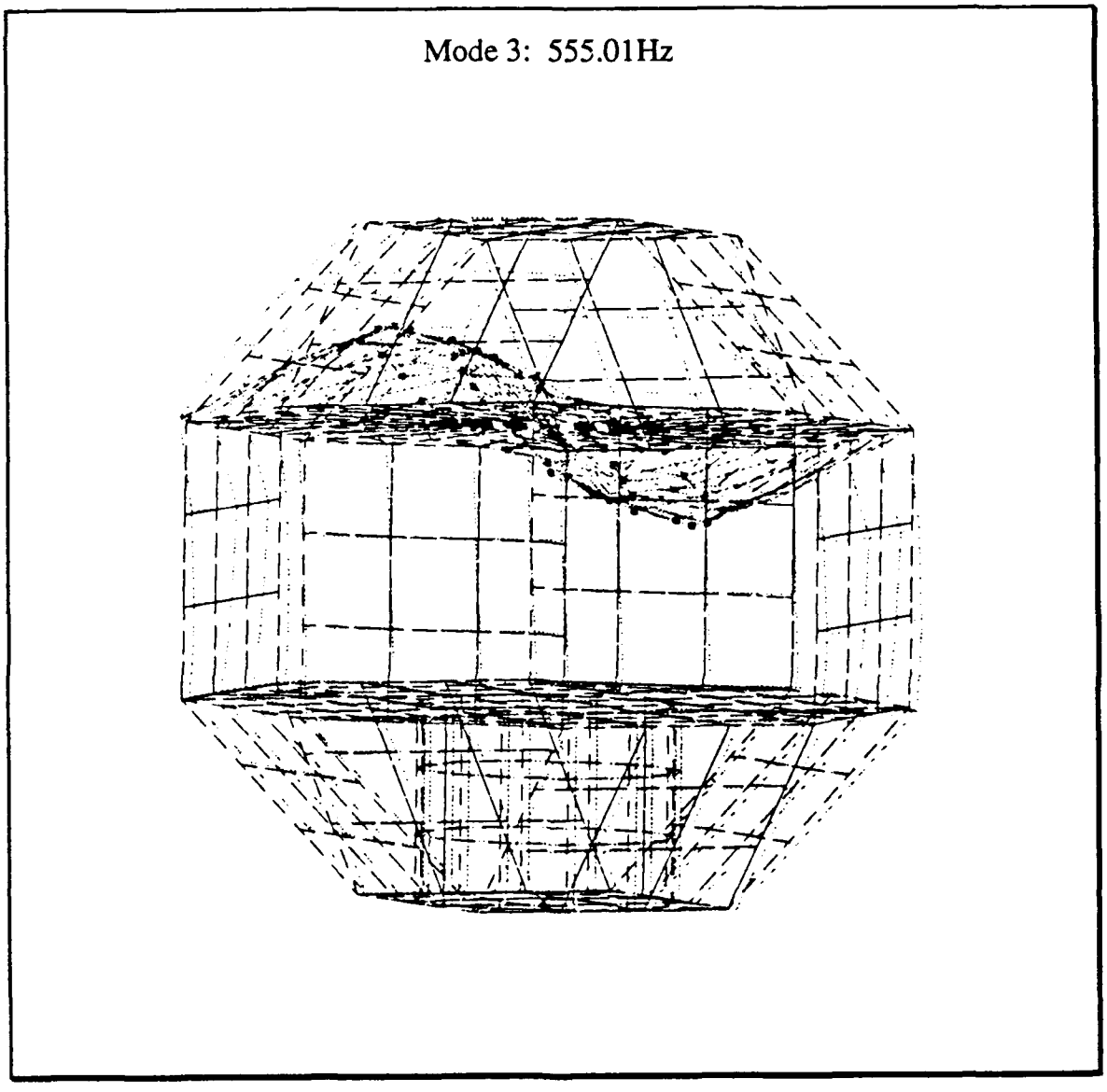

Figure 50. Mode 3, Structure Alone

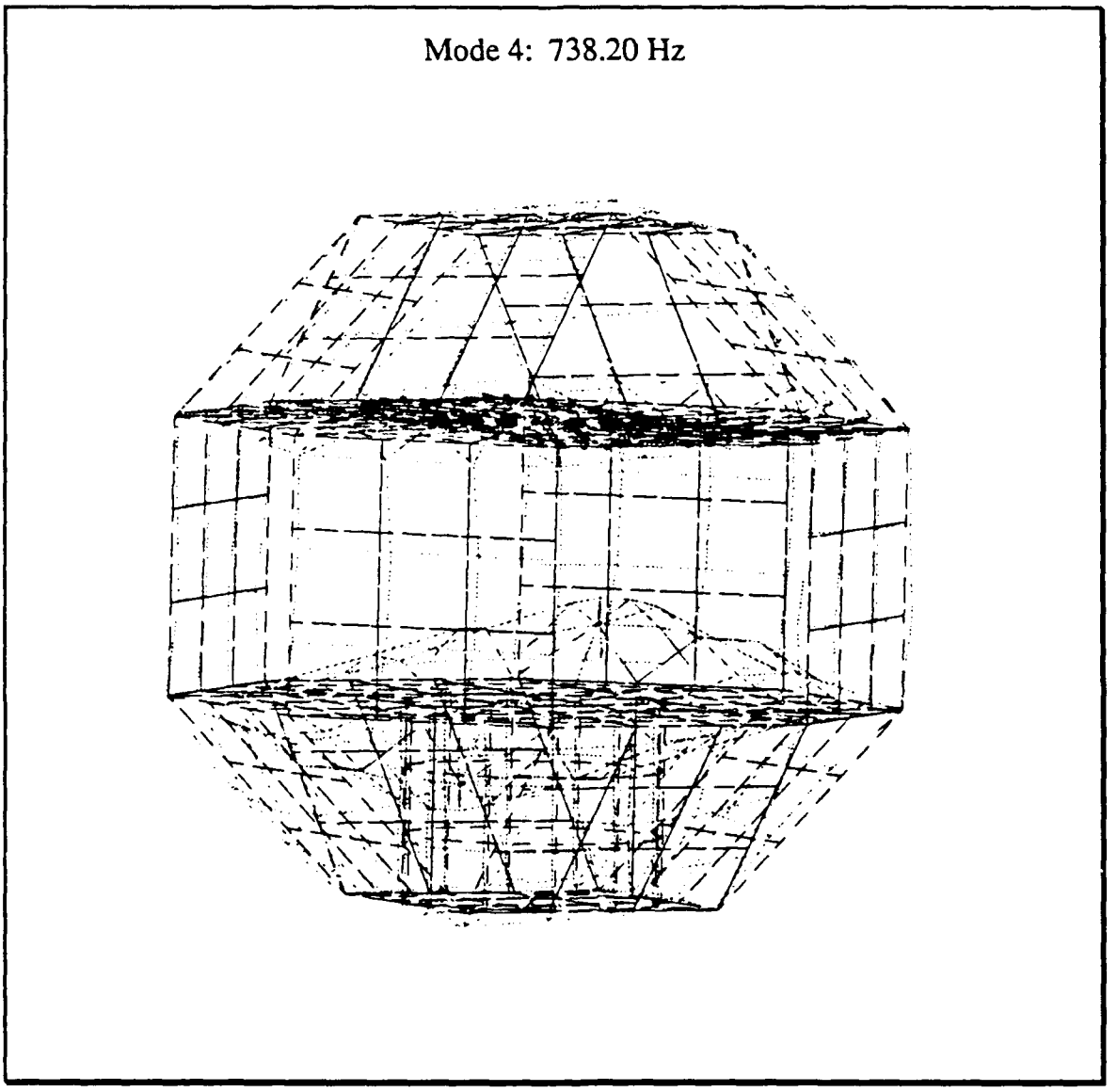

Figure 51. Mode 4, Structure Alone

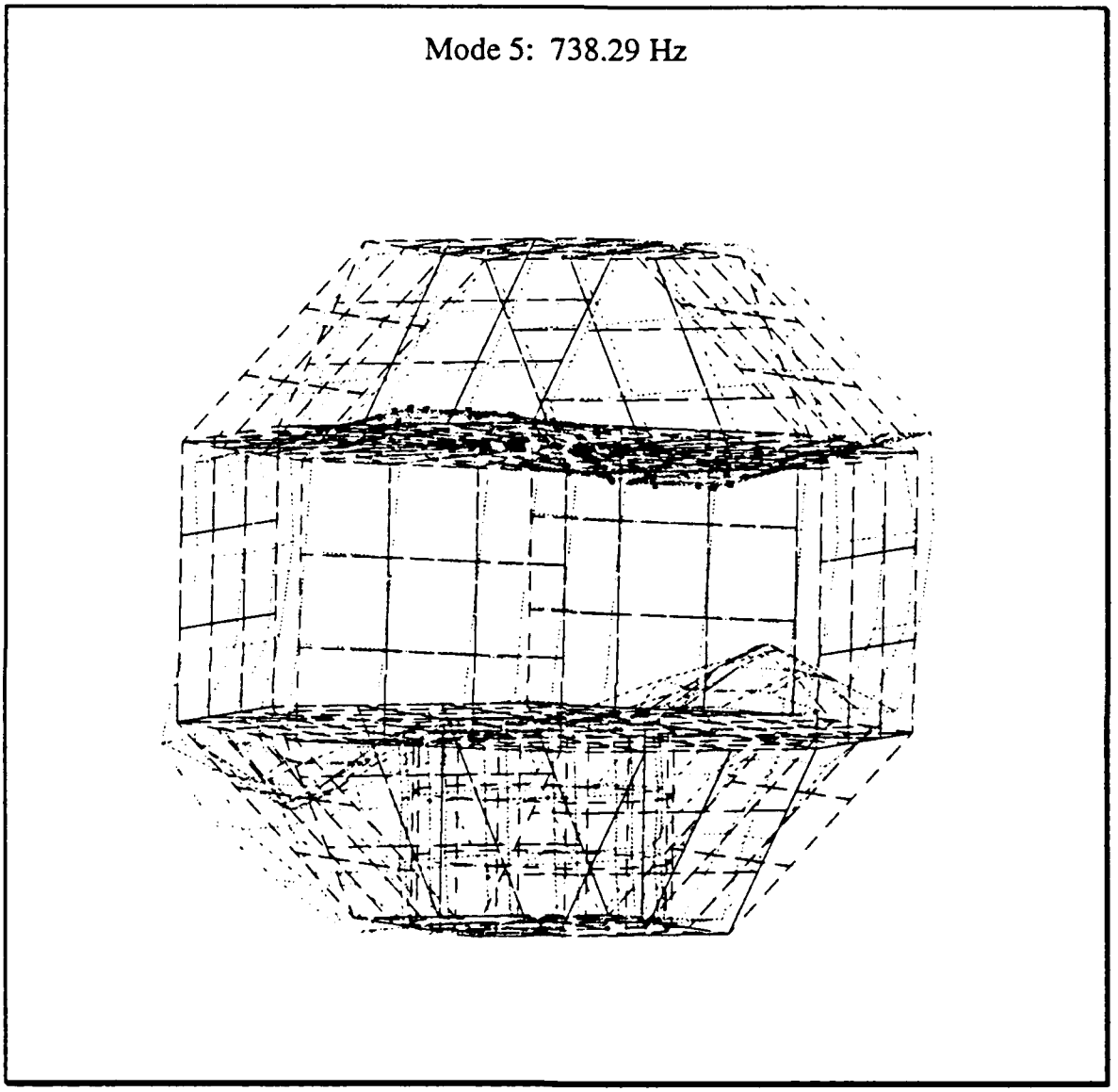

Figure 52. Mode 5, Structure Alone

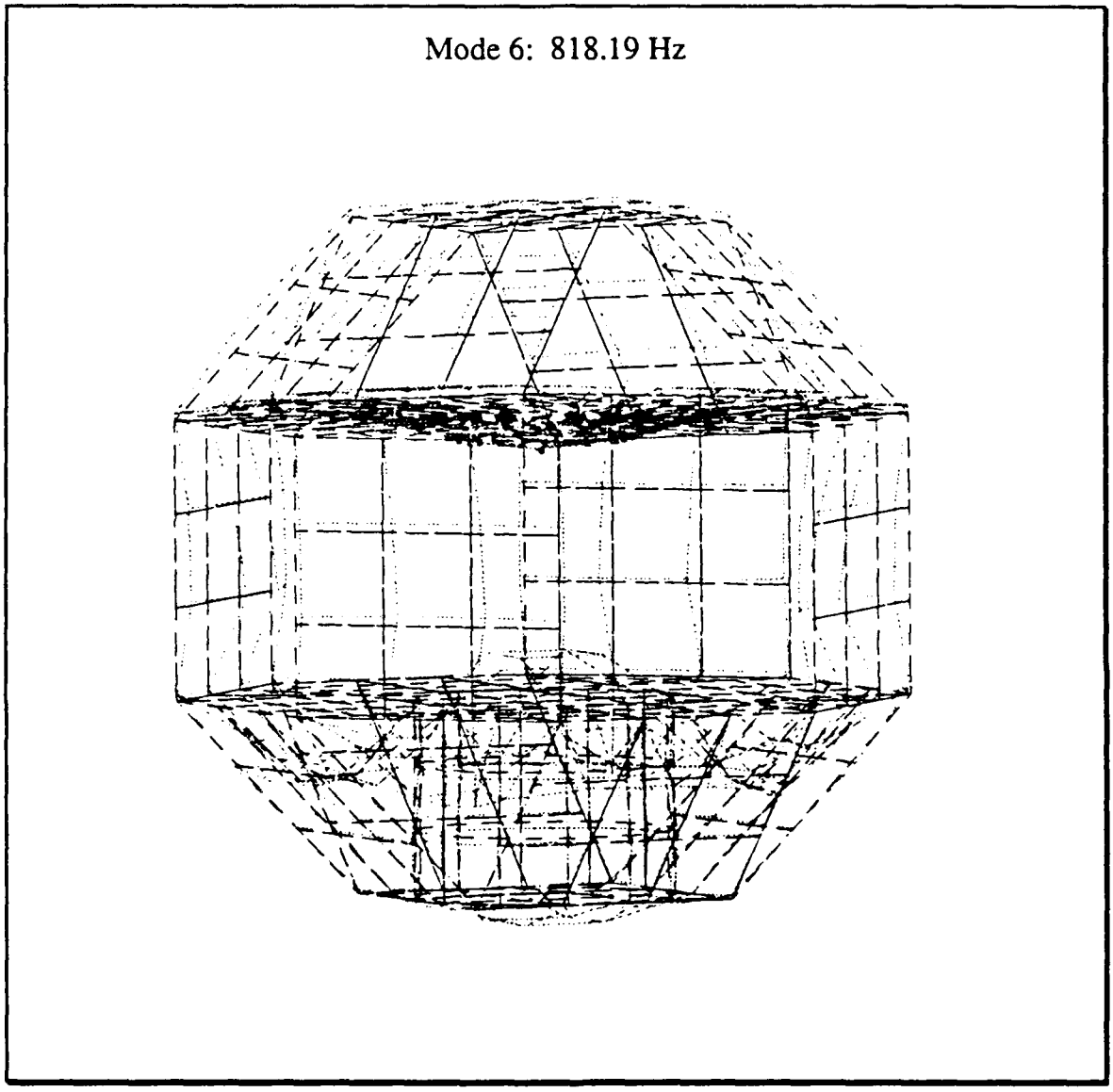

Figure 53. Mode 6, Structure Alone

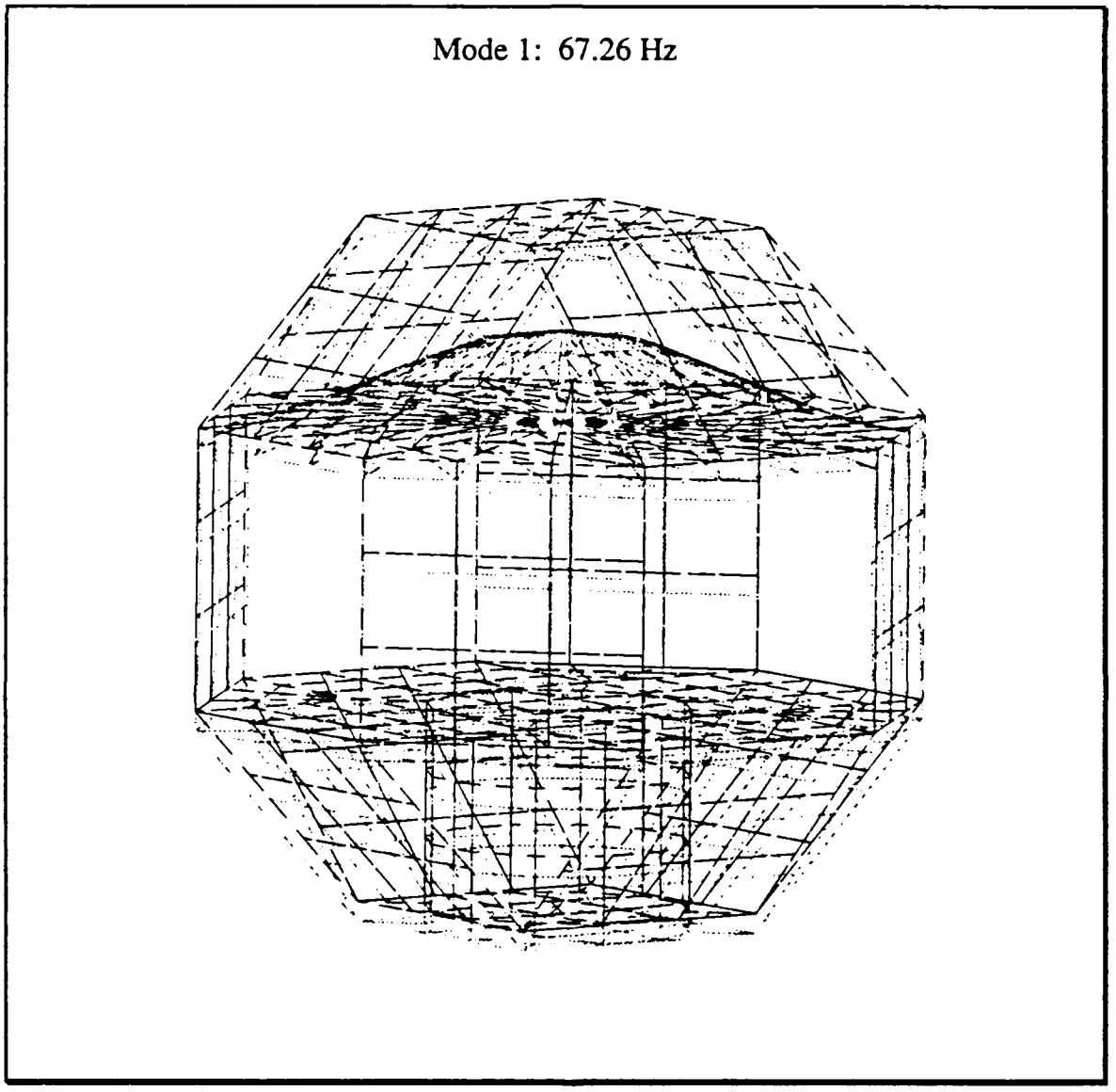

Figure 54. Mode 1, Structure with Component Mass

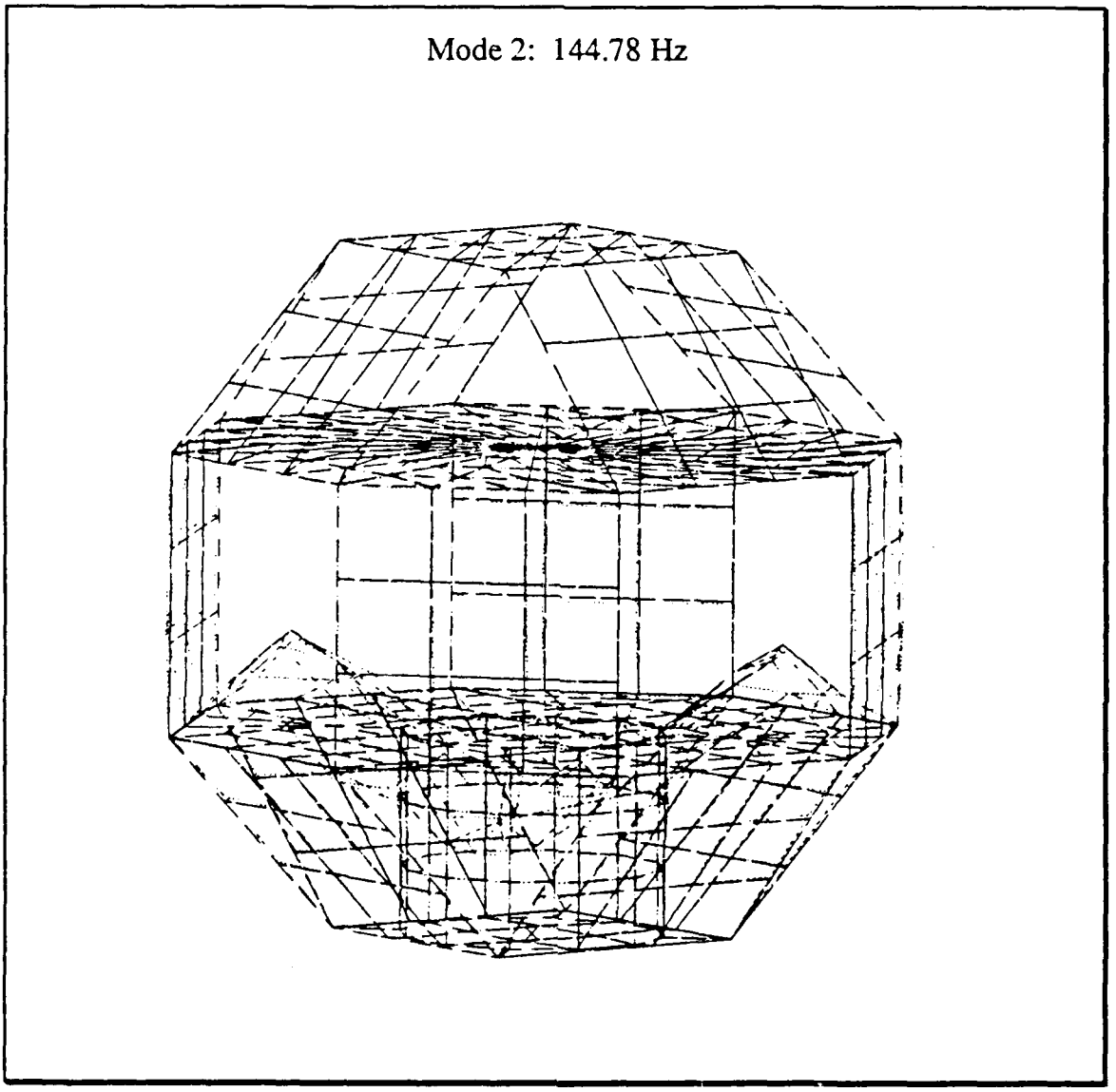

Figure 55. Mode 2, Structure with Component Mass

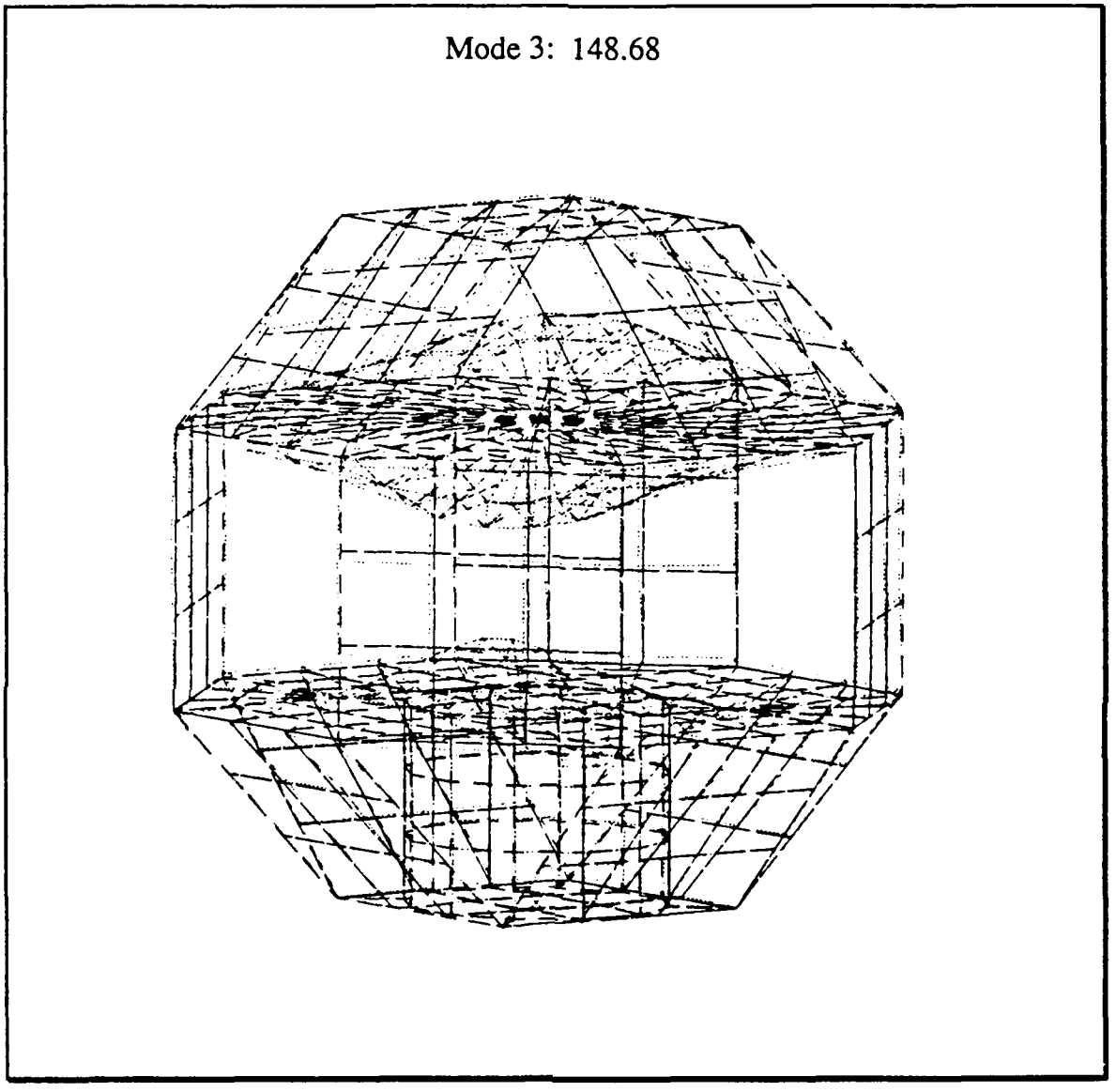

Figure 56. Mode 3, Structure with Component Mass

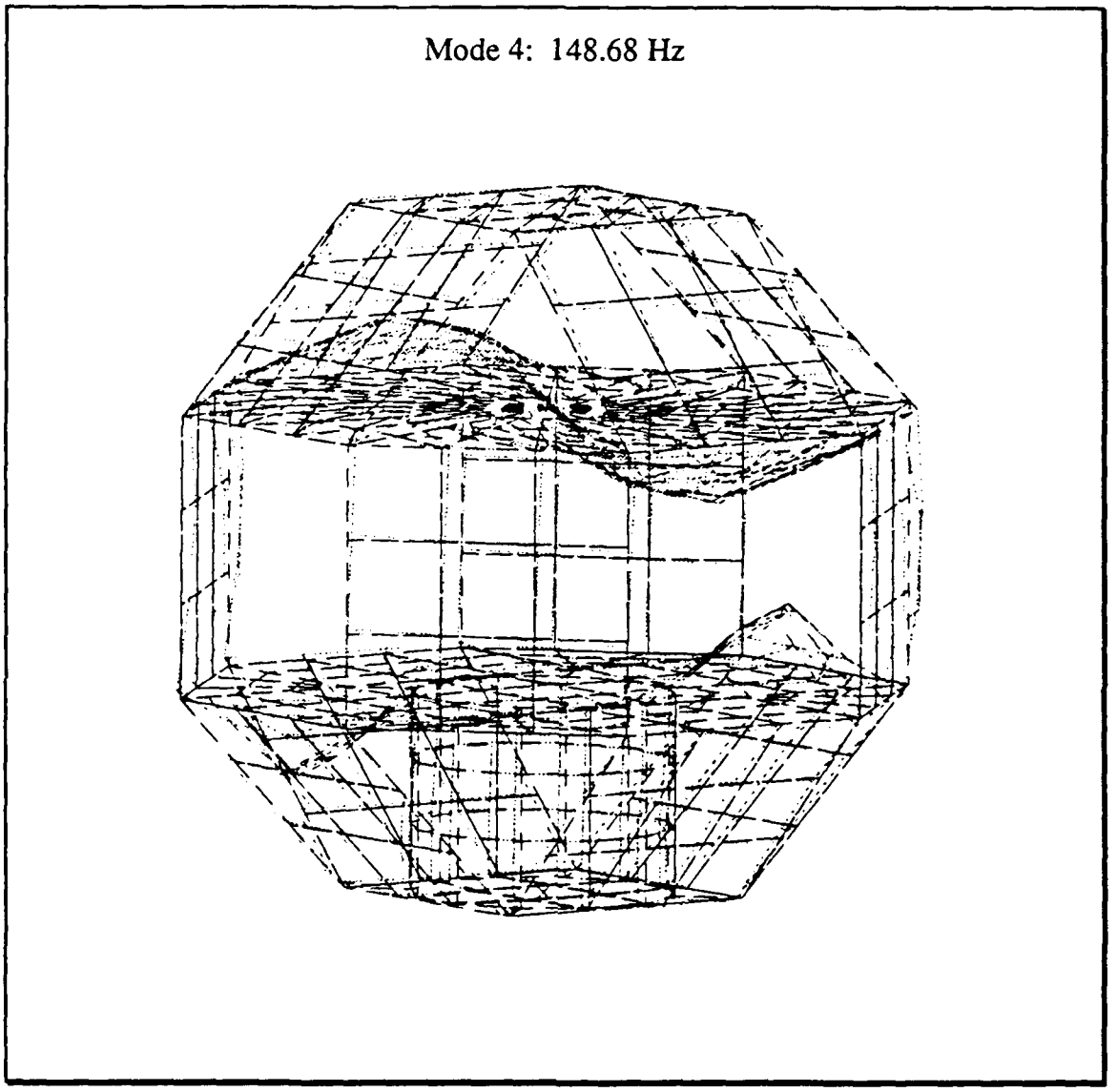

Figure 57. Mode 4, Structure with Component Mass

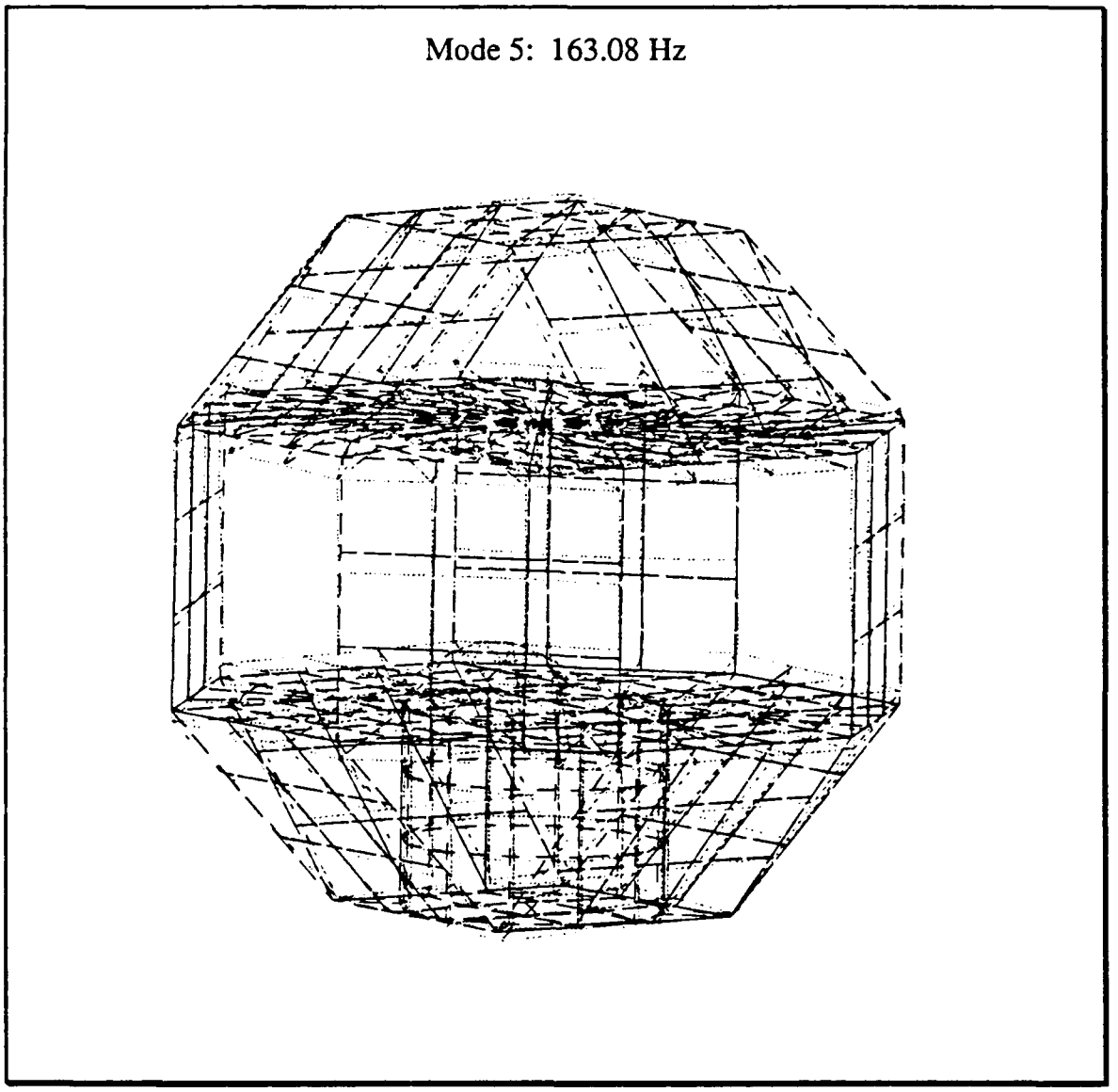

Figure 58. Mode 5, Structure with Component Mass

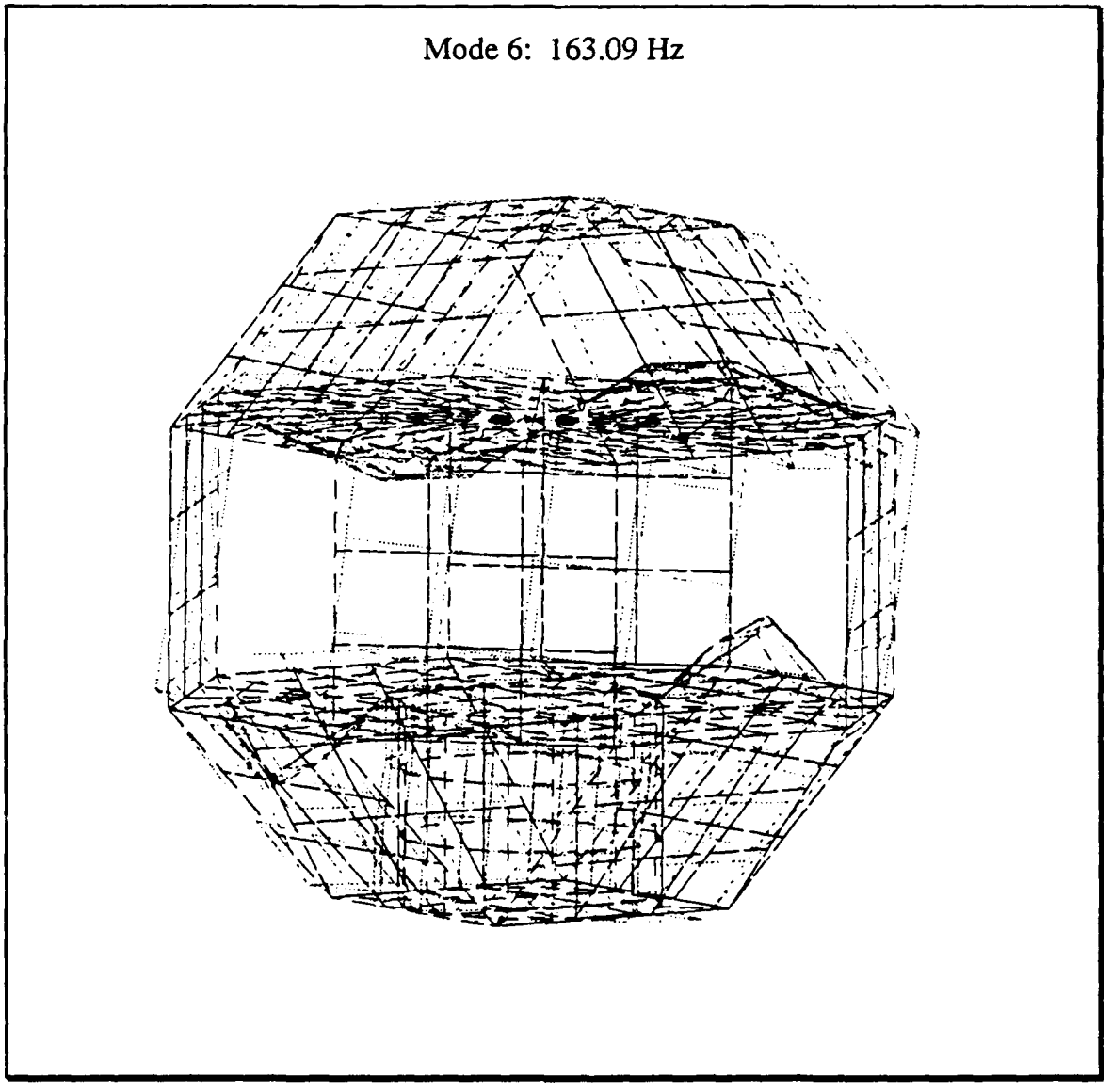

Figure 59. Mode 6, Structure with Component Mass

REFERENCES

1. The Aerospace Corporation, Report No. TOR-0091(6508-05)-1, *Experimenter's Planning Guide for Department of Defense Space Test Program*, by F. L. Knight and H. T. Sampson, 8 June 1991.

2. *Get Away Special Payloads Safety Manual*, National Aeronautics and Space Administration, Goddard Space Flight Center, May 1986.

3. Letter from NASA Technical Manager, Special Payloads Division, to Payload Manager for NPS payload G337, Subj: Experiment G337, 28 November 1990.

4. CASA/GIFTS, Inc., *GIFTS User's Reference Manual*, September 1985, (copyright © University of Arizona, 1979).

5. Structural Dynamics Research Corp., *Test User's Guide*, 1990.

6. Ewins, D. J., *Modal Testing: Theory and Practice*, Research Studies Press, Somerset, England, 1984.

7. Structural Dynamics Research Corp., *Finite Element Modeling User's Guide*, 1990.

8. NASA Contract Report, CR-912, *Shell Analysis Manual*, by E. H. Baker, *et al.*, April 1968.

9. Agrawal, B. N., *Design of Geosynchronous Spacecraft*, Prentice-Hall, Inc., Englewood Cliffs, NJ, 1986.

INITIAL DISTRIBUTION LIST

1.	Defense Technical Information Center Cameron Station Alexandria, Virginia 22304-6145	2
2.	Library, Code 0142 Naval Postgraduate School Monterey, California 93943-5002	2
3.	Chairman, Code (AA) Department of Aeronautics & Astronautics Naval Postgraduate School Monterey, California 93943	2
4.	Chairman, Code (SP) Space Systems Academic Group Naval Postgraduate School Monterey, California 93943	3
5.	Prof. Ramesh Kolar, Code (AA/Ko) Naval Postgraduate School Monterey, California 93943	2
6.	Prof. Young Shin, Code (ME/Sg) Naval Postgraduate School Monterey, California 93943	1
7.	Prof. Brij N. Agrawal, Code (AA/Ag) Naval Postgraduate School Monterey, California 93943	1
8.	Mr. Daniel Sakoda, Code (SP/Sd) Naval Postgraduate School Monterey, California 93943	2